ARGON ION LASER MODIFIED AND MONITORED GROWTH OF III-V SEMICONDUCTORS BY CHEMICAL BEAM EPITAXY.

Thesis submitted in accordance with the requirements of the University of Liverpool for the degree of Doctor in Philosophy.

By Adam Robert Boyd

September 1996.

ABSTRACT

The aim of this research work was to investigate the effect of focused argon ion laser radiation on the growth rate and morphology of GaAs growth using chemical beam epitaxy (CBE), and the development of surface topography during annealing of (001) GaAs wafers and subsequent CBE growth of GaAs, AlGaAs and InGaAs layers using laser light scattering (LLS). The precursors used were triethylgallium, trimethyamine-alane, trimethylindium and arsine thermally cracked to As_2 in an injector cell.

In the substrate temperature range 313-450°C the local growth rate of GaAs was found to be increased with argon ion laser radiation by a factor of up to 20 depending on the laser power density, substrate temperature, and group V: group III flux ratio. The greatest enhancement was observed at power densities above $500W/cm^{-2}$, a substrate temperature of 313°C, and V:III flux ratios above 4:1. Under these conditions sharply defined features were produced due to a sharp knee in the growth rate with laser power density relationship. For substrate temperatures greater than 360°C the results show a strong photothermal contribution to the enhancement. A rippled surface topography developed during assisted growth at power densities of above $500W/cm^{-2}$ and substrate temperatures in the range 360-450°C consistent with thermally induced elastic strain resulting in local variations in growth rate.

Above 490°C laser irradiation resulted in a local GaAs growth rate reduction consistant with local substrate heating. At laser power densities above around $200W/cm^{-2}$ a 'cross-hatch' pattern of ridges aligned along the <110> directions was observed extending up 6mm from the irradiated area. These are believed to be associated with dislocations which lie parallel to the surface. An etch pit density study revealed no increase of threading dislocations (terminating at the surface). This indicates that the thermally induced plastic strain from the laser irradiation was accommodated by the movement of threading dislocations from the underlying substrate.

Using LLS a wide range of behaviour was observed during the pre-growth anneal of GaAs substrates. It is suggested that this was due to the desorption of previously deposited species from the cryopanel as a result of radiant heating from the substrate, leading to contamination of the wafer surface. Procedures to minimise this contamination are outlined.

LLS was also used to study the development of surface topography during growth. Development of of elliptical islands during the growth of GaAs and AlGaAs, and the onset of the 'cross-hatch' pattern during the growth of InGaAs were observed. Interference oscillations in scattered light intensity during the growth of multilayer structures are also shown to be observable using LLS.

PREFACE

This thesis describes research carried out in the Department of Material Science and Engineering at The University of Liverpool between Ocober 1992 and September 1995. None of this work has previously been submitted for a degree at this or any other university.

The work reported is original and was performed under the supervision of Dr T J Bullough. The work of others has been freely drawn upon and duly referenced. A full alphabetical list of referees is given at the end of the text.

Some portions of the work described within this thesis have been published as follows:

'The origin of misfit dislocations and the surface cross-hatch pattern in low-misfit strained epitaxial layers'
R Beanland and A R Boyd
Proc. 9th Int Conf Microscopy of Semiconducting Materials, Oxford 95

'An in-situ laser light scattering study of the development of surface topography during GaAs and $In_xGa_{1-x}A$ s chemical beam epitaxy'
A R Boyd, T B Joyce and R Beanland
J. cryst. Growth 164 (1996) 51-57

'Growth mechanisims and morphology of Ar^+ laser assisted CBE of GaAs'
A R Boyd, T J Bullough, T Farrell and T B Joyce
J. cryst. Growth 164 (1996) 71-76

ACKNOWLEDGEMENTS

First and foremost I would like to thank Alison Johnson, my mother, father, and brothers Nathan and David for continual support during this work.

I am indebted to all my collegues at Liverpool, and in the field of CBE, for their contributions and assistance, some of which particularly by the technicians, may have seemed unnoticed. In particular, special thanks must go to my supervisor Dr. Tim Bullough, and Prof. Peter Goodhew for useful comment, to Dr. Trevor Farrell for getting the research work up and going, to Dr. Tim Joyce for keeping the system running, and to Dr. Richard Beanland for encouraging me to study InGaAs on GaAs heteroepitaxy. I would also like to thank all the semiconductor group at Liverpool for discussions, particularly Simon Westwater for keeping me company during evenings and putting me up after I had left Liverpool. I would also like to thank EPSRC for my studentship and the purchase of the laser, all those who helped with characterisation and those at The University of Cadiz, especially Prof. Raphael Garcia Roja, for making my stay there a pleasant and productive one.

Finally I would like to thank the departmental student football team for giving me a well needed break from writing this august with a fractured finger.

CONTENTS

CHAPTER ONE: INTRODUCTION

1.1 Background.
- 1.1.1 GaAs Epitaxy
- 1.1.2 Laser Modified CBE
- 1.1.3 Optical Monitoring of CBE and laser modified CBE

1.2 Aims of this research project.

1.3 Summary of this research work.

1.4 Synopsis of thesis contents

CHAPTER TWO: EPITAXIAL GROWTH AND MORPHOLOGY OF SEMICONDUCTORS

2.1 Introduction to GaAs and related III-V semiconductors

2.2 Epitaxial growth techniques
- 2.2.1 Molecular Beam Epitaxy
- 2.2.2 Metal-organic Vapour Phase Epitaxy
- 2.2.3 Chemical Beam Epitaxy and related techniques

2.3 Surface preparation for epitaxial growth

2.4 Chemical Beam Epitaxial growth of GaAs

2.5 Epitaxial growth of low compressively strained thin films: $In_XGa_{1-X}As$ on GaAs ($X < 0.25$)

2.6 Epitaxial growth of high compressively strained thin films: InAs on GaAs

CHAPTER THREE: OPTICAL PROCESSING AND MONITORING

3.1 Optical processing of semiconductors.
- 3.1.1 Introduction
- 3.1.2 Mechanisms for direct laser writing
- 3.1.3 Mechanisms of laser modified CBE

3.2 Optical monitoring by laser reflectometry.
- 3.2.1 Reflection and transmission of light at a surface.
- 3.2.2 Reflection and transmission of light by a single film.
- 3.2.3 Application of laser reflectometry.

3.3 Optical monitoring by laser light scattering
- 3.3.1 Description of a surface.
- 3.3.2 Rough surface scattering.
- 3.3.3 Smooth surface scattering.
- 3.3.4 Point scattering.
- 3.3.5 Scattering of light from a single film.
- 3.3.6 Application of laser light scattering

CHAPTER FOUR: EXPERIMENTAL METHODS

4.1 The chemical beam epitaxial growth facility

4.2 Beam flux calibration

4.3 Substrate temperature control and calibration

4.4 The argon ion laser

4.5 Experimental set up for laser assisted CBE

4.6 In situ laser light scattering and laser interferometry

4.7 Post-growth optical microscopy techniques

4.8 Post-growth profilometry techniques

4.9 Post-growth secondary ion mass spectrometry

4.10 Post-growth etch 'pit' density measurements

CHAPTER FIVE: LASER LIGHT SCATTERING STUDIES OF THE GROWTH OF GAAS, ALGAAS, AND INGAAS ON GAAS

5.1 Substrate preparation
- 5.1.1 Introduction to substrate preparation
- 5.1.2 Typical LLS results for substrate annealing with and without chamber outgassing
- 5.1.3 Summary of LLS results
- 5.1.4 Atomic force microscopy results
- 5.1.5 Discussions

5.2 Growth of GaAs and AlGaAs
- 5.2.1 Morphology changes during the growth of GaAs and AlGaAs
- 5.2.2 Laser light scattering interference oscillations
- 5.2.3 Discussions

5.3 Low compressively strained layer growth: $In_xGa_{1-x}As$ (x<0.25) on GaAs
- 5.3.1 Laser light scattering results
- 5.3.2 Atomic force microscopy results
- 5.3.3 Discussions

5.4 High compressively strained layer growth: InAs on GaAs

5.5 Summary of chapter

CHAPTER SIX: LASER MODIFIED CHEMICAL BEAM EPITAXY

6.1 Low temperature laser assisted growth of GaAs
- 6.1.1 General growth rate results
- 6.1.2 Modelling of growth rates to temperature rise
- 6.1.3 Chopped beam results
- 6.1.4 Effect of group V-III flux ratio
- 6.1.5 Growth rate and Carbon incorporation profile
- 6.1.6 Morphology results
- 6.1.8 Discussions

6.2 High temperature laser inhibited growth of GaAs
- 6.2.1 Growth rate results
- 6.2.2 Morphology results
- 6.2.3 Discussions

6.3 Summary of chapter

CHAPTER SEVEN: CONCLUSIONS

7.1 Laser Modified CBE

7.2 Laser light scattering studies

7.3 Suggestions for further work

REFERENCES

CHAPTER ONE
INTRODUCTION

1.1 Background.

1.1.1 GaAs Epitaxy

1.1.2 Laser Modified CBE

1.1.3 Optical Monitoring of CBE and laser modified CBE

1.2 Aims of this research project.

1.3 Summary of this research work.

1.4 Synopsis of thesis contents

1.1 Background

1.1.1 GaAs Epitaxy

The semiconductor industry is now one of the most profitable and rapidly advancing industries in the world. Many of the advances in semiconductors have been at least partly due to the provision of improved materials and processing, to enable the fabrication of advanced device structures. A wide range of techniques for material growth and fabrication have been developed. This thesis details studies based upon the use of Chemical Beam Epitaxy (CBE) to grow GaAs, AlGaAs and InGaAs epitaxial layers upon GaAs substrates, and in particular the use of light to modify and monitor that growth.

Most semiconductor devices are based on the growth of a single crystal layer of different electrical properties on a single crystal wafer. The difference in electrical properties is usually achieved by the introduction of dopant atoms, but it may be achieved by a difference in composition or thickness. Structures are usually defined laterally across the wafer in a plan or selective area process and vertically by the formation of a series of layers. The plan or selective area process is usually masking and re-growth or selective area etching, both are usually performed outside of the growth system.

The growth of a layer of single crystal material upon a single crystal substrate so that the lattices are in exact registration with each other is called epitaxy. There are two classes of epitaxy, homoepitaxy, where the layer and substrate are of the same material and heteroepitaxy, where the layer and substrate are of different materials. Homoepitaxy is widely used in semiconductor device fabrication. Layers of differing electrical properties are achieved by dopant incorporation either during growth or by implantation. Heteroepitaxy is not widely used at present due to differing thermal expansion coefficients, and lattice parameters, which results in lattice strain. Strain leads to a change

in electrical properties and both can result in defect generation which reduces the potential for device fabrication. However, if the problems of heteroepitaxy are overcome, accommodated, or even utilised, it will allow a greater diversity in semiconductor devices.

Currently, the vast majority of semiconductor devices produced are based on silicon. There is however considerable interest in 'compound semiconductors' which covers III-V, II-VI and IV-VI material systems. In terms of electronic and optoelectronic devices the most significant progress has been made in the III-V material system based on GaAs and InP.

GaAs has a number of advantages over silicon for electronic devices. Higher electron mobility and drift velocity enable higher frequency operation, and 'semi-insulating GaAs wafer substrates can be produced, providing good electrical isolation for overlying devices. GaAs, and other III-V compounds, are useful for optoelectronic devices due to high efficiency direct radiative recombination and optical transparency in the near IR region, allowing the use of GaAs in light emitting, detecting and modulating devices. However, compared with silicon, GaAs has a short minority carrier lifetime, a higher density of crystal defects, a lack of a stable native oxide and a higher material and processing cost. This has resulted in GaAs still being used only as a specialist material for microwave and optoelectronic devices and not for VLSI.

GaAs and InP based alloys form the basis of most light emitting diodes (LEDs). These are a major commercial outlet and are usually grown by liquid phase epitaxy and zinc diffusion used to form the p-n junction. LPE is used since it the cheapest method of growing GaAs layers. More advanced devices, such as quantum well (QW) injection lasers (Dupuis et al 1978), heterojunction bipolar transistors (HBTs) and high electron mobility transistors (HEMTs) incorporate many layers, often QWs from 0.28nm (one

monolayer) to 10nm in thickness. These devices require precise control of composition, dopant concentration and thickness during growth. Epitaxy is the only method to produce these layers, and the need for these devices has led to an increasing requirement for more advanced epitaxial growth systems. These systems are discussed in chapter 2.

Chemical Beam Epitaxy (CBE) is one of the most advanced growth systems. It was developed from molecular beam epitaxy (MBE) by the substitution of solid evaporation cells by gaseous sources, initially from metal organic vapour phase epitaxy (MOVPE). It was developed to overcome some of the problems associated with the two systems. The problems included poor group V flux control and morphological defects in MBE, and a lack of monolayer thickness control in MOVPE. CBE does relieve these problems, although the MBE problems have been reduced at the same time but does entail problems of its own such as difficulty in obtaining accurate (±1%) ternary and quaternary compositions due to its strong dependence on temperature.

CBE has a unique potential in selective area epitaxy by the use of masks blocking the chemical beams, and also by the use of laser (or lamp) irradiation to locally effect the decomposition of the gaseous sources used.

1.1.2 Laser Modified CBE

The growth rate in the CBE growth of GaAs using triethylgallium (TEG) as the gallium precursor falls from its maximum value at ~500-550°C to almost zero at ~320°C. This has prompted several studies of locally enhancing the rate by irradiating a substrate held at ~310-450°C with focused laser light, thus offering the prospect of selective area growth.

Both pulsed UV excimer lasers (e.g.. Farrell et al, 1992) and cw argon ion lasers (e.g. Iga, Sugiura and Yamada, 1993) have been used to locally enhance the growth of GaAs.

The photon energy of the excimer lasers is sufficient to photo-dissociate the metalorganic molecule (Beuermann and Stuke, 1989) and this offered the prospect of non-thermal local area growth. However GaAs is strongly absorbing at the UV laser wavelengths and this leads to local heating of the substrate. With the fluences required to enhance the growth the temperature rise per laser pulse can be several hundred degrees, and the resulting surface morphology contains pronounced ripples (e.g.. Donnelly and McHulley, 1989) and a dislocation defect structure heating effect the origin of the growth rate enhancement due to pulsed excimer lasers is generally regarded as thermal.

On the other hand the temperature rise under a cw Ar+ laser footprint is much smaller at the power densities required for enhancement, it has been reported as only 20°C to regain the full maximum growth rate from 400°C (Iga, Sugiura and Yamada, 1993). Thus cw Ar+ laser irradiation has recently been more favoured for laser assisted CBE. The low modelled temperature rise also lead to the proposal that the enhancement was due to photo-dissociation of the metalorganic molecules (Sugiura et. al. 1988). However the photon energy is not sufficient to photo-dissociate the molecules in the gas phase (Beuerman and Stuke, 1989) although it has not been established whether it is sufficient when the molecules are absorbed on a GaAs substrate, as was suggested. The origin of the enhancement has thus not been established uniquely, also little attention has been paid to the morphology of Ar+ laser assisted growth.

Ar+ laser irradiation has also been reported to cause growth rate inhibition by enhancing precursor desorption by locally raising the temperature above 550°C. This, being near the standard growth temperature, has been investigated (Iga, Sugiura and Yamada, 1993), along with changes in composition and growth rate of InGaAs at this temperature due to a local temperature rise. A laser diode was demonstrated which operated at two wavelengths due to the laser changing the thickness and InGaAs composition of part of the active region.

1.1.3 Optical Monitoring of CBE and laser modified CBE

Optical monitoring techniques are gaining widespread recognition as valuable tools for in-situ analysis of the tools for in-situ analysis of the epitaxial growth of semiconductors and other thin films. These techniques include laser interferometry (also known as dynamic optical reflectometry - DOR) (Farrell, Armstrong and Kightley, 1991), laser light scattering (LLS) (Smith et. al., 1991), ellipsometry (Aspnes, Quinn and Gregory, 1990), and reflectance anisotropy (Kamiya et. al., 1992). One reason for the increasing use of such tools is that they are non-UHV environments.

Although reflection high energy electron diffraction (RHEED) remains the most widely used monitoring tool in CBE, optical monitoring techniques are valuable in CBE. Laser interferometry and LLS are particularly suited to CBE growth since they can be used under normal growth conditions with substrate rotation. Both are also suited to laser modified CBE since they utilise either the laser itself as a probe, or a co-aligned laser as the probe. Using the laser to self monitor the growth is a simple method of monitoring the growth exactly in the laser irradiated area.

Laser interferometry is achieved by growing a layer of differing refractive index, which can be correlated to the composition of ternary alloys. Armstrong et. al. (1992) demonstrated that by co-aligning a visible laser with a focused excimer laser the growth rate of excimer laser assisted CBE could be measured.

LLS is a technique used to monitor surface topography, monitoring is achieved by placing a telescope and detector at an angle to the specular reflected beam and detecting light scattered by both reflection and refraction from surface and underlying features. These features can be treated as a sinusoidal diffraction grating or a distribution of

diffraction centres depending on their profile (Church, Jenkinson and Zavada, 1979). These treatments show the intensity of scattered light to be proportional to the square of the height of the roughness. LLS is simple to apply to CBE and laser assisted CBE since it only requires a laser beam incident on the substrate and a detector, and is reasonably tolerant to substrate rotation

1.2 Aims of this research work

The initial aim of this research work was to investigate the use of an argon ion laser to locally modify the growth of GaAs on GaAs by chemical beam epitaxy.

The objectives were identified as follows:

(i) To identify the dominant mechanism responsible for laser modified CBE.

(ii) To identify and develop techniques for in-situ monitoring, particularly laser interferometry, laser light scattering and post growth characterisation for laser modified CBE.

(iii) To be able to model the effects of laser irradiation on the growth rate of GaAs from knowledge of (i), the responsible mechanism.

(iv) To determine the effect of laser modified growth on the surface and structural morphology, and on unintentional dopant incorporation.

(v) To determine the feasibility of selective area laser modified growth and to give information on the growth conditions most suited to obtain selective area growth. Also to investigate methods of obtaining patterns.

As the research progressed it was found that the surface morphology of laser modified growth was influenced by the substrate cleaning and growth of underlying unmodified layers. There was also considerable interest in using the argon ion laser as a probe for LLS measurements. This a further objective (vi) was set to use LLS to investigate changes in the surface morphology during the substrate cleaning and subsequent growth of GaAs, AlGaAs and InGaAs.

1.3 Summary of this research work.

All structures were grown by CBE in a Vacuum Generators V8OH system configured for all vapour sources. Arsine, thermally cracked to As_2 in an injector source, was used as the group V source and triethylgallium (TEG), trimethylamine-alane (TMAA) and trimethylindium (TMI) were used as the group III precursors. epi-ready (001) GaAs substrates were used, thermally cleaned in-situ under a As_2 flux, for the growth of GaAs, AlGaAs and InGaAs.

A cw 514.5nm Ar+ laser was directed by mirrors and focused by a 0.5m focal length concave mirror, to the substrate at near normal incidence. This resulted in an elliptical laser spot on the surface of major and minor axis of approximately 2mm and 0.2mm respectively. From 0.25 - 2.5W of laser power was used to modify the growth and ~10mW when the laser was used as a probe.

The growth rate of layers grown was measured using laser reflectometry, by timing interference intensity oscillations in the specular reflected beam during the growth of layers of differing refractive index. LLS was employed to monitor the development of surface morphology by measuring the intensity of light scattered at 23° from the specular reflected beam using a telescope and photo-multiplier tube, this resulted in maximum

sensitivity to periodic roughness of ~1.2 microns. Characterisation techniques were used to evaluate the growth and assist interpretation, these were: secondary ion mass spectroscopy (SIMS) for compositional analysis, and Nomarski optical interference microscopy (NOM) and atomic force microscopy (AFM) for surface morphological analysis.

The results in terms of the objectives were:

(i) The dominant mechanism of Ar+ laser modified CBE was found to be thermal. Growth rate variation as a function of laser beam chopping frequency was found to be consistent with a thermal model. Also the growth rate alteration was consistent with a local temperature rise at most temperatures. The fitted temperature rise was around 30% above that expected from a heat conduction equation assuming infinite substrate dimensions. This difference may have been due to the finite substrate dimensions. Unintentional carbon incorporation was also consistent with the thermal model. However at substrate temperatures below approximately 360°C there is some deviation in growth rate from a fit to growth rate with temperature which indicates the presence of a non-thermal contribution.

(ii) Laser reflectometry (also known as laser interferometry) was found to be a valuable tool for measuring the growth rate of laser assisted GaAs. However due to the changes in refractive index with temperature and the small variation in growth rate with temperature above 500°C laser reflectometry was less successful for monitoring the growth rate in this region. Laser light scattering could also be used to monitor the changes in surface morphology.

(iii) Above 360°C the growth rate and unintentional dopant incorporation can be modelled assuming a purely thermal mechanism, using a thermal conduction equation but allowing for the finite substrate dimensions.

(iv) Laser irradiation was found to result in plastic deformation, by the movement of dislocations, above ~500°C and ~0.5W laser power. However the residual strain from this irradiation is only around 0.05% and the number of threading dislocations was not increased. Plastic deformation was accompanied by a surface 'cross-hatch' pattern. Below this temperature plastic deformation was not observed but above 360°C a ripple pattern, 6nm high and 180nm period was observed after laser modified growth using above 1W laser power. Elastic deformation followed by lateral growth rate variations are suggested as the origin of this ripple pattern.

(v) Laser modified selective area growth was demonstrated. The largest selectivity was achieved at 313·°C and high laser powers (above 1W) with a large (5:1) group V:III ratio, At this substrate temperature and group V:III ratio at step increase in growth rate with laser power was identified around 0.75W. Above 0.75W a well defined laser enhanced region was observed by Nomarski, and selectivity in excess of 10 times was measured. Diffractive optic gratings were used to produce arrays of laser assisted hillocks on substrates, but patterning was found limited by the 0.3m distance between the substrate and viewport, and system vibration, and little progress was made.

(vi) LLS, using AFM to aid interpretation, was used to investigate surface morphology development during substrate clearing, and subsequent growth of GaAs AlGaAs and InGaAs.

During thermal substrate cleaning changes in scattered light intensity are usually attributed to oxide desorption (e.g.. Smith et. al., 1991). However it was found that a wide range

of behaviour was possible depending on the growth history of the chamber. It is suggested that this was due to desorption of previously deposited species from the cryopanel as a result of radiant heating from the substrate. Procedures to minimise this contamination were developed.

GaAs growth typically did not result in large changes in the mean (orientation averaged) intensity of scattered light independent of whether the surface was initially rough or smooth. This showed that epitaxy did not dramatically alter the height of the surface roughness at around the 1μm scale. However, variation with substrate orientation was often observed showing islands already present elongating and become elliptical.

Growth of AlGaAs resulted in interference oscillations comparable in wavelengths to those observed in specular laser interferometry.

The development of a 'cross-hatch' pattern of surface ridges during the growth of pseudomorphic InGaAs on GaAs was monitored by LLS. This development, associated with dislocations, was found to be related to the critical thickness of layer.

The development of 3-D islands during deposition of InAs on GaAs was shown to be identifiable by LLS.

1.4 Synopsis

This thesis is divided into seven chapters:

Chapter 1 introduces the research work and places it in perspective with semiconductor growth.

Chapter 2 describes epitaxial growth modes and kinetics, along with epitaxial growth techniques. In particular it details the reaction mechanisms in conventional CBE, along with strain relaxation during pseudomorphic InGaAs on GaAs heteroepitaxy.

Chapter 3 describes the use of lasers and other light sources to modify and monitor epitaxial growth. The first part describes the area of lasers to modify growth, often referred to laser writing, and the possible mechanisms are discussed. The second part describes some of the theories used to interpret laser reflectometry and LLS.

Chapter 4 describes the CBE system and optical system used during the research work. It also describes the various post growth characterisation techniques used.

Chapter 5 describes and discusses the results of experiments using LLS, along with post-growth characterisation to aid interpretation. Results during the pre-growth annealing are presented along with details to improve the cleaning process. The surface topographical development during GaAs, AlGaAs, InGaAs and InAs epitaxy are discussed.

Chapter 6 describes the results of experiments on laser modified CBE. These include studies on laser assisted and inhibited growth of GaAs. Growth rate, surface morphology and carbon incorporation results are presented and discussed in terms of dominant mechanisms.

Chapter 7 details the conclusions of this research work along with suggestion for further work.

CHAPTER TWO
EPITAXIAL GROWTH AND MORPHOLOGY OF SEMICONDUCTORS

2.1 Introduction to GaAs and related III-V semiconductors

2.2 Epitaxial growth techniques

2.2.1 Molecular Beam Epitaxy

2.2.2 Metal-organic Vapour Phase Epitaxy

2.2.3 Chemical Beam Epitaxy and related techniques

2.3 Surface preparation for epitaxial growth

2.4 Chemical Beam Epitaxial growth of GaAs

2.5 Epitaxial growth of low compressively strained thin films: $In_XGa_{1-X}As$ on GaAs (X < 0.25)

2.6 Epitaxial growth of high compressively strained thin films: InAs on GaAs

2.1 Introduction to GaAs and related III-V semiconductors

The GaAs based AlGaAs and InGaAs material systems are potentially useful for high-speed digital, high-frequency, and electro-optic device applications. This potential is due to higher electron mobility and drift velocity than Si enabling higher frequency operation, the production of semi-insulating substrates enabling electronic isolation of devices, optical transparency in the near IR and high efficiency direct radiative recombination, and the growth of multilayer structures of differing compositions.

The growth of heterostructures is a fundamental part of III-V semiconductor application. Many III-V compounds, and in particular GaAs, AlAs, InAs and InP form crystals with the same structure, the zinc-blende arrangement. The structure is based on the cubic space group $F\bar{4}3m$, where atoms are tetrahedrally bound, with four III-V molecules in a unit cell. Because of the same structure and the small lattice constant difference between GaAs and AlAs (0.5653nm for GaAs and 0.5661nm for AlAs) their ternary alloys are the easiest to grow epitaxially since the effect of lattice strain is almost negligible. This has led to the growth of relatively defect free layers of differing band gap and refractive index. Since InAs has a lattice constant 7.2% greater than GaAs growth of InGaAs on GaAs is accompanied by strain, and its relaxation during epitaxial growth has been the subject of detailed study (see sections 2.10 and 2.11). One monolayer of AlGaAs and InGaAs (when unstrained) is half a unit cell, for unstrained GaAs this is 0.2826nm. Material parameters for AlGaAs are given in Adachi (1985), optical parameters in Aspnes et al. (1986) and a review of semiconductor and other properties of GaAs in Blakemore (1982), and Brodsky (1990).

2.2 Epitaxial growth techniques

A variety of epitaxial growth techniques have been used for the growth of III-V semiconductors. Early techniques were liquid phase epitaxy (Nelson 1963) and vapour phase epitaxy (Effer, 1963). Because of the need for more accurate control of composition and thickness and a wider range in materials composition and doping the relatively advanced techniques of MBE and MOCVD were developed in the late sixties and CBE (and related techniques) in the early eighties.

2.2.1 Molecular Beam Epitaxy

MBE is conceptually a refined form of vacuum evaporation in which atomic and molecular beams, evaporated from thermal effusion sources, impinge on a heated substrate under ultra high vacuum (UHV). However, since its evolution from a technique for surface kinetic studies of Ga and As_2 beams with GaAs (Arthur, 1968) or silane with Si (Joyce and Bradley, 1966) to the growth of thin films for devices (Cho, 1971), it has become a complex and expensive technique requiring stainless steel chambers, complex pressure pumping and load locks. Readers are referred to reviews by Foxon and Joyce (1981) and Parker (1985) for fuller descriptions. MBE suffers from low growth rates with respect to other techniques and substantial down time, although this is now much reduced with larger source material cell design.

The UHV conditions of MBE growth enable the use of in-situ analytical techniques such as reflection high energy electron diffraction (RHEED) and mass spectrometry. RHEED is of particular use in MBE since it yields information on the surface reconstructions (Joyce et al. 1984) and growth rate. During 2D growth oscillations in the intensity of the diffracted beams occur every monolayer. Step edges on the surface act as scattering

centres. The intensity of the specular reflected beam and those caused by diffraction from the periodic surface reconstructions, which also act as scattering centres varies due to the oscillatory density of the step edges on the surface. The growth rate of epilayers is measured by RHEED thus by monitoring the intensity of either a diffracted beam or more commonly the specular reflected beam. A fuller description is given in Neave et al. (1984).

2.2.2 Metal-organic Vapour Phase Epitaxy

Metal organic vapour phase epitaxy (MOVPE) is a low (typically 0.1 - 1 atmosphere) pressure technique. Metalorganic and hydride precursors are injected into a cold wall reactor, usually a quartz tube, and growth results from thermal decomposition of the molecules on a heated substrate parallel to the flow in the reactor as they pass over it. The growth is controlled by the gas flow into the chamber. Readers are referred to Stringfellow (1991) for a more detailed review.

2.2.3 Chemical Beam Epitaxy and related techniques

Chemical Beam epitaxy and related techniques were essentially developed as hybrids of both MBE and MOVPE, using the precursors of MOVPE in an MBE system, but have advanced as stand alone techniques with their own modified systems, pumping, and precursors. The techniques are commonly recognised in the literature as:

1. CBE - if the sources are vapour (metalorganic) for group III and vapour (hydrides or metalorganic) for group V.
2. Metalorganic MBE (MOMBE) - if the sources are vapour (metalorganic) for group III and solid (effusion cells) for group V.

3. Gas source MBE (GSMBE) - if the sources are solid for group III and vapour (hydride or metalorganic) for group V.

However since the hydride group V sources are often thermally cracked to the same elemental beams in the injector cell the difference between GSMBE and MBE, and between MOMBE and CBE often only result in flux controllability due to source temperature control for MBE and MOMBE, and pressure control for GSMBE and CBE. Also systems use different sources for group III and doping across CBE and MOMBE (including solid sources), and some GSMBE and MBE systems now employ gaseous sources making the categories pretty vague, indeed many authors accept the acronym of MOMBE across CBE, MOMBE and GSMBE.

Panish (1980) investigated the use of cracked phosphine and arsine in the epitaxial growth with solid group III sources, followed by the additional use of metalorganic group III sources by Veuhoff et al. (1981). CBE, as an acronym, was invented by Tsang (1984) and device quality GaAs, InGaAs and InP demonstrated. CBE has produced very high quality GaAs (Tsang, 1990), although background doping levels, particularly of carbon, are higher than for MBE.

2.3 Surface preparation for epitaxial growth

Substrate preparation is necessary prior to epitaxial growth by MBE and related techniques, such as CBE, to remove the oxide layer, and ideally produce an atomically smooth and contaminant free semiconductor surface. In practice a step - terraced surface with an even terrace spacing is preferred for abrupt interfaces, which are required for device fabrication. The terraces should ideally be in the same direction and of the greatest width without nucleating islands during growth. Impurities on the surface provide

nucleation sites for defects such as stacking faults, and may effect the electrical characteristics of the interface.

Semiconductors such as silicon and gallium arsenide form native oxide layers under ambient conditions, which are not easily removed thermally or chemically in growth systems to reveal atomically smooth or evenly step - terraced surfaces. *Ex-situ* etching and re-oxidation are often performed to produce a smooth native oxide layer on a defect free substrate, which can be thermally or chemically removed *in-situ* after loading into the vacuum growth system.

In silicon MBE the native oxide can be thermally removed *in-vacuo* by the reaction

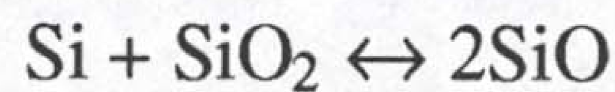

$$Si + SiO_2 \leftrightarrow 2SiO$$

producing the volatile SiO. Using transient mass spectrometry and Laser Light Scattering (LLS), during thermal oxide removal at 850°C, Robbins *et al* (1987) found that the excess Si required for the reaction was supplied by the substrate and once holes had formed through the oxide these holes supplied Si for the reaction by diffusion of Si to the edge of the holes where the reaction predominantly occurred. This resulted in pits in the substrate surface after the oxide had been removed, a small proportion of which were believed to cause the nucleation of defects such as stacking faults and micro-twins. The use of a reactive Si - beam to etch the oxide layer also resulted in these pits, since the reactive Si - beam whilst supplying Si for the reduction of SiO_2 revealed holes in the oxide layer which then acted as an additional source of Si. The evolution of the pits was observed as a rise using LLS and occurred after much of the oxide had desorbed. On continued heating, without the reactive Si-beam, they found the scattered light intensity rose further due to thermally induced roughening of the bare silicon surface.

GaAs under ambient conditions forms a conformal native oxide layer predominantly of Ga_2O_3 (Vasquez, Lewis and Grunthaner, 1983). In III -V MBE and related techniques

epi-ready (requiring no *ex-situ* preparation prior to substrate loading after supply from the manufacturer) nominally (001) GaAs substrates are routinely annealed at ~600°C in the vacuum growth chamber to remove the native oxide layer. This is performed under an As_2 or As_4 flux to maintain an As stable surface and avoid As loss from the surface after the oxide has been removed. Removal is often determined by the appearance of a 2 x 4 arsenic stable surface reconstruction observed by RHEED (Rolleau and Park, 1992). It has also been followed by monitoring the MBMS desorption peak for Ga_2O (atomic mass unit/ charge 156), the predominant oxide observed desorbing and by an LLS intensity rise (Celli *et al.* 1993).

The desorption of predominantly Ga_2O suggests the most likely reaction between the GaAs and the oxide to be:

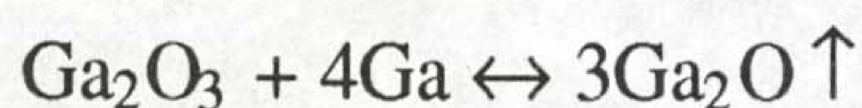

$$Ga_2O_3 + 4Ga \leftrightarrow 3Ga_2O\uparrow$$

proposed by Smith *et al.* (1993). They observed a sharp order of magnitude LLS intensity rise during annealing in an MBE chamber and attributed the rise to the development of pits supplying Ga to reaction sites at the edges of holes through the Ga_2O_3. The pits, observed by AFM, were much deeper (~6nm and up to 25nm) than the oxide layer thickness (~1.5nm) suggesting that they were not present before desorption of the oxide, and were formed during the oxide removal process. The LLS intensity rise during thermal cleaning in an MBE chamber occurred over a temperature interval smaller than 0.4°C but at a temperature dependent on the oxide layer thickness and substrate temperature heating rate (Lavoie *et al.* 1992) rendering it dangerous as a substrate calibration point. This suggests that previous to the holes developing a much slower and temperature dependant process occurs, perhaps of Ga diffusing through the oxide layer to react on the surface, but once holes have formed in the oxide layer the oxide is rapidly removed due to surface diffusion of Ga to react at the edge of the holes. Smith *et al.* (1993) reported that the pit density was much lower, and the pits smaller in size, when the oxide was desorbed from a deliberately re-oxidised epilayer, demonstrating that the

desorption process is not intrinsically inhomogeneous. This suggests that diffusion through the oxide layer occurs. They also proposed that the pits formed at 'defects' which weaken the oxide or expose bare GaAs, although there has been no observations of these. Whitaker et al. (1996) recently showed that the native oxide layer could be removed with tris(dimethylamino)arsenic (TDMAAs) at a reduced substrate temperature of ~400°C by the etching of the oxide by the thermally decomposed TDMAAs to reveal a superior topography in contrast with substrates prepared using conventional thermal cleaning.

2.4 Chemical Beam Epitaxial growth of GaAs

The growth rate of GaAs by CBE, using TEG and arsine cracked to As_2 in an injector cell, increases with substrate temperature up to around 490°C. Above this temperature it is observed to decrease. The growth rate has been measured by a number of techniques including laser interferometry (Armstrong et al. 1992), RHEED (Martin et al. 1992) and post growth cleaved edge TEM (Joyce et al. 1992). Figure 1.1 shows the results of Joyce et al. (1992), showing the temperature dependence to be affected by the group III flux. The reaction kinetics are more complicated in CBE than MBE, which is based mainly on surface atom migration. The cracking pattern for TEG was determined by Modulated Beam Mass Spectrometry (MBMS) by Martin and Whitehouse, (1990). Five regions of growth were identified as: 0/ no growth below 350°C, TEG decomposes to DEG but the DEG desorbs. 1/ onset of growth between 350 and 440°C due to DEG decomposition. 2/ growth rate decreasing slowly with T due to DEG desorption between 440-590°C. 3/ more rapid reduction in growth rate due to DEG desorption, between 590-660°C. 4/ Above 660°C a rapid reduction in growth rate with temperature due to Ga desorption.

The growth rate was found to be predominantly dependent on the ratio of decomposition of DEG (Martin et al. 1992). Foord et al. (1990) showed that the blocking of active

reaction sites by arsenic dimers and metalorganic molecule fragments was a limiting factor at low temperature (regions 0,1). This blocking effectively controls the desorption to decomposition of DEG ratio. This was backed by temperature programmed desorption studies and is consistent with the variation of temperature dependence with V:III flux ratio. Further work by Kaneko et al. (1992) has shown that the absolute As flux, along with the V:III ratio controlled the growth.

CBE growth of high quality GaAs has been achieved (Houng, 1990) by growing at the peak growth rate temperature. However accurate control of ternary and quaternary compounds has been difficult in CBE. Temperature controllability and uniformity across substrates has only been of a few degrees. So far the precursors used for growing quaternary compounds have not had common substrate temperatures where small variations in temperature (<5°C) do not result in large (~5%) variations in growth rate. Much present research is focused at finding compatible precursors and better temperature measurement, control and uniformity and also in situ monitoring of growth.

2.5 Epitaxial growth of low compressively strained thin films: $In_XGa_{1-X}As$ on GaAs ($X < 0.25$)

The growth of intentionally strained layers has recently attracted much interest. Previously strained layer heteroepitaxy was avoided due to the possibility of defects, but due to increased understanding of the strain relief process defect free metastable strained layers with properties differing from those of the corresponding bulk material may be routinely grown if the layers are grown to tight constraints. Such structures have proven to be successful in novel microelectronic (Zipperan *et al.* 1988) and optoelectronic (Huang *et al.* 1989) devices.

$In_xGa_{1-x}As$ on GaAs heteroepitaxy occurs by the two-dimensional growth mode for $x \leq 0.25$ under standard growth conditions in CBE, MBE and MOVPE. This is due to the strain energy relieved by a corrugation from three-dimensional growth being less than the increase in surface free energy associated with the corrugation(Tsao, 1992). Relaxation of the strained $In_xGa_{1-x}As$ epilayer occurs through misfit dislocation introduction.

The introduction of misfit dislocations has been described by several models. The models give rise to a 'critical thickness' for the onset of plastic deformation. The Matthews and Blakeslee models are most widely favoured, being based on energy or force derivation. For a detailed analysis of critical thickness the reader is referred to reviews by Fitzgerald (1991) and Beanland, Kiely and Pond (1994). Dunstan et al (1991) approximated the critical thickness for the introduction of misfit dislocations, h_c, to $h_c = (0.2 \pm 0.1)/\varepsilon_0$ nm, where ε_0 is the misfit.

Under two-dimensional growth mode conditions these misfit dislocations cannot enter the epilayer through the sides of islands, so the relaxation can only occur as a result from glide of already present dislocations, or by dislocation generation. Dislocations present in semiconductor substrates are termed threading dislocations. At around the critical thickness (h_c) threading dislocations, originating from the substrate and replicated through the growing epilayer, which have 'bent over' to leave a 60° misfit dislocation segment at the $In_xGa_{1-x}As$ / GaAs epilayer interface have been observed (Barnet *et al.* 1994). It was observed that not all the threading dislocations 'bend over' at the critical thickness perhaps due to there being a number of types of threading dislocations. With high quality GaAs wafers it was also observed that some of the misfit dislocations extended to the edge of the wafer .

The density of threading dislocations arising from the substrate is typically below $10^4 cm^{-2}$ in high quality GaAs. If each threading dislocation bends over to leave a misfit

dislocation to the edge of the wafer, the maximum strain that can be relieved is only 0.05% in layers grown on 5cm GaAs wafers. Nevertheless, in layers which are sufficiently thick, strains of several percent are relieved by misfit dislocations. Dislocation generation must therefore occur in $In_xGa_{1-x}As$.

The possibility of homogeneous half loop generation from the surface was discussed by Fitzgerald (1991). The strain required to activate the sources was estimated to be ~4%, well above that produced in $In_xGa_{1-x}As$ / GaAs ($x \leq 0.25$) heteroepitaxy. Heterogeneous half loop generation due to defects arising from the substrate cleaning or during growth may play a role in relaxation. This is because the strain field of the defect may add to the existing stress. Studies of the relaxation of low misfit $In_XGa_{1-X}As$ on GaAs ($X \leq 0.25$) have shown the amount of strain relieved is reproducible (e.g. Dunstan *et al.* 1994, Drigo *et al.* 1984).This suggests that the process in not dominant in most systems.

Dislocation multiplication by the operation of a spiral source (Beanland, 1992) or Frank-Read source (Frank, 1950) are further possible mechanisms. Both rely on dislocations segments in the epilayer bowing out to form a misfit dislocation at the interface.

The onset of significant relaxation is accompanied by the development of a surface 'cross-hatch' pattern in the <110> directions (Olsen, 1975). Celii et al. (1993) suggested that the cross-hatch is due to the formation of atomic steps on the surface due to the generation of dislocations, and followed the development with LLS. However Fitzgerald (1991) suggested that the origin of the cross hatch pattern was a laterally varying strain field due to the presence of misfit dislocations, resulting in a local growth rate variation.

2.6 Epitaxial growth of high compressively strained thin films: InAs on GaAs

The 7.2% compressively mismatched heteroepitaxial growth of InAs on GaAs substrates is now recognised as a key technology in applications such as InAs - based devices on semi - insulating GaAs substrates (Kitabayashi and Waho, 1995), and has recently been used to build high - speed tunnelling devices (Brown *et al.* 1991). Also findings that the three - dimensional islands formed at the early stages of highly compressively strained layer heteroepitaxy can remain coherent has lead to the possibility of the natural formation of quantum - wire and - box structures. Quantum - boxes and - wires formed in this way have been shown to possess an inherently low density of defects as compared with those introduced during lithographic methods (Fukui et al. 1990), and laser action has been observed after insertion of such formed quantum - boxes into an active region of laser structures(Egorov et al. 1994).

The initial growth mode in lattice mismatched heteroepitaxy is not simple. Strain energy and surface free energies both play important roles in the epitaxial growth kinetics. Strain energy provides a driving force towards three - dimensional growth occurring. Quantum - boxes are obtained in structures where the three - dimensional growth mode occurs to result in distinct islands on the surface which are then overgrown with the an unstrained material. The production of quantum boxes thus requires only a few monolayers to be deposited before complete coverage, and that full isolated islands form before this thickness due to the three - dimensional growth mode. Furthermore to utilise the islands as quantum dots no misfit dislocations should be present, so the height of the islands must be below the critical thickness for dislocation introduction. In discussions of thickness the term monolayer (ML) is used as the thickness of half a unit cell of the deposited material and is an average thickness.

For lattice - mismatched heteroepitaxy of InAs on GaAs, with a compressive strain of 6.8%, Nabetani *et al.* (1995) found that InAs, grown by MBE, grew by the Stranski -

Krastinov growth mode. Using *ex-situ* photoluminescence (PL), atomic force microscopy (AFM) and transmission electron microscopy (TEM) they observed:

(a) InAs grew pseudomorphically and two-dimensionally for 1.5 ML, due to the lower surface energy of InAs as compared with GaAs.

(b) The InAs grew three - dimensionally and small (<25nm) hemispherical InAs islands nucleated at about 1.8ML, this they believed to occur suddenly and not only by newly deposited atoms but also by atoms already sited. At least 1ML was expected to cover the entire GaAs substrate to minimise surface energy. An InAs wetting layer was observed in overgrown quantum boxes by Xie et al. (1995) using cross - sectional TEM, estimated to be 1.7 ML for 2 ML of deposited InAs.

(c) Above 2.0 ML larger (>40nm) InAs islands were observed with dissimilar shapes and a density about 1/40 of that of the smaller islands but increasing with layer thickness.

(d) The size of the smaller islands was almost constant with thickness but the larger islands took various shapes as the thickness increased from 2 to 4 ML.

(e) It was suggested that after the islands had nucleated it would be favourable for only a few islands to increase in size, and these would coalesce to form the observed larger islands.

(e) Misfit dislocations were introduced in the larger islands above around 3 ML in agreement with a calculated critical thickness of InAs / GaAs by a valence - force field theory.

Le Corre *et al.* (1994) suggested a similar behaviour for the growth of InAs on InP, to that above, with a two - dimensional to three - dimensional growth mode transition of around 1.5 ML in spite of the lower lattice mismatch (3.6%). However they observed a reduction in island size on going from 1.5 ML to 2.5 ML which they explained to be due to interaction between islands being greater at 2.5 ML due to a higher density and limiting the island size. They claimed that InAs islands in InP would remove the possible problem of InAs /GaAs intermixing.

Jeppesen *et al.* (1994) showed that CBE is a potential source of growing quantum - dots of InAs on GaAs, They found the thickness of the transition from two - dimensional to three - dimensional growth is suppressed by higher As_2 and by higher substrate temperature, but was independent of the growth rate. They also showed that the islands formed at step edges and the dot assembly could be controlled using patterned substrates.

The role of the growth of the capping layer has also been studied For InAs boxes in GaAs Xie *et al.* (1995) showed with high resolution TEM that defect free islands and wetting layers could be grown without substantial InAs / GaAs mixing using low temperature migration enhanced epitaxy (LTMEE) to grow the GaAs cap layer. The InAs island induced strain field effects the adatom migration during the growth of the GaAs capping layer (Xie *et al.* 1994). Strain - driven migration away from the islands was found to result in depressions above the InAs islands. This was found to be temperature dependent and no depressions were observed in samples where the capping layer was grown at a reduced temperature of 420°C (from 480°C). Jeppesen *et al.* (1995) demonstrated that this growth inhibition around the InAs islands could be used to vertically stack InAs quantum boxes since another layer of InAs islands would nucleate in the depressions under certain conditions, adding another dimension to the periodicity of the quantum boxes.

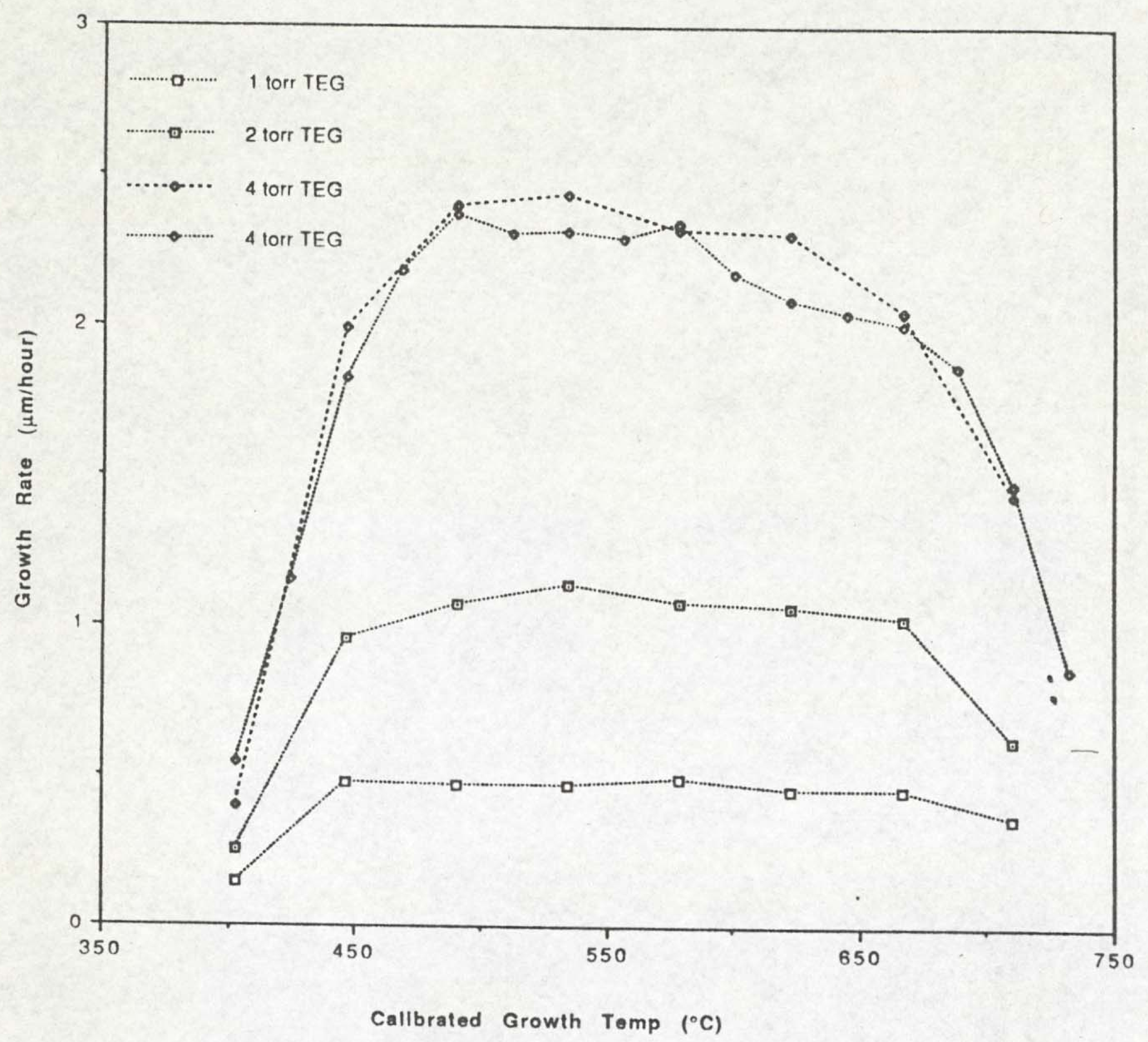

Figure 2.1: Temperature dependent growth rate of GaAs (from Joyce *et al.* 1992).

CHAPTER THREE
OPTICAL PROCESSING AND MONITORING

3.1 Optical processing of semiconductors.

3.1.1 Introduction

3.1.2 Mechanisms for direct laser writing

3.1.3 Mechanisms of laser modified CBE

3.2 Optical monitoring by laser reflectometry.

3.2.1 Reflection and transmission of light at a surface.

3.2.2 Reflection and transmission of light by a single film.

3.2.3 Application of laser reflectometry.

3.3 Optical monitoring by laser light scattering

3.3.1 Description of a surface.

3.3.2 Rough surface scattering.

3.3.3 Smooth surface scattering.

3.3.4 Point scattering.

3.3.5 Scattering of light from a single film.

3.3.6 Application of laser light scattering

Optical processing of semiconductors has been used as a method of producing selective area growth in a number of growth systems, particularly MOVPE and CBE. In section 3.1 a basis for this processing will be given and the various processes and techniques will be discussed.

Optical monitoring techniques are gaining widespread recognition as valuable tools for *in-situ* analysis of the epitaxial growth of semiconductor thin films. These techniques include laser reflectometry (also known as Dynamic optical reflectometry) (e.g. Farrell *et al.* 1991), ellipsometry (e.g. Aspnes *et al.* 1990), reflectance anisotropy (e.g. Kamiya *et al.* 1992), and laser light scattering (also known as diffuse optical reflectometry) (e.g. Smith *et al.* 1991). One reason for the increasing use of such tools is that they are non-intrusive and can be applied to non-UHV environments. In the case of CBE this is significant, since they can be used under conditions when the growth chamber pressure is too great to facilitate RHEED or mass spectrometry. Another is that they are relatively simple to apply and maintain, only requiring optical viewports.

In sections 6.2 and 6.3 a theoretical basis will be given for the two techniques used in this work, laser reflectometry and laser light scattering. These were chosen because they can give information on laser-assisted growth by monitoring the specular and diffusely reflected light intensity of the laser used to effect the growth. This provided real time information on the growth processes of the exact area of the laser footprint. Both techniques give a useful insight into the processes going on and combined will be shown to be very powerful, they are also the two techniques which are likely to be of greatest use in device fabrication.

3.1 Optical processing of semiconductors.

3.1.1 Introduction

Laser-induced surface modification processes are currently being investigated in many laboratories as an alternative to photo-, or electron beam-lithography based fabrication or to alter microstructures. The main advantages of using lasers to modify growth or microstructure is the wide variation in focal diameter, fluence and exposure time. The application is in theory simple, focusing a laser beam onto a substrate either during growth to alter deposition or after to effect changes in the microstructure. Laser annealing and alloying processes involving purely laser solid interactions will not be discussed here.

Laser modified growth has been studied for a wide range of materials. This work is based on the laser modification of GaAs grown by CBE, and only the directly relevant work will be reviewed. For a more broader review the reader is referred to Rytz-Froidevaux *et al.* (1985).

3.1.2 Mechanisms for direct laser writing

The mechanisms involved during direct laser writing have been the subject of study since laser writing was first attempted as early as the 1930s (e.g. Laidler (1942). Depending on the material, growth system and laser wavelength and power a number of different origins to the deposition were found. The deposition can be based on photolytic, pyrolytic (photothermal) or photoelectrochemical (photocatalytic) reactions.

(a) Photolytic reactions.

The photo-dissociation of molecules consists of the excitation of one of the molecular bonds by absorption of one or more photons. Such photo-dissociation involves transition between vibrational and/or electronic states. The process can occur by a combination of both. Vibration state excitation can be achieved by a number of transitions each by one or more photon, whereas electronic excitation may only involve one photon either dissociating the molecule or breaking one bond. The quantum yield of the process, the ratio of transitions to photons necessary to induce the transition, of the vibrational excitation is typically very low, but the photon energy may be as low as that corresponding to a wavelength in the infrared. Electronic transitions typically have much greater yields but require photons of energy to dissociate the molecule or bond, typically corresponding to radiation in the ultraviolet, around 200-300nm in wavelength. The deposition rate will be proportional to the laser power / radius for gas phase photo-dissociation and to laser power density (at one wavelength) (power/ radius squared) at the surface for molecules physisorbed to a surface, since the quantum efficiency will be constant and the number of photons passing near the molecules will vary as such. Photolytic processes are also very wavelength dependent.

Photolytic growth is often accompanied by the development of a surface ripple pattern of lateral period near that of the laser (e.g. Brueck and Ehrlich, 1982). This pattern is believed to be the result of a stimulated surface wave. Surface roughness induced light scattering from the incident wave initiates the development of a periodic variation in photo-dissociation due to lateral modulation of the optical intensity as a result of interference between the scattered and incident fields. Once initiated, the periodic ripple will add to the scattering and reinforce the local growth rate variation.

(b) Photoelectrochemical reactions (photocatalytic).

Photoelectrochemical reactions involve photons absorbed within the semiconductor bulk by the production of a conduction electron - hole pair. Thus it requires photons of above band gap energy. These photo-generated electron - hole pairs can modify growth one of two ways. They can non-radiatively recombine near or at the surface and pass energy to the adsorbed molecule. Alternatively an electron or hole can move to the molecule altering its charge and chemistry. Photocatalytic reactions are expected to be dependent on the power density.

(c) Pyrolytic reactions.

Photothermal effects require absorption of above band gap energy photons creating electron - hole pairs, followed by non-radiative recombination resulting in a local temperature rise. This temperature rise results in the molecules being pyrolised at the surface identically to raising the substrate temperature by any other means. This temperature rise is estimated by assuming that all heat is lost by conduction through the semiconductor, and thus that the substrate dimensions are semi-infinite. By making such assumptions it is possible to estimate the temperature rise by solving a time independent heat flow equation. The temperature rise ΔT from irradiation of constant power density over a radius r_c is given by Carslaw and Jaeger (1959) as:

$$\Delta T = \frac{W_I(1-R)}{4k_s r_c} \qquad \text{Equation 3.1}$$

where W_I is the incident power, R is the reflectivity and k_s is the thermal conductivity. A similar result for laser irradiation of gaussian profile is given by Lax (1977). This local temperature rise will result in compressive strain in the laser area due to the thermal expansion. Hussein et al. (1990) stated that there was a critical temperature rise above which plastic deformation would occur, this was only ~50°C at a temperature of 500°C.

3.1.3 Mechanisms of laser modified CBE

Ar+ laser assisted growth rate enhancement has been reported for CBE grown GaAs (e.g. Sugiura et al. 1988) at substrate temperatures below 400°C, using TEG and arsine cracked to As_2 in an injector cell. However, the dominant process responsible for laser Assisted CBE has not been uniquely identified since a number of processes may simultaneously be occurring. The laser radiation is above the band gap and thus is absorbed, resulting in a temperature rise due to non-radiative recombination. Thus also there is the possibility of photoelectrochemical assistance due to the carriers charging the adatoms or recombining at the surface and passing energy to the adatoms.

The photon energy is not sufficient to efficiently photo-dissociate the molecules in the gas phase. The adsorption of TEG in the gas phase falls rapidly to nearly zero above wavelengths of 220nm (Fischer *et al.* 1988). However photolysis was suggested as the dominant mechanism for laser assisted CBE, due to growth rate enhancements above that expected from the calculated and measured temperature rise (Sugiura et al. 1988). This was justified by experiments to photo-dissociate TEG on cold Quartz tubes, although this only demonstrated the possibility. Further evidence was given as a lack of growth rate dependence on chopped beam frequency, and deposition on transparent substrates. Studies by other workers have shown results consistent with a photothermal origin to most of the enhancement (e.g. Dong et al. 1992). Little attention has been paid to the morphology of laser assisted growth however, and most of the studies have moved on to the use of different group III and group V precursors (e.g. Dong *et al.* 1994). CBE also offers the prospect of growth rate reduction from the temperature of maximum efficiency. A temperature rise would result in a growth rate reduction due to desorption of adatoms or elemental material. This was demonstrated by Iga et al. (1992) along with compositional modification during the growth of InGaAs alloys. Both were attributed to photothermal effects. The status of laser assisted CBE has been reviewed by Tu *et al.* (1995) and Iga *et al.* (1993).

3.2 Laser reflectometry.

3.2.1 Reflection and transmission of light at a surface.

Application of the Maxwell equations to a boundary lead to the well known Fresnel reflection and transmission coefficients (Heavens, 1955).

3.2.2 Reflection and transmission of light by a single film.

The Fresnel coefficients may be applied to the determination of the reflection and transmission coefficient of a single thin film by the well known method of summation (Heavens, 1955). This will be shown here for a single non-adsorbing film, bounded on either side by semi-infinite non-adsorbing layers. The results give interpretation of laser reflectometry of single layers.

Suppose that a parallel beam of light of unit amplitude and of wavelength λ falls on a plane, parallel sided, homogeneous and isotropic film of thickness d and refractive index n_1, supported on a substrate of refractive index n_2, from a medium of refractive index n_0 at an angle of incidence ϑ_0 (figure 3.1).

We may write the amplitudes of successively reflected and transmitted beams in terms of the Fresnel coefficients, as shown in figure 3.1. These are denoted as r_n and t_n for reflection and transmission at the n_{n-1} to n_n boundary and as r_n' and t_n' for propagation from n_n to n_{n-1}. Since it can be seen that $r_n' = - r_n$, r_n' will be written as $-r_n$.

Also δ_1 is the change in phase of the wave as it transverses the film, where:

$$\delta_1 = \frac{2\pi}{\lambda} \cdot n_1 d_1 \cos\theta_1 \qquad \text{equation (3.2)}$$

The reflected amplitude for the thin film can be obtain by summing the individual beams in the n_0 direction:

$$R = r_1 + t_1 t_1' r_2 e^{-2i\delta_1} - t_1 t_1' r_1 r_2^2 e^{-4i\delta_1} + \ldots\ldots$$

$$\Rightarrow R = r_1 + \frac{t_1 t_1' r_2 e^{-2i\delta_1}}{1 + r_1 r_2 e^{-2i\delta_1}} \qquad \text{equation (3.3)}$$

This may be further simplified by writing the Fresnel transmission coefficients in terms of r_1, r_2. From conservation of energy we have:

$$t_1 t_1' = 1 - r_1^2 \qquad \text{equation (3.4)}$$

So that equation (3.3) becomes:

$$R = \frac{r_1 + r_2 e^{-2i\delta_1}}{1 + r_1 r_2 e^{-2i\delta_1}} \qquad \text{equation (3.5)}$$

The transmitted amplitude is given by:

$$T = t_1 t_2 e^{-i\delta_1} - t_1 t_2 r_1 r_2 e^{-3i\delta_1} + t_1 t_2 r_1^2 r_2^2 e^{-5i\delta_1} - \ldots.$$

$$\Rightarrow T = \frac{t_1 t_2 e^{-i\delta_1}}{1 + r_1 r_2 e^{-2i\delta_1}} \qquad \text{equation (3.6)}$$

Equations (3.5) and (3.6) are generally valid. For non-normal incidence each takes on two forms, depending on the state of polarisation of the incident beam. If any of the media are adsorbing the values of n are replaced with the complex values of refractive index.

The values have so far been expressed in terms of amplitude. In terms of energies equations (3.5) and (3.6) become:

$$n_0RR^* = \frac{n_0\left(r_1^2 + 2r_1r_2\cos 2\delta_1 + r_2^2\right)}{\left(1 + 2r_1r_2\cos 2\delta_1 + r_1^2r_2^2\right)} \qquad \text{equation (3.7)}$$

$$n_2TT^* = \frac{n_2t_1^2t_2^2}{\left(1 + 2r_1r_2\cos 2\delta_1 + r_1^2r_2^2\right)} \qquad \text{equation (3.8)}$$

Equations (3.7) and (3.8) are valid for a wave of unit amplitude, in terms of unit energy they must be divided by n_0, thus:

$$\mathbf{R} = \frac{\left(r_1^2 + 2r_1r_2\cos 2\delta_1 + r_2^2\right)}{\left(1 + 2r_1r_2\cos 2\delta_1 + r_1^2r_2^2\right)} \qquad \text{equation (3.9)}$$

$$\mathbf{T} = \frac{n_2}{n_0} \cdot \frac{t_1^2t_2^2}{\left(1 + 2r_1r_2\cos 2\delta_1 + r_1^2r_2^2\right)} \qquad \text{equation (3.10)}$$

In terms of Fresnel coefficients at normal incidence the reflectance and transmittance are given by:

$$\mathbf{R} = \frac{-4n_0n_1^2n_2 + \left(n_0^2 + n_1^2\right)\left(n_1^2 + n_2^2\right) + \left(n_0^2 + n_1^2\right)\left(n_1^2 + n_2^2\right)\cos 2\delta_1}{4n_0n_1^2n_2 + \left(n_0^2 + n_1^2\right)\left(n_1^2 + n_2^2\right) + \left(n_0^2 + n_1^2\right)\left(n_1^2 + n_2^2\right)\cos 2\delta_1} \qquad \text{equation (3.11)}$$

$$\mathbf{T} = \frac{8n_0n_1^2n_2}{4n_0n_1^2n_2 + \left(n_0^2 + n_1^2\right)\left(n_1^2 + n_2^2\right) + \left(n_0^2 + n_1^2\right)\left(n_1^2 + n_2^2\right)\cos 2\delta_1} \qquad \text{equation (3.12)}$$

3.2.3 Application of laser reflectometry.

Laser reflectometry involves monitoring the intensity of reflected light during the growth of a thin film on a substrate. As the thickness d changes with time the intensity will oscillate as shown in equation (3.12). Turning points will occur at thicknesses $d = M\pi / \delta_1$ and $d = (2M + 1)\pi / 2\delta_1$, where M is an integer and, at normal incidence, $\delta_1 = 2\pi N/\lambda$, where N is the refractive index of the growing layer. From the oscillation period τ the growth rate is determined as $\lambda / 2n\tau$ where n is the real part of the refractive index of the growing layer. The refractive index can be calculated from measurement of the oscillation amplitude or the mean reflectivity (Armstrong *et al.* 1992). Laser reflectometry or laser interferometry, as the application to growth of multilayer structures, has been used to monitor the growth rate in a number of material and growth systems. For example the growth of GaAs and AlGaAs by CBE (Armstrong *et al.* 1992), carbon doped GaAs and AlAs (Joyce *et al.* 1995), and MOCVD growth of HgCdTe / ZnTe / CdTe on GaAs (Irvine *et al.* 1992). It has also been applied to the monitoring of Excimer laser assisted GaAs on AlGaAs (Farrell *et al.* 1992).

3.3 Laser light scattering

Whereas laser reflectometry is primarily dependant on the bulk properties of a thin film, laser light scattering is primarily sensitive to the surface morphology. In the previous sections it was assumed that the surface was infinite and accommodated the infinitely wide plane of unique frequency supposed to be upon it. If the surface is not infinite then light will be reflected and refracted at angles other than those discussed. In terms of laser reflectometry this limitation is not of great importance, because for the surfaces investigated the intensity removal from the specular cone is small.

For laser light scattering it is the radiation away from the specular beam which is detected, and it is the morphology of the surface which is of primary interest.

3.3.1 Description of a surface.

The most widely used description of surface roughness is the rms. height of the roughness. The rms. height of roughness is usually determined by some means of stylus profilometry. These techniques range from simple profilers such as Dektak through AFM to STM in terms of lateral range, lateral resolution and tip radius. A surface may yield different values of roughness by the differing techniques, since it may have a differing roughness on differing scales. An example of this is semiconductor surfaces which may appear to have a smooth stepped surface under a 100nm x 100nm STM scan but to have an island morphology on a 10μm x 100μm AFM scan with several nm of roughness but appear smooth to a 10mm scan stylus profilometer. A similar phenomenon is found with in-situ monitoring. Pickering (1991) used laser light scattering and ellipsometry simultaneously and shown that ellipsometry is sensitive to morphology with a lateral period below the wavelength of light used whereas laser light scattering is most sensitive to morphology of lateral period above that of the wavelength of light used. It was shown that both have a sub-nanometre height sensitivity, but can show contrasting results.

The most fundamental quantity describing the scattering of radiation in reflectance from a surface is the bi-directional reflectance distribution function, or BRDF (Church *et al.* 1977). The BDRF is a function of the angles of incidence and scattering as shown below:

$$BDRF = f(\theta_i, \varphi_i; \theta_s \varphi_s) \qquad \text{equation (3.13)}$$

where subscripts i and s represent the incident and scattered waves respectively and the angles are defined in figure 3.2. It is also a function of the wavelength and polarisation of the incident and scattered waves. To obtain the morphology of the surface using scattered light the BDRF must first be obtained for the range $0 \leq \theta \leq \pi / 2$ where either ϑ_i, φ_i or

ϑ_s, φ_s could be altered, laser light scattering only samples a small range, due to its fixed geometry and will not give complete understanding of the morphology, although with post growth characterisation such as angle resolved light scattering (Pidduck, 1989) or atomic force microscopy (Smith *et al.* 1991) the results may be correlated to surface features.

3.3.2 Rough surface scattering.

Observations of reflected sunlight from rippled water, roads and similar surfaces lead workers (e.g. Schooley, 1962) to postulate a facet theory for ground radar return. The majority of light observed from a rippled water surface is from facets angled such that they reflect the incident light toward the observer, where the angle of reflectance equals the angle of incidence to the facet which is inclined to the surface normal.

In the case of laser light scattering a parallel beam impinges on the surface and the light is detected at a defined angle to the surface. If the surface is represented as small flat plane facets, it can be seen that light will only be detected from facets with their normal half-way between the incident beam direction and the detection direction. The intensity of light detected is thus proportional to the area of facet with this normal. It follows that by varying the detection or incident beam geometry the slope distribution of the surface (facets) can be obtained, however the scale could not. This geometric optic approach assumes zero wavelength and the results should be wavelength independent. This is clearly not in accordance with the results discussed (e.g. Pidduck *et al.* 1989) but would be reasonable for large roughness with lateral periods $>>\lambda$ where these effects dominate.

Two modifications were made to this basic model to consider the actual reradiation pattern of finite sized facets at finite wavelengths, and on establishing the effective number of facets from the wavelength. Schooley (1962) produced a theoretical model

predicting the effective scattering area of a facet from its size and the wavelength of radiation used. He also showed that facets will reradiate over a finite angle depending on their size relative to the probing radiation wavelength, and established an angular beam width at half power relationship.

3.3.3 Smooth surface scattering.

Most surfaces of interest to this thesis come within the regime labelled smooth surface scattering, where the facet slopes are generally much below that which would give significant scattering by the rough surface model.

In the limit where the vertical height of the surface roughness is much less than the wavelength of the radiation - the smooth surface limit - the scattering intensity depends only on the second order statistical properties of the surface roughness. The angular distribution of the scattered light intensity (i.e. the B.D.R.F) is then a mapping of the two - dimensional power spectral density (PSD) of the surface roughness in wavenumber space. In wavenumber space the radiation vector magnitude is given by $k = 2\pi /\lambda$ and the surface roughness vector magnitude is given by $K = 2\pi /d$, where d is the period of the surface roughness. The smooth surface approximation is valid for regions where $(ka)^2 < 10^{-2}$, where a is the vertical amplitude of the roughness (Church *et al.* 1979). For the Ar+ laser wavelength of 514.5nm this corresponds to roughness of vertical amplitude of around 10nm or less.

For a simple surface composed of a single one dimensional sinusoid on a perfectly reflecting surface of profile

$$Z(x) = a \sin(2\pi a /d)$$

radiation will be scattered in the form of a pair of first order diffraction lines with positions

$$\sin \theta_s = \sin \theta_i \pm \lambda/d$$

In the smooth surface limit the intensity of each of these diffraction lines is (Church *et al.* 1979):

$$\sim (ka \cos \theta_i)^2$$

Thus the intensity of scattered radiation is proportional to the vertical height of the roughness squared, and the angular position determined by the reciprocal of the wavelength of the roughness.

A real surface can be represented as a superposition of surface height variations of sinusoidal form with different transverse wavelengths. Laser light scattering with a fixed angular geometry will thus be sensitive to the Fourier component of the surface morphology corresponding to its position in the PSD.

The scattering geometry is shown schematically in figure 3.3. The incident and scattered beams, if monochromatic and coherent, will have a vector magnitude of k ($=2\pi/\lambda$) in directions as shown in figure 3.3. The scattering geometry corresponds to diffraction by the Fourier components of the surface height variation in the x - y plane of wavenumbers p - q given by projecting the incident and scattered wavenumber vectors to the x - y plane.

Projection of the incident beam to the x - y plane gives a magnitude k $\sin\theta_i$ and projection of the scattered beam k sin θ_s. The distance between the scattered and incident vectors in the p and q directions are given by

$$p = k\,((\sin\theta_s \cos\varphi_s) - \sin\theta_i)$$

$$q = k\,(\sin\theta_s \sin\varphi_s)$$

The magnitude of the vector between the scattered and incident beams is thus given by

$$K = (p^2 + q^2)^{0.5} \qquad \text{equation 3.14}$$

The scattering geometry will be most sensitive to surface roughness of period $2\pi/K$ where K is given by the above equation.

3.3.4 Point scattering.

So far a surface with a continuous roughness has been discussed, however, sometimes it is more applicable to treat a surface as perfectly smooth except for a distribution of features, such as particles, lumps, mounds, pits, scratches, troughs etc. each which can be treated as point scatterers.

For particles with radii $<<\lambda$ Barber and Hill (1990) assumed that they could be approximated to point dipoles, with an isotropic scattering cross section. For a particle of radius, a, using the Rayleigh model the scattered light intensity would be independent of angle and α a^6. Neglecting the interaction between particles the Rayleigh scattered intensity I for N particles is given by equation (3.15):

$$I \alpha \sum_{i=1}^{N} a_i^6 \qquad \text{equation (3.15)}$$

Where a_i is the radius of the ith particle. For N particles all of radius a, this becomes:

$$I \alpha N a^6 \qquad \text{equation (3.16)}$$

Mathis and Bonnot (1996) used this model to explain the growth of diamond particles on silicon substrates, and stated that the growth rate could be inferred from the slope of the scattered light intensity with time. They did acknowledge that interactions cannot be ignored. It is also fair to say that the scattering from most point scatterers will not be isotropic.

The 'shot model' (Church, *et al.* 1979) approached scattering from a distribution of defects by separating the roles of defect distribution and shape, and examining them separately.

For simplicity a one-dimensional distribution of N identical defects was considered flat on an otherwise flat surface. The surface profile can thus be written as:

$$Z(x) = \sum_{n=1}^{N} Z_0(x - x_n) \qquad \text{equation (3.17)}$$

where $Z_0(x)$ is the shape of the defect and x_n denotes the position of the nth defect. Church *et al.* (1977) showed that this leads to:

$$W_1(p) = \frac{1}{2L} \cdot \left| \sum_{1}^{N} e^{ipx_n} \right|^2 \cdot \frac{1}{2\pi} \left| \int_{-L}^{+L} e^{ipx} Z_0(x) dx \right|^2 \qquad \text{equation (3.18)}$$

This equation is split into three parts:

$$W_1(p) = \frac{1}{2L} \cdot S(p) \cdot \quad F(p) \qquad \text{equation (3.19)}$$

where 1 / 2L is the reciprocal length of the scattering surface, S(p) the structure factor and F(p) the form factor.

The structure factor is the interaction effects between the point scatterers, and is independent of their shape, shown as:

$$S(p) \equiv \left| \sum_{1}^{N} e^{ipx_n} \right|^2 \qquad \text{equation (3.20)}$$

The form factor is the scattering from a single defect and is only dependent on its shape. This is given by:

$$F(p) \equiv \frac{1}{2\pi} \left| \int_{-L}^{+L} e^{ipx} Z_0(x) dx \right|^2 \qquad \text{equation (3.21)}$$

The structure factor can be rewritten as:

$$S(p) = N + 2 \sum_{m>n}^{N} \sum_{n}^{N} \cos[(x_m - x_n)p] \qquad \text{equation (3.22)}$$

For a random distribution of defects the second term can be seen to tend to zero over the range $p >> 2\pi / L$, since it can be seen that many values of x_m-x_n will be present. Thus for a completely random distribution $s_p \rightarrow N$, as was assumed previously in equation (3.3). Thus the scattered light intensity is proportional to the number of scattering centres. For a periodic array of scattering centres the intensity of the diffracted light is

proportional to the number squared. The angle of the diffracted light will be identical to that of periodic roughness.

3.3.5 Scattering of light from a single film.

Scattering of light from a single film can be treated in as similar way to reflectance from a single film. Scattering, or diffuse reflection or transmission, may occur at either or both the n_0 - n_1 or n_1 -n_2 interfaces, where n_0 is the real part of the refractive index of the substrate, n_1 the epilayer, and n_2 the air or vacuum above the epilayer. This leads to a large number of beams to be summed.

The scattering at each interface (i.e. the surface and the film / substrate interface) will be dependent on the morphology of the interface, and also on the refractive indices of the two media. If we assume smooth surface scattering then it is the scattering at a vector in terms of wavelength and refractive index that is dependent on the morphology, and the scattering angle for a lateral period of roughness will be dependent on the value of n in the media where the scattered wave propagates, in the same way as the specular beam vector changes on passing into n_1 from n_0. This means the PSD with angle for an interface will be independent of the fact that the interface is below a thin film. Also the scattering intensity in reflectance and transmission are relative to the intensity of specular reflected and transmitted beams. This is because the scattering is from the transmitted and reflected beams, and also unit amplitude scattering must be divided by the respective refractive index to obtain the intensity related scattering, as is for specular reflection and transmission. Thus for identical morphologies, scattering in reflection and transmission from both the surface and the film / substrate interface will all have an identical contribution and the oscillations in scattered light intensity are expected to be identical in amplitude and phase if near normal.

The intensity of scattered light is proportional, in the smooth surface limit, to the height squared at the correlation lateral period of the wavelength and geometry as inferred from equation (3.14), it may also be due to lateral variations in n. A small difference in the morphologies (or lateral variation in n) of the surface and film / substrate interface may thus cause scattering from the rougher of the two to dominate and the amplitude of the oscillations to alter.

3.3.6 Application of laser light scattering

Laser light scattering has been applied to pre-growth annealing and growth of Si (e.g. Pidduck *et al.* 1989), III-V semiconductors (Smith *et al.* 1991)and diamond (Mathis and Bonnot, 1996) thin films.

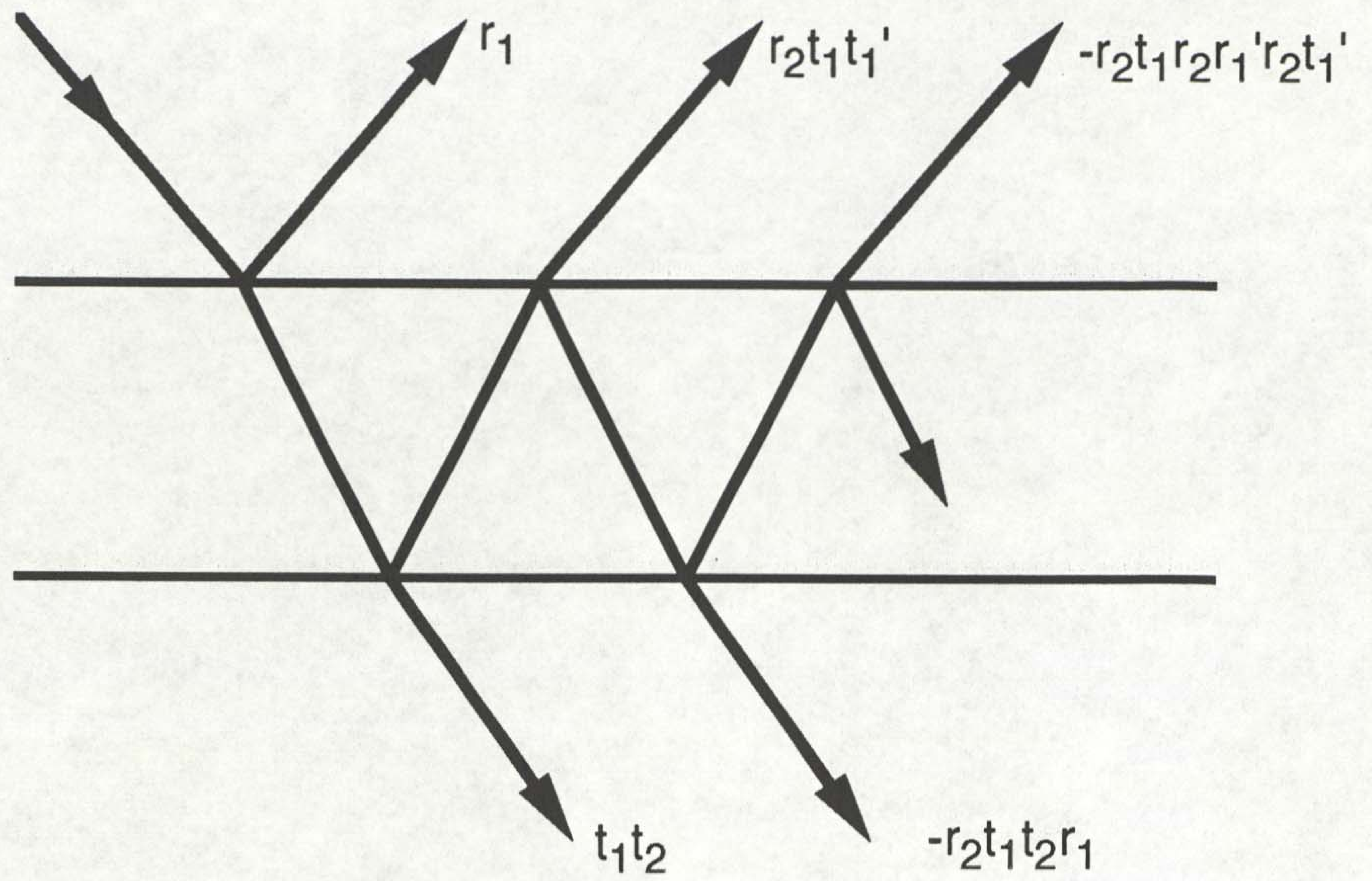

Figure 3.1: Amplitudes of succesively reflected and transmitted beams for light incident on a single thin film.

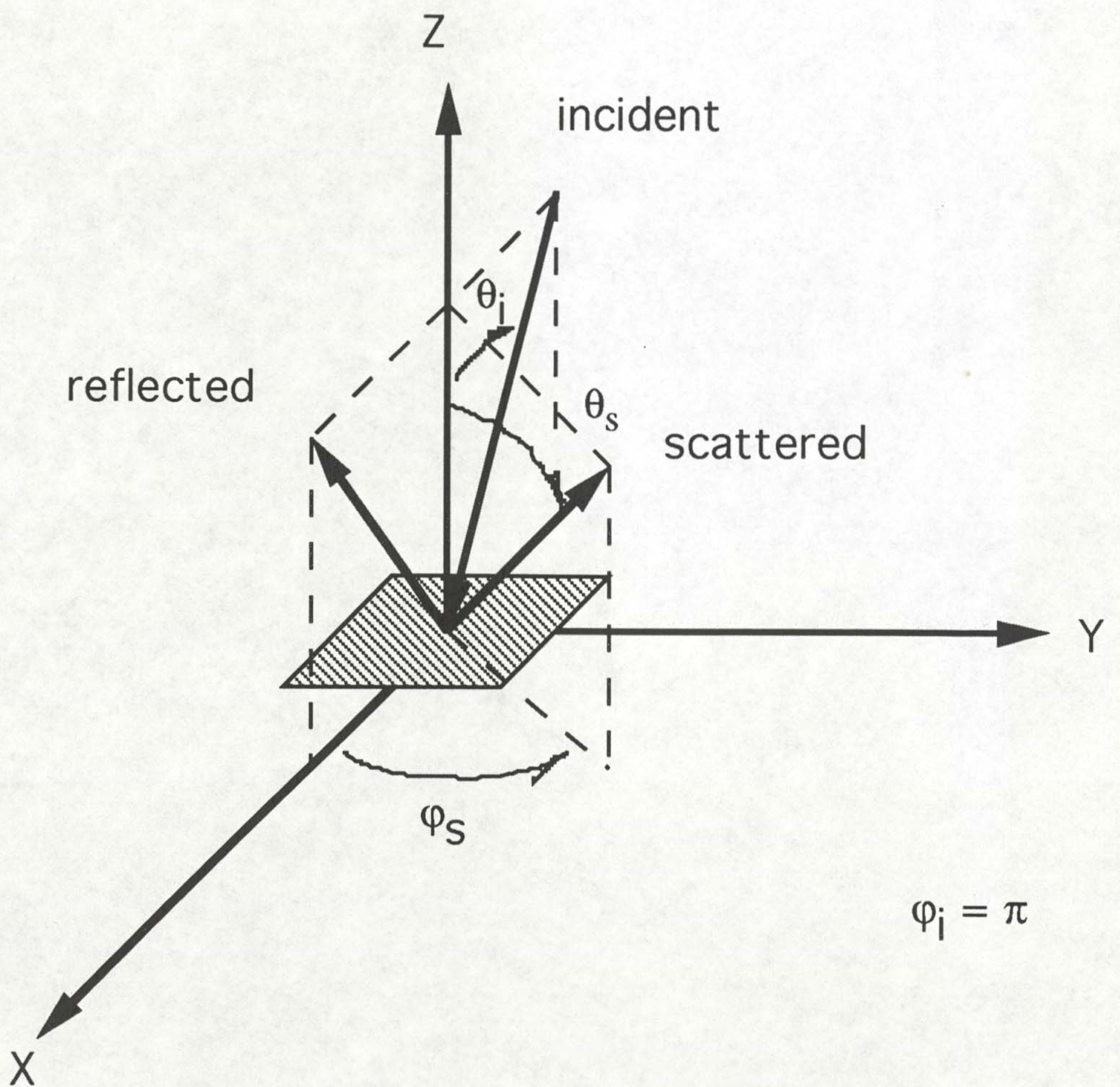

Figure 3.2: Diagram showing the angles of incidence and scattering for LLS.

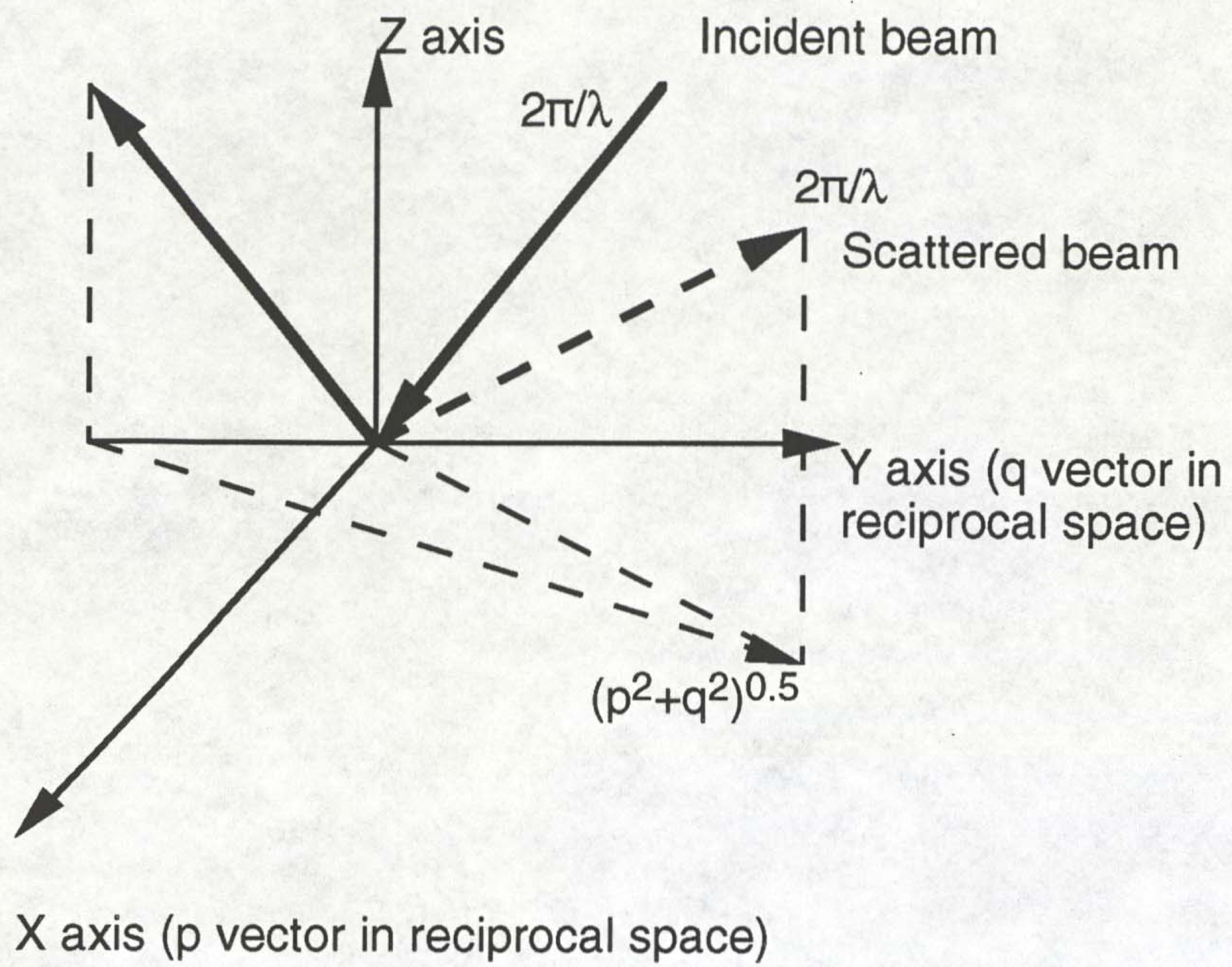

Figure 3.3: Schematic of the scattering geometry in reciprocal space showing vector magnitudes of incident, scattered beams and the difference in the p-q plane.

CHAPTER FOUR
EXPERIMENTAL METHODS

4.1 The chemical beam epitaxial growth facility

4.2 Beam flux calibration

4.3 Substrate temperature control and calibration

4.4 The argon ion laser

4.5 Experimental set up for laser assisted CBE

4.6 In situ laser light scattering and laser interferometry

4.7 Post-growth optical microscopy techniques

4.8 Post-growth profilometry techniques

4.9 Post-growth secondary ion mass spectrometry

4.10 Post-growth etch 'pit' density measurements

4.1 The chemical beam epitaxial growth facility

The growth chamber is a standard V80H MBE chamber, constructed by VG Semicon and modified for CBE. Figure 4.1 shows a schematic of the chamber. UHV pumping is provided by an E06 diffusion pump fitted with a CCT liquid nitrogen cold trap. Condensable species within the growth chamber are pumped by a large surface area liquid nitrogen cryopanel. A detailed description of the chamber is given in Joyce (1993).

The growth chamber is fitted with two group III alkyl injector cells each with two alkyl precursor lines, and two high pressure group V hydride cracker cells, each with a single arsine line. TEG (triethyl gallium), TMAAl (trimethyl amine alane) and TMI (trimthyl indium) are used as the Ga, Al and In precursors respectively. These are held in containers, often referred to as bubblers, within the gas handling cabinet, and heated with temperature controlled heating tape.

The pressure controlled gas handling system was described by Mifsud *et al.* (1990). The system for group V control is shown in figure 4.2. Control of group III is similar but with omission of the valve PV6, the addition of a turbo-pump and Penning gauge in the exhaust line to a separate rotary pump, and the use of a group III gas cell. A 'baratron' capacitance manometer monitors the pressure between the inlet control valve (CV1) and the gas cell valve (PV5) and the system automatically adjusts the pressure the set value using the control valve. When a rapid reduction in pressure is required the exhaust flow control valve is also opened. When the gas cell valve (PV5) is open gas is admitted to the chamber via a fixed orifice and thus the flux is directly related to gas line pressure. Further valves allow the lines to be purged with nitrogen and pumped.

All cells inject precursors at 22° from the substrate normal, when it is facing the central optical - pyrometer viewport. A second viewport at 60° to the substrate normal is fitted

for optical - pyrometry. For detecting scattered laser light a further window was added in a redundant injector cell position at 22° from the normal, although the optical alignment is nearer 23°. The viewport for LLS and the central pyrometer viewport, used for laser incidence and reflectivity measurements, were equipped with all metal UHV valves to protect the windows from coating by condensation of metalorganic species .

4.2 Beam flux calibration

When calibrating an MBE system relative beam fluxes are often calculated from the Knudsen equation for the K - cell. However none of the gas injector cells used in the Liverpool CBE system are genuine Knudsen sources, so accurate calculation of flux is complicated. This is because there is around 2 metres in length of gas line between the 'baratron' pressure control and cell orifices of unknown bore diameters, indeed the gas restricting orifice is an aperture upstream of the cell . Thus, neither the equilibrium pressure in the cell (P_{eq}) or the area of the orifice (A_e), required for the Knudsen equation, are accurately known.

In spite of this, a calculation was made using available data and using some assumptions about pressures and orifice sizes, and comparing with growth rate and ion gauge results (Joyce et al. 1992). The impinging flux J_e at the substrate will depend on the cell - substrate distance (r_{cs}) as follows (Joyce, 1993);

$$J_e = 1.118\times10^{22} \frac{P_{eq} A_e}{r_{cs}^2 \sqrt{MT}}$$ Equation 4.1

Where M is the molecular weight of the molecules and T the source temperature, P_{eq} is in Torr and other units are in cgs units.

For the V80H CBE system used in this work r_{cs} = 18cm. For typical group V values;

P_{eq} = 700torr (typical baratron pressures 100 - 1000torr)

T = 1100K

A_e = 1 x 10^{-4}cm^2 (estimate)

M = 150 (As_2)

the arsenic flux would be;

$$\Rightarrow J_e = 6.0 \times 10^{15} \text{ As}_2 \text{ dimers / cm}^2 \text{ / sec}$$

For the typical values given below for TEG;

P_{eq} = 4torr (typical baratron pressures 0.1-4torr)

M = 157 (for TEG)

T = 300K

A_e = 1.96 x 10^{-3}cm^2 (gas line 9)

the TEG flux would be;

$$\Rightarrow J_e = 1.25 \times 10^{15} \text{ Ga atoms / cm}^2 \text{ / sec}$$

Now a growth rate of one monolayer per second is equivalent to an incorporated flux of 6.25 x 10^{14} Ga atoms / cm^2 / sec. Thus the calculated flux for 4torr TEG is equivalent to a growth rate of 2.0 ML / sec. This value compares favourably with experimentally measured growth rates of 2 to 2.3 ML / sec(at a substrate temperature of 500°C where the incorporation efficiency is expected to be near unity). Thus it appears that the calculation

LIVERPOOL UNIVERSITY LIBRARY

is reasonably valid. Correlation with experimentally found fluxes using ion gauge measurements were previously reported in Joyce and Bullough (1992).

The V/III flux ratio is of importance for CBE growth since it has an effect on the growth rate and dopant incorporation. Using the above calculated values the V/III flux ratio for 700torr arsine and 4torr TEG is 4.8 (6×10^{15} As_2 dimers / cm^2 /s / 1.25×10^{15} Ga atoms / cm^2 /s).

Run to run flux control is reported to be very good in CBE and run to run calibrations are not necessary (Davies *et al.* 1991). Thus growth rates for laser assisted layers measured on different growth runs can be directly compared with the assumption of constant beam fluxes with time. However there is some lateral flux variation across the wafer. The sources are angled at 22° to the normal, off - centre to the substrate, with the intercept of the centre axis of the various beams to the wafer centre of rotation, a few cm behind the wafer. This design is to enable good growth rate uniformity of below 1% over the entire substrate with the substrate in rotation. For laser assisted CBE substrate rotation is not used so the growth rate is not uniform and the growth rate in the laser irradiated area depends on position on the wafer to a greater extent than growth run number. The laser beam was thus always directed to the same area of the wafer (with respect to the chamber geometry) each time for laser assisted growth and each set of data was collected in one growth run. This area was near the centre of the wafer so that the measured unmodified growth rates would be comparable to those measured with rotation. Movement of the beam to a new area for growth rate measurements was achieved by substrate rotation, thus keeping the laser beam position constant with respect to the sources.

4.3 Substrate temperature control and calibration

The need for substrate rotation in CBE to give lateral growth rate and composition uniformity leads to difficulties in the measurement of substrate temperature. The substrate is heated by a resistively heated tantalum foil (or foils) behind the substrate holder. The substrate temperature is measured by a thermocouple between the heater and substrate, but not in contact with the substrate since it (along with the heater) remains stationary. Without direct contact with the substrate the thermocouple temperature (a result of radiation from the heater and the substrate) will be different from the true substrate temperature. In laser - assisted CBE this is not entirely a bad thing since the thermocouple temperature will not be very sensitive to laser - induced substrate heating and very little feedback is expected. In this thesis 'substrate temperature' refers to the temperature measured by the thermocouple referred to as °VG or the pyrometer measured temperature as °C. The term substrate temperature will not be used to refer to the locally increased temperature under the laser where laser - assisted growth occurs.

The difference between °VG and °C was calibrated using optical pyrometry and by monitoring RHEED transition temperatures. The optical pyrometer used to monitor the apparent temperature was a Minolta-Land Cyclops 52 with an operating wavelength of 900 - 1100nm. Reliable measurements could only be obtained using the central pyrometer viewport and thus could not be used simultaneously with laser interferometry, LLS or laser assisted CBE. Furthermore reliable measurements could only be taken when the window was clean (and it was found to coat up during growth runs) and the pyrometer was unable to measure temperatures below 400°C, as used in laser assisted CBE. Thermocouple temperatures were calibrated using figure 4.3. Temperature variations between growth runs was less than ±5°C for 2" n+ GaAs substrates.

4.4 The argon ion laser

Argon and krypton ion lasers constitute one of the most important classes of lasers. These lasers produce reliable high power in cw operation at a multitude of wavelengths across the visible and in the near ultraviolet and infrared. As a result, cw ion lasers have found applications as diverse as retinal surgery and high resolution microscopy. Argon ion lasers are potentially suited to laser modified growth for a number of reasons; they are very stable resulting in consistent results and allowing the beam itself to be used for self monitoring; they are relatively simple to use compared to excimer lasers; they operate at a number of wavelengths from the visible to the near UV which can be selected with relative ease; they can be used at a wide range of powers from a few milliwatts to a few Watts. In noble gas ion lasers, laser action occurs between highly excited energy levels in either singly or doubly ionised atoms. The atoms are principally excited by one or more electron impacts, and the ions relax to lower states by one of many possible relaxation routes, emitting a photon.

A Coherent Innova 90-5 laser was used for this project which was capable of producing 6.8W of laser power in multiline mode, and powers for individual lines as shown in table 4.1 below. The wavelength required is selected by the use of an intracavity etalon in conjunction with a wavelength selector prism. The etalon is a Fabry-Perot interferometer, made from a piece of fused silica. Wavelength selection is achieved by tilting the etalon, and thus varying the effective thickness, and fine tuning by varying the index of refraction by temperature tuning. Multiline operation is achieved by replacing the etalon with a dummy spacer. The output power is monitored using a beam-splitter and a photocell in the laser head. The output of the photocell is used to control the current in light regulation mode.

Wavelength (nm)	Laser Power (W)
514.5	2.7
501.7	0.50

496.5	0.90
488.0	2.6
476.5	1.1
472.7	0.20
465.8	0.10
457.9	0.50
454.5	0.010
Multiline(465.8-514.5)	6.8
UV(351.1-363.8)	0.35

Table 4.1: Maximum power output at selected laser line wavelengths, and in multiline operation, for the laser used in this study.

In this work the laser was operated using the 514.5nm single line mode offering a maximum power of 2.7W. An aperture is provided to limit the beam diameter and so prevent higher transverse modes from operating. In this work the widest aperture (4mm diameter) was used for multimode operation, allowing many transverse modes. This provided the highest power output, but also the highest beam width and divergence. The output transverse profile from the laser thus resembled a top hat.

4.5 Experimental set up for laser assisted CBE

The output from the laser was directed by two plane mirrors and focused by a 0.5m focal length concave mirror to the substrate at near normal incidence through the central pyrometer viewport, as shown in figure 4.4. The focusing mirror was mounted on an optical bench and its' distance from the substrate was varied until the spot size on the substrate, viewed with a telescope through a side window, was minimised. Since the laser light was off axis on incidence with the focusing mirror, the beam was focused to an ellipse on the substrate. This ellipse was found to have widths in major and minor axis of 2 and 0.15mm (see section 6.2). The substrate was held stationary during growth of the laser modified layers.

Beam chopping was achieved by inserting a rotary beam chopper in the path between the directing and focusing mirrors. Arrays of dots and lines were achieved by substituting the focusing mirror for a plane mirror and inserting two 0.1m convex lenses in a telescope arrangement for focusing along with a pinhole or grid as a diffractive optic after the last mirror. The grids used were copper TEM sample grids which were not degraded by the laser heating.

4.6 In situ laser light scattering and laser interferometry

Growth rates for laser modified growth were determined in real time from interference oscillations using laser interferometry (also called DOR, Armstrong et al. (1992)). The intensity of the specular reflected beam from the Ar^+ laser was monitored using a large area photodiode protected by suitable filters. The incident beam was directed so that it passed through the upper half of the viewport and the substrate was oriented so that the reflected beam passed through the lower. The reflected beam was deflected using a small planar mirror through a focusing lens onto the photodiode. Focusing was required to collect the entire reflected beam, which was diverging due to the focusing at the substrate and the local nature of the growth. An interference filter was placed over the photodetector window to improve the signal to noise ratio, along with interchangeable neutral density filters to reduce the intensity to a level suitable for detection. The voltage produced in the photodiode was fed through an A-D converter to a 386 PC microcomputer for real time display, storage and processing.

Unassisted growth rate measurements were made using a low laser power (12mW) which was found not to effect the growth to a significant extent. To monitor interference oscillations a thin film of AlGaAs (usually of thickness $\lambda/4$) was grown, followed by GaAs. The growth rate was calculated from the time intervals of the first 4 turning points in the interference oscillation.

Laser light scattering was used to monitor the surface morphology evolution at high laser power during laser modified CBE growth of GaAs, and at low power during conventional substrate cleaning and growth of GaAs, AlGaAs, InGaAs and InAs. This was achieved by monitoring the intensity of normally incident Ar+ laser irradiation diffusely reflected through a viewport at an angle of 23° from the wafer normal. In section 3.2 it was shown that this geometry corresponds to a maximum sensitivity to roughness of lateral period 1310nm.

Detection of the scattered light was accomplished using a 50mm diameter (video camera) telescope focusing the scattered light via an optical fibre into a photo-multiplier tube. Sensitivity was maximised by imaging the laser spot by eye and using the telescope aperture to reduce the field of view to the laser spot. (This aperture when used with a CCD array acts as a light level aperture, but due to effectively viewing from infinity will now lie on the image plane). This reduces the light detected from the rest of the substrate and the heater stage. The lights in the CBE room were dimmed and the telescope covered. A 514.5nm interference filter was placed over the entrance to the optical fibre along with neutral density filters when using high laser power for laser modified growth studies. The output from the photo-multiplier tube was converted to 0-10V by a picoammeter and fed through an A-D converter (along with the laser interferometry information) to the PC. To accommodate the intensity varying by over 4 orders of magnitude during some growth runs the range of the picoammeter was manually switched by order of magnitude increments when necessary during growth, and the data corrected later.

Measurement of scattered light intensity with axial substrate orientation was achieved by substrate rotation and normal data acquisition. The substrate was rotated with a period of 6s, which is slower than the normal period of ~1s, so that data could be collected about every 3° if necessary without the data files becoming too large, and to reduce noise. Even

so, many of the files were of the order of 30,000 data points which took ~300Kbytes of memory. During LLS the specular reflected beam was always reflected again internally either off the chamber internal surfaces, or partially off the normal incidence viewport window. Without substrate rotation, the substrate was oriented such that the doubly reflected laser spot was not coincident on the substrate with the area collected by the telescope aperture. During substrate rotation this was more difficult to achieve, but only occasionally caused spikes in the LLS traces. Even without this routine, when laser interferometry was used simultaneously, the data was of sufficient quality to observe the changes of interest. Laser interferometry during rotation was achieved by using a data sampling program which analysed the reflected intensity only when the reflected laser beam passed across the photocell.

4.7 Post-growth optical microscopy techniques

A number of post-growth optical techniques were used to image the laser affected area and the surface morphology within. Most of the laser-modified areas, on the otherwise smooth wafer surfaces, took the form of hillocks, rounded in vertical profile, less than 1μm in height and of lateral dimensions 2 x 0.15mm, which proved difficult to find and characterise.

The most successful method of locating the laser areas was to reflect a slightly diverging light source off the wafer surface, viewing the reflected beam either by eye or preferably on a screen. Features undetectable by normal microscopy methods can then be observed. This technique is known as Makyoh topography (e.g. Kugimiya, 1992) and proved to be a simple technique to apply. However quantitative profiling was not possible.

Dark field optical microscopy was occasionally used to locate the laser affected area when the laser irradiation produced a change in surface morphology but not profile. The main

imaging techniques used were based upon interference microscopy, a group of optical microscopy techniques used in a large number of areas. In this work the differential contrast method invented by Nomarski (1952), and described by Miller and Rozgonyi (1978) was used. The technique of Nomarski interference optical microscopy (NOM) was found to be suitable for locating and imaging the laser affected area produced by laser affected CBE during this work. With NOM the affected area could be imaged due to the profile of its surface morphology. However, height measurements of the profile or morphology could not be obtained because of the large lateral dimensions with respect to height.

NOM utilises a "Nomarski" device which is essentially a beam splitting instrument, usually built into a standard optical microscope. The schematic arrangement is shown in figure 4.6. Referring to figure 4.6, light enters from the left, passes a polariser set at 45° and is reflected by a half silvered mirror through the Nomarski prism, where the light is split, and then through the objective lens onto the object. The two beams reflect off the object, pass back through the lens, the prism, the half silvered mirror, an analyser polariser set at 135° and an eyepiece to the eye or to photographic film. The Nomarski prism consists of two separate birefringant quartz prisms, cemented together with perpendicular optic axis. The two components of the beam entering the prism see different refractive indexes (due to the birefringent quartz) and thus have different velocities. When the two components meet the glue joint they form two divergent beams. The angle of divergence is arranged so that it matches the focal length of the lens so that the two beams are parallel but displaced in relation to each other when focused on the object. The reflected beams are recombined by the prism to form a single beam. When they recombine the phase difference between the two is dependant on the local surface orientation of object in the direction of the divergence and on the thickness transversed in the prism by each component. If the thickness transversed within the prism is equal for the two components, the analyser (set at 135°), will extinguish the beam when the surface

of the object is flat (i.e. oriented at 90°to the beam direction in the direction of the displacement).Features i.e. deviations from this orientation result in an increase in intensity. Due to the dark background observed this condition is referred to as a dark mode or null condition The thickness and thus relative phase of the two beams can be altered by moving the prism in the displacement direction, altering the relative thickness transversed by the beams each side of the glue joint. When a phase difference is present a flat surface will appear grey and vertical relief on the scale of the beam horizontal displacement, typically 0.2μm, will result in an increase or decrease in imaged intensity depending on whether the surface gradient brings the phases apart or together respectively.

The condition with a small phase difference set by the prism (called the off null position) gives the most easily interpreted image since changes of object surface orientation result in apparent shading and highlighting. Since the beam separation of 0.2μm is below the resolving power of the microscope the beam displacement will not be observable and only the intensity change seen. The technique is only sensitive to variations in height in the displacement direction over ~0.2μm. Surfaces with the same orientation in the displacement direction have the same contrast independent of overall vertical height, and no contrast is observed perpendicular to the displacement direction. Step heights as low as 3nm and corresponding slopes (3nm in ~0.2μm) can be detected corresponding to islands of lateral dimensions ~1μm and vertical height ~8nm. However the sensitivity is dependent on the NOM phase difference, magnification, and roughness form and lateral scale, causing differences in vertical resolution for different features. Specifically linear features aligned perpendicular to the horizontal displacement are more resolvable than islands of the same height.

In practice the Nomarski prism results in differing phase conditions along the displacement direction across the viewed sample region, particularly at low

magnification. This results in a dark 'null state' band perpendicular to the displacement direction. Then the sign of the contrast (i.e. direction of the apparent shadow or 'light source') is reversed on either side. Absolute elevation (whether a feature is a hill or pit) can be determined with reference to a known feature (the substrate circlip mark in this work, known to be a depression) imaged on the same side of the null point.

For measurement of height a feature must be adjacent to a flat surface, since the NOM contrast is only a function of local surface orientation. Height measurement is thus only possible for isolated features and not for continuously varying morphology. Height contrast is achieved by the insertion of a different prism which produces a separated double image, similar to the standard Nomarski prism but with a displacement of the order of 0.1mm (in this work the prism used was called a polarisation interferometer Nomarski prism. Using monochromatic light on a perfectly flat surface would then result in accurately straight and parallel interference fringes. If one point departs from true flatness its depth (or height) will result in a local fringe displacement of ζ times the fringe separation (where ζ is a number typically between 0.5 -10) corresponding to a depth of $1/2\zeta\lambda$. This technique was found to be successful in locating and gaining information on the shape of the laser effected area and was more sensitive than the standard NOM, but could not give accurate height information due to the overlapping of the images of the laser areas.

4.8 Post-growth profilometry techniques

A Dektak stylus profilometer was used to measure the laser-affected area profiles, and a Nanoscope III atomic force microscope was used to measure the surface morphology within and outside the laser-affected area.

The principle of a Dektak profilometer is that a diamond tipped stylus is held on the sample surface and then scanned over a few mm in length. A piezoelectric crystal was used to convert the stylus height to an electric signal displayed on a screen. The lateral accuracy is around 1μm and the height accurate to around 20nm. The force exerted by the stylus was not expected to have caused significant damage to the semiconductor surface and no line was observed by NOM.

Atomic force microscopy (AFM) was invented by Binning et al. (1986) to overcome the limitation of the scanning tunnelling microscope (STM) to conductive samples. Operationally it is very similar to STM but functionally it is like a profilometer. In essence a very sharp tip at the end of a flexible cantilever scans across a surface at close distance tracing the surface contour.

A schematic of the AFM is shown in figure 4.7. In 'constant height mode' the sample is scanned in the X and Y axis and inter - atomic, frictional, magnetic and electrostatic forces attract or repel the cantilever. This force causes a deflection in the flexible cantilever. A laser beam, used as the sensing system, is focused onto the cantilever and the reflected beam directed onto a split photodiode. The deflection in the cantilever moves the position of the beam on the split photodiode and from the differential signal from the photodiode a sensitive measure of the tip deflection and thus sample 'contour' can be obtained. However this is usually too sensitive with only a few nm range in height so in 'constant force mode' the Z - axis piezoelectric varies the height of the sample to maintain a constant tip deflection (as measured by the photodiode) and thus contact force. In this study the 'constant force mode' was used in air.

The presence of a native oxide layer has been reported (Bluhm *et al.* 1994) not to disturb the capability of AFM to image the as-grown surface morphology, since it grows conformally, and atomic steps on the as grown surface may still be imaged. The images

presented in section 5.1 were taken after only 30 minutes in air to achieve the best results possible. Best results were found with a very low contact force. A cantilever with a spring constant of 0.06N/m was used and the contact force was ~4nN. For characterisation of laser effected growth the area was found initially either by eye with a parallel light source or by sequentially moving the AFM tip across the sample and maximising changes in surface morphology.

More recently Martin *et al.* (1989) developed a method called "non contact AFM" in which the tip is oscillated over the sample and changes in phase or frequency are related to changes in force from the sample. It was reported that this method provided better results than contact AFM because less charge is trapped in the surface.

A difference between AFM and Dektak profilometry is that AFM scans and rasters relatively fast (a few seconds per frame) in both the X and Y direction, producing a 3D 'image' whereas the Dektak only scans a line producing a 2D slice. Secondly horizontal scanning is motor driven in the Dektak and by piezoelectric crystal in the AFM. Thirdly the surface contour is measured directly by the voltage induced in the piezoelectric crystal from the stylus height in the Dektak profilometer, but independently by a laser beam reflecting off the cantilever onto a split photodiode measuring the tip deflection in the AFM. Because of the measurement and scanning differences AFM can be used so as to exert a lower force on the object and have a better resolution.

4.9 Post-growth secondary ion mass spectrometry

To address the problem of dopant and impurity profiling Secondary Ion Mass Spectroscopy (SIMS) was utilised. The results presented in chapter 5 were performed by A. Chew of Loughborough Consultants, and those in chapter 6 by Mats. UK,

Merseyside. SIMS has played a major role in semiconductor characterisation since the late 1970s and is now regarded as an established technique. A fuller description can be found in Benninghoven *et al.* (1987).

In SIMS the sample is bombarded in vacuo by an energetic beam of primary ions, in this study caesium ions at 5keV with a current of 80nA. As a result some particles are sputtered from the sample. Sputtered ions (negative in this case) are extracted into a mass spectrometer and separated according to their mass to charge ratio. With a rastered focused primary Cs+ beam the surface in the bombarded area is etched in a controlled way. By monitoring the intensity of one or more mass - to - charge ratio peaks with time a concentration profile both laterally and in terms of depth is possible. This is achieved by measuring the crater depth (e.g. by stylus profilometry) after a known bombardment time, and knowledge of parameters such as analysed area, sputter rate and sample density, and a calibration by a standard. The primary ions, of energy 5keV, penetrate around 10nm creating mixing only on this thickness scale, and the secondary ions have an escape depth of around 2-3 atom layers enabling detection of very thin layers such as interface contamination. SIMS was employed in this thesis to identify impurities at the substrate - epilayer interface in chapter 5.

As described in chapter 6, SIMS was used to identify variations in dopant concentration in laser effected layers. Hall measurements and Capacitance - Voltage Profiling both required a larger analysing area than the laser irradiated area and were thus not suited to analysis of laser effected growth. SIMS detection from an area of 50x50μm on the wafer surface was feasible, although it gives no information on electrical activation of dopant atoms. To align the SIMS ion beam with the laser affected area a parallel light source and a CCD camera had to be used. The light source was directed through a viewport at around 30° to the sample normal and the light was detected with the CCD camera focused on the sample through an opposing port also at about 30° from the normal. The laser affected area could not be seen using the secondary electron image commonly used. Data

was acquired for the entire 0.5x0.5mm crater split into pixels (of size ~5x5μm). Once the SIMS profiling was complete an image of the laser area at any depth was obtained and from this the concentrations at the centre found by electronic gating. A lower SIMS background level of carbon incorporation was found by detecting AsC- as opposed to C-.

4.10 Post-growth etch 'pit' density measurements

Etching of semiconductors is a widely used method of preparing substrates and patterning structures. However some etchants are material and defect sensitive. The defect sensitivity during etching has been exploited as a simple method of identifying and quantifying defects such as threading dislocations. Reported defect sensitive etchants for (001) GaAs include molten KOH (Grabmaier and Watson, 1969), AB etchants (Abrahams and Buiocchi, 1965) and CrO_3-HF aqueous solutions (van de Ven *et al.* 1986). In this study a CrO_3-HF aqueous solution was used to reveal threading dislocations and 'misfit' dislocations in GaAs layers grown by laser effected CBE. Van de Ven *et al.* (1986) reported that threading dislocations are revealed as hillocks and underlying misfit dislocations to result in ridges on the surface. A complex etching process was proposed dependant on the concentrations of CrO_3 and HF along with the GaAs carrier type and level, temperature and the presence of agitation and light. Essentially, under most conditions, the HF is responsible for the GaAs etching by oxidative dissolution of GaAs and the CrO_3 is responsible for the selectivity. During the etching the Cr^{VI} is reduced to form an adsorbed species on the surface. This layer inhibits the etching and is reported to be thicker at areas of high strain and thus these areas have slower etch rates. Etching of defects, such as threading dislocations, with an associated strain field result in a lower etch rate and are revealed as hillocks.

Selective etching of defects is of use to laser assisted CBE since it can be used to measure changes in threading dislocation density at levels below the sensitivity of TEM. The

samples were placed in a 1.5M HF and 1.2M CrO_3 aqueous solution at room temperature and normal light conditions for 5 minutes without agitation which was found to etch ~500nm of defect free GaAs (which was reported to be great enough to reveal all defects present). The defect concentration was measured using NOM.

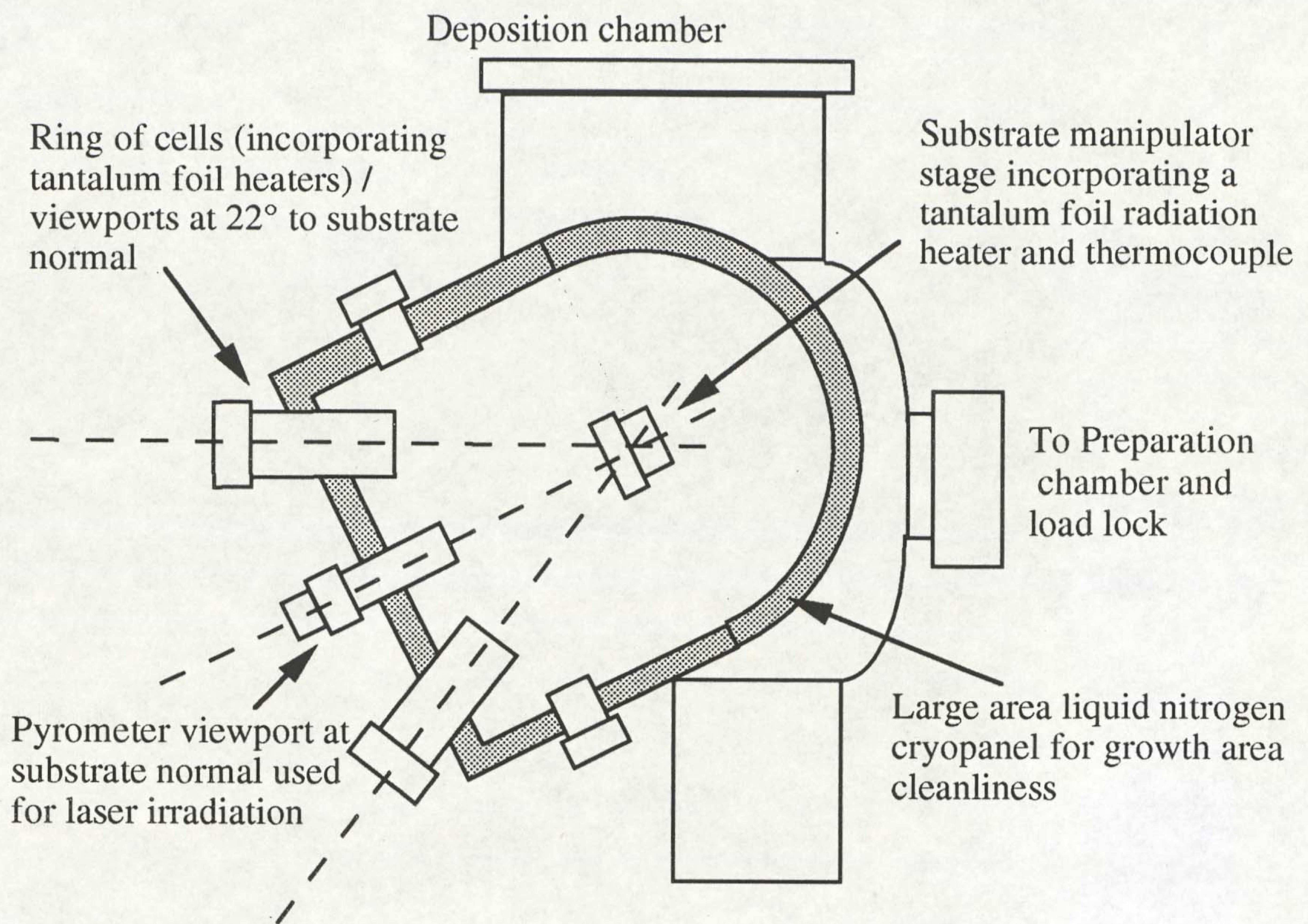

Figure 4.1 Sectional diagram of the CBE growth chamber. The preparation chamber is not shown.

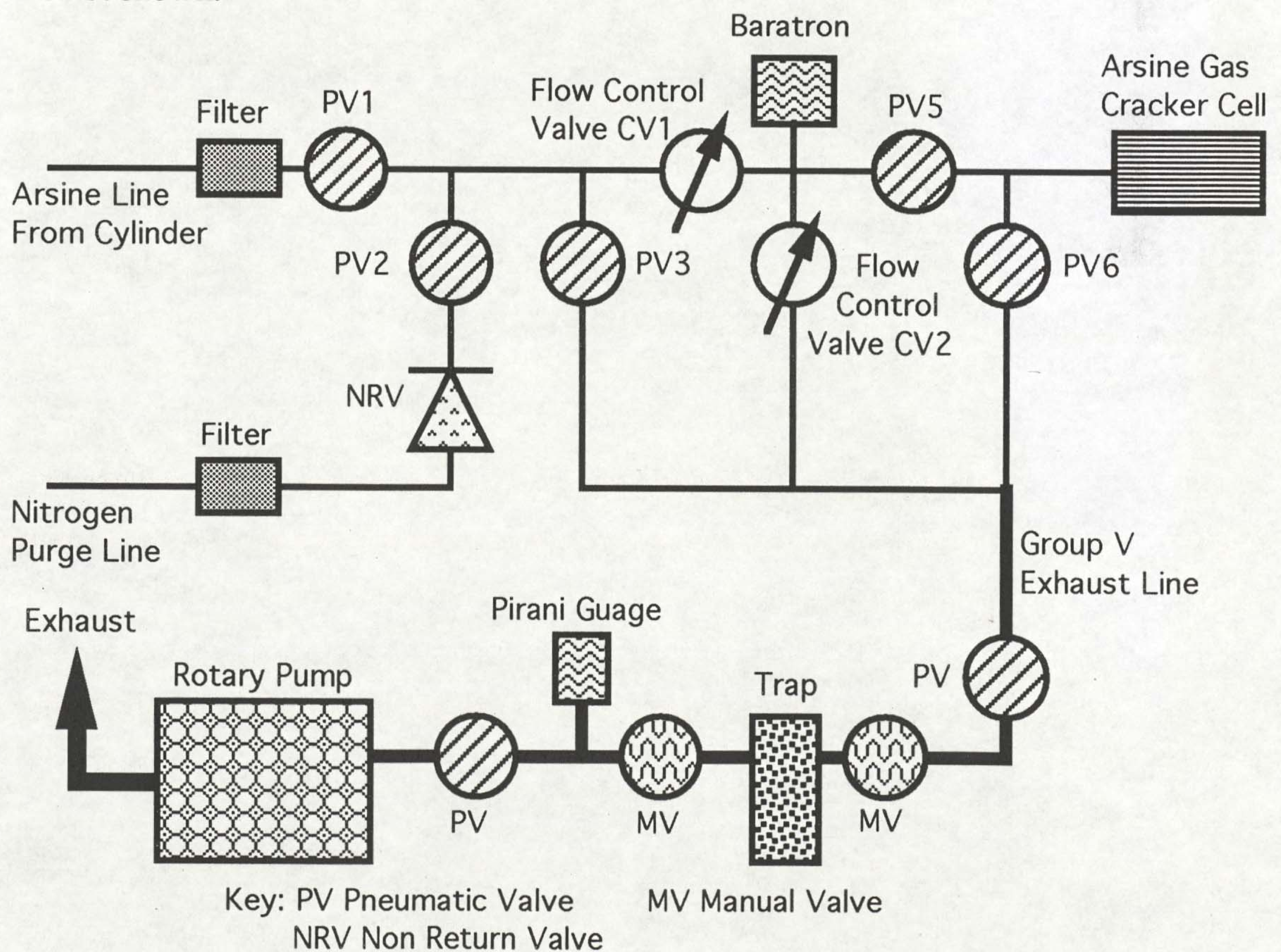

Figure 4.2 Schematic diagram of the group V gas handling and exhaust system.

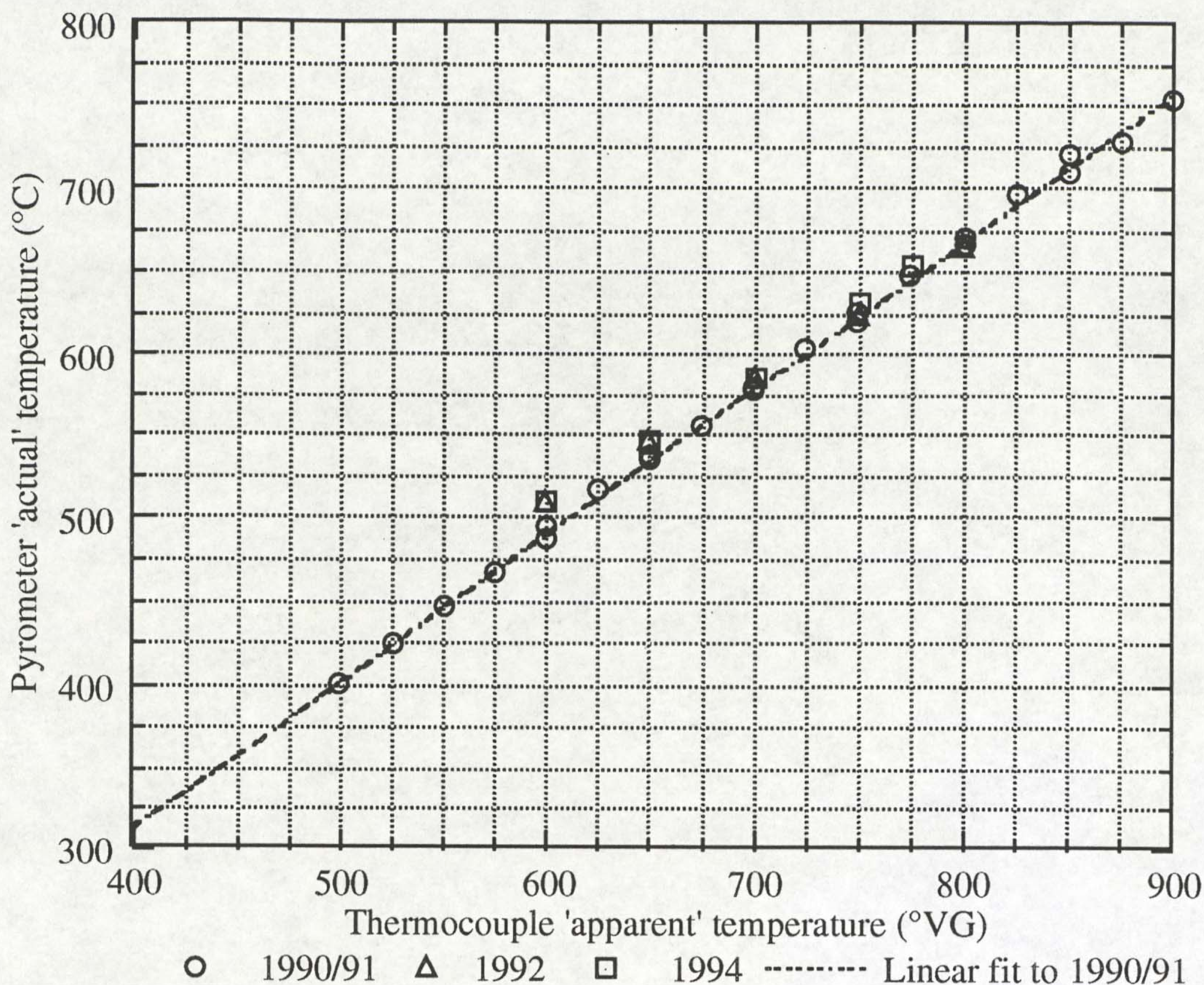

Figure 4.3: Callibration from thermocouple temperature (°VG) to degrees centigrade (°C) by an optical pyrometer temperature for 2" n+ substrates.

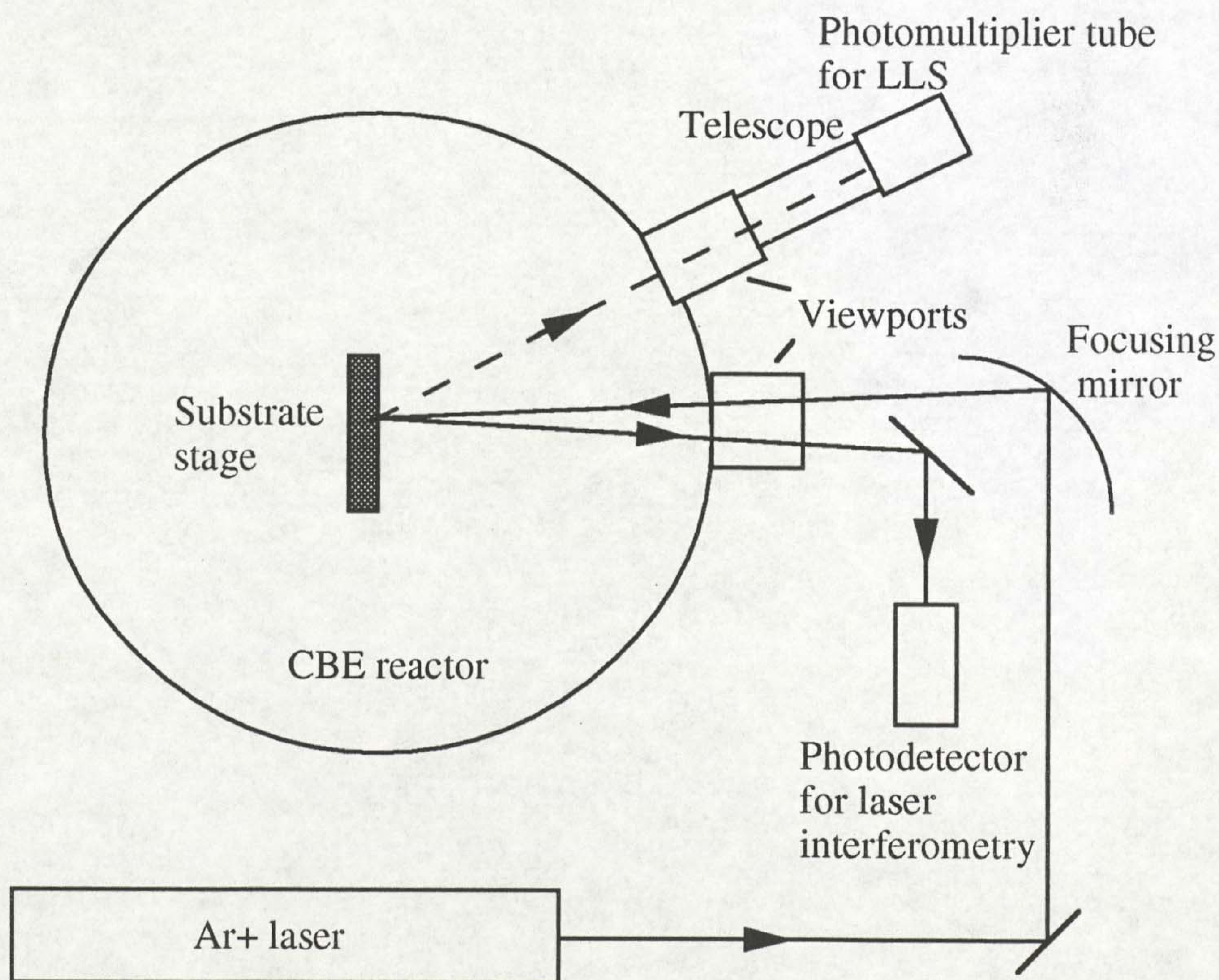

Figure 4.4 Schematic diagram of the experimental arrangement for laser assisted CBE plus laser interferometry and LLS measurements.

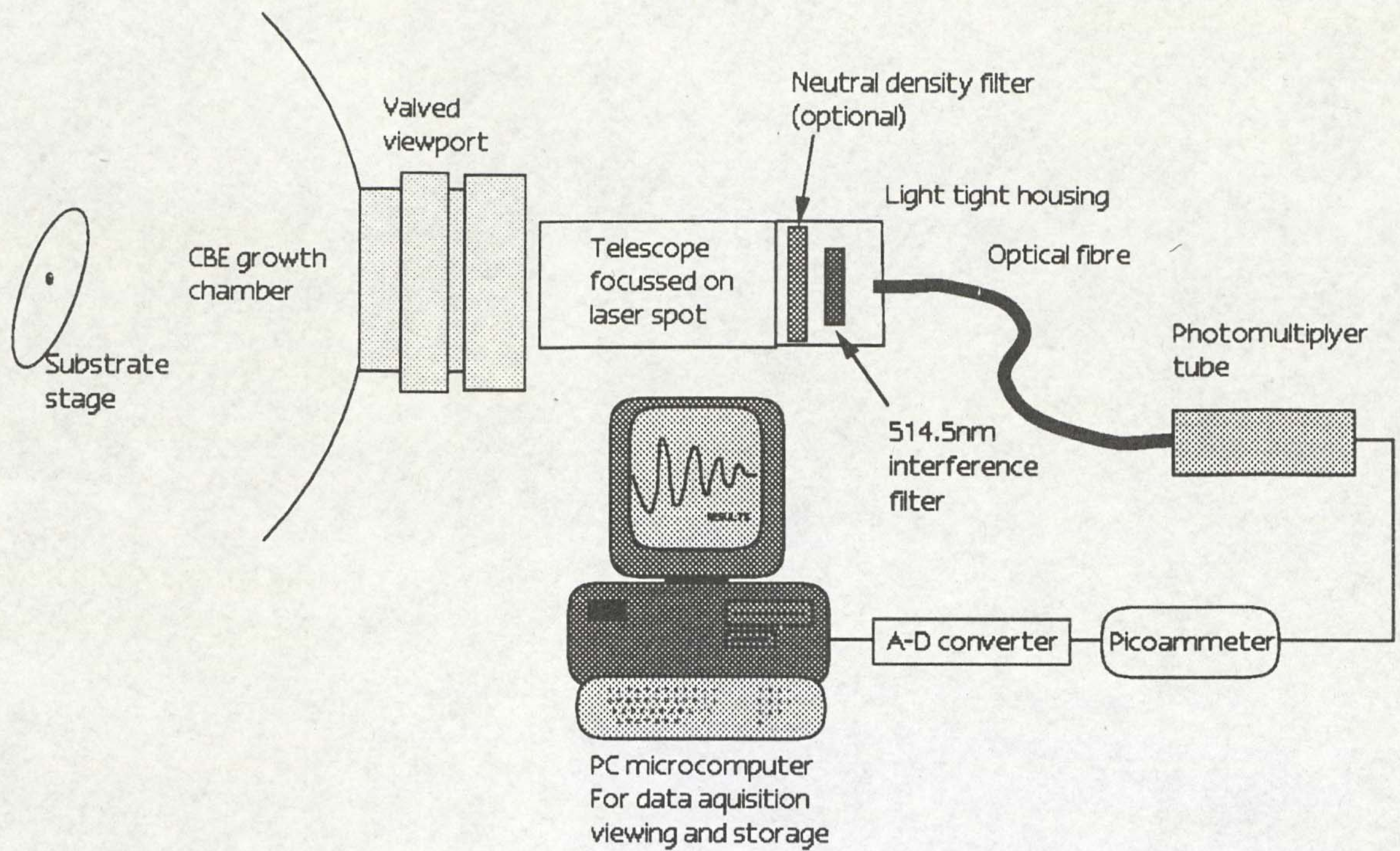

Figure 4.5 Laser light scattering components.

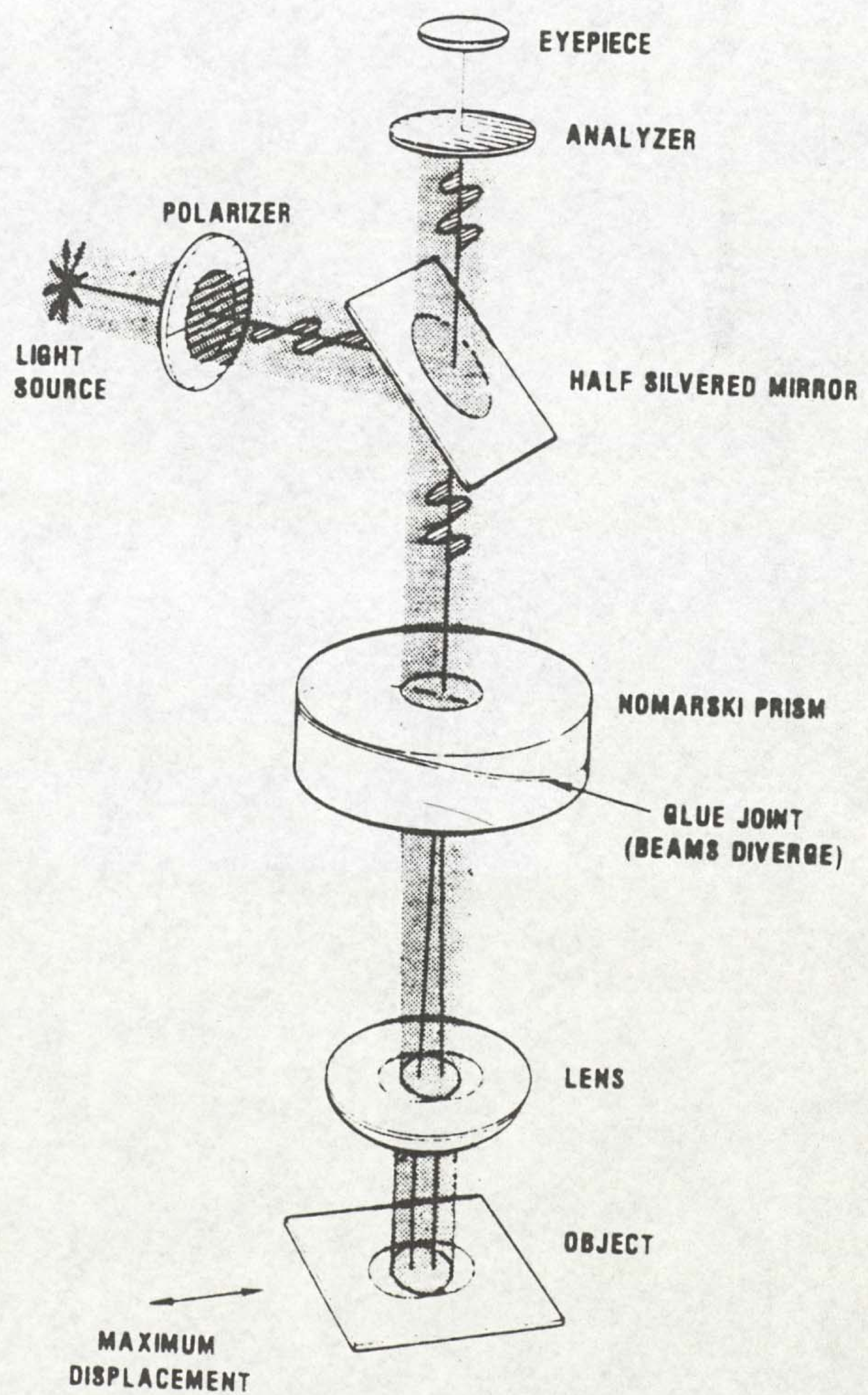

Figure 4.6 Schematic diagram of the arrangement of essential parts of a microscope used for Nomarski optical microscopy (from Miller and Rozganyi 1978).

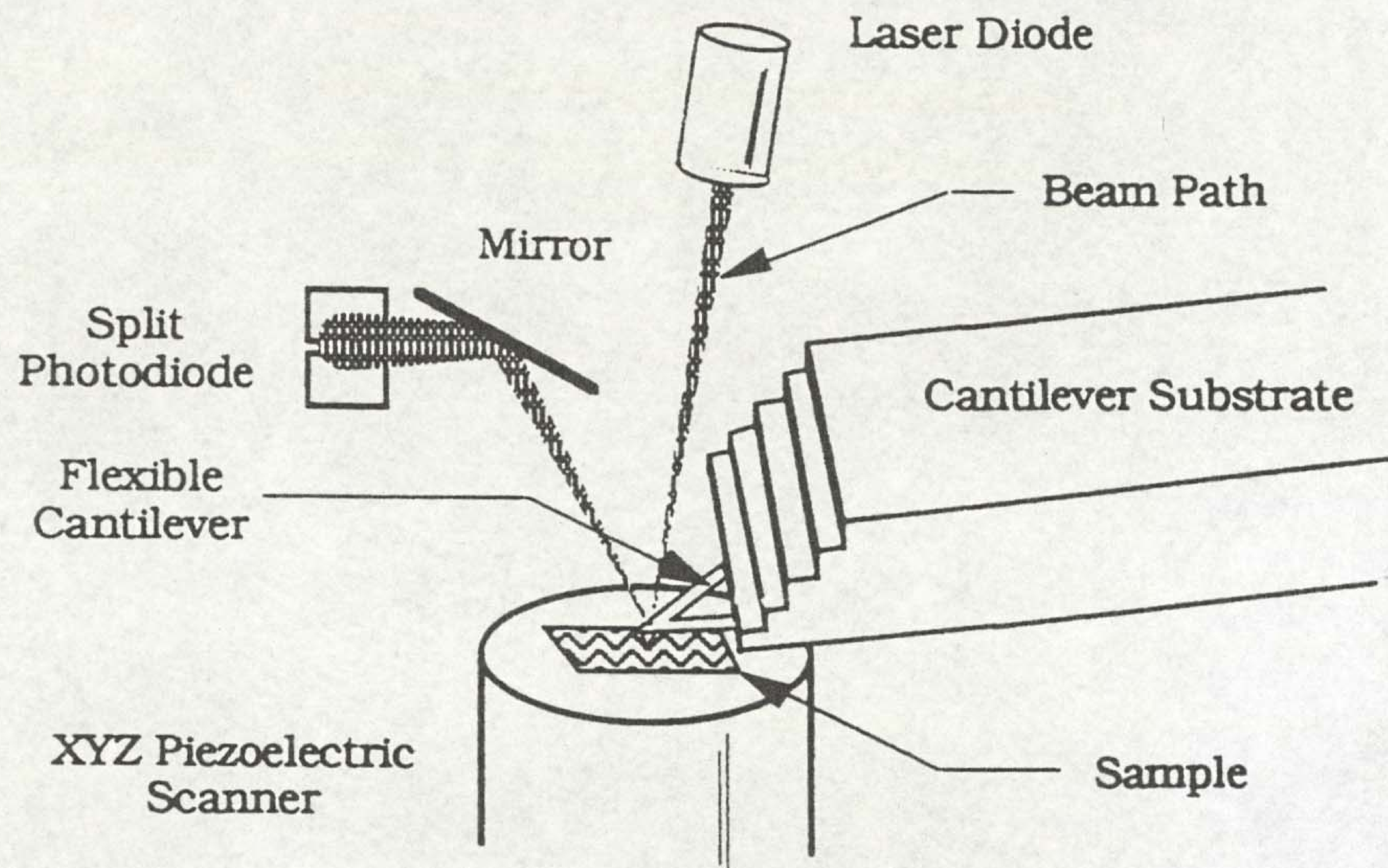

Figure 4.7 Schematic diagram of the atomic force microscope (from Nanoscope III AFM instruction manual).

CHAPTER FIVE

LASER LIGHT SCATTERING STUDIES OF THE GROWTH OF GaAs, AlGaAs, AND InGaAs ON GaAs

5.1 Substrate preparation

5.1.1 Introduction to substrate preparation

5.1.2 Typical LLS results for substrate annealing with and without chamber outgassing

5.1.3 Summary of LLS results

5.1.4 Atomic force microscopy results

5.1.5 Discussions

5.2 Growth of GaAs and AlGaAs

5.2.1 Morphology changes during the growth of GaAs and AlGaAs

5.2.2 Laser light scattering interference oscillations

5.2.3 Discussions

5.3 Low compressively strained layer growth: $In_xGa_{1-x}As$ (x<0.25) on GaAs

5.3.1 Laser light scattering results

5.3.2 Atomic force microscopy results

5.3.3 Discussions

5.4 High compressively strained layer growth: InAs on GaAs

5.5 Summary of chapter

5.1 Substrate preparation

5.1.1 Introduction to substrate preparation

Epi-ready 2" n+ nominally (001) GaAs substrates are routinely annealed in-situ at a thermocouple temperature of 700°VG corresponding to an apparent substrate temperature of ~600°C as measured by optical pyrometry. Substrates are routinely heated to ~600°C at a heating rate of 0.5°VG/s, and held for ~1000s, under an As_2 flux of 200torr (corresponding to a flux density of 1.71 As_2 dimers/cm^2/sec). Reflectance High Energy Electron Diffraction (RHEED) is usually used to ascertain the removal of the native oxide by the change in diffraction pattern from diffuse to that characteristic of a 1x1 surface reconstruction as the oxide becomes thin to that characteristic of a 2x4 surface reconstruction when the oxide is removed (Tu et al. 1989). RHEED is a useful technique in that it gives information on the surface structure and thus the presence of the oxide layer, but it gives little information on the morphology development and processes occurring. Modulated Beam Mass Spectrometry (MBMS) has been employed to determine the molecular species desorbing from the substrate during the process and gives an insight to the reactions occurring, but is not an easily applied technique. Van Buuren *et al.* (1991) found that the predominant oxide desorbing was Ga_2O suggesting the native oxide is reduced by the reaction:

$$Ga_2O_3 + 4Ga = 3Ga_2O$$

to produce the volatile Ga_2O. MBMS however gives no information on the morphological development

This study centres around the use of Laser Light Scattering (LLS) to monitor the morphological development during the substrate annealing. It gives no information on the material present but measures changes in the surface morphology. Combined with results from RHEED, MBMS and *ex-situ* characterisation it can give an insight into the

substrate cleaning process. In this study the intensity of scattered light from a 514.5nm wavelength Ar+ laser was measured during the heating and anneal as detailed in section 4.6. The wafer was rotated with a period of 6 seconds so that variations with substrate orientation and/or probe position could be monitored.

5.1.2 Typical LLS results for substrate annealing with and without chamber outgassing

Figure 5.1 shows a plot of the laser light scattering intensity against time for one such substrate anneal and subsequent growth (of a substrate labelled M491). Initially, and on heating to approximately 600°VG, the intensity varied randomly with orientation with a 360° period. This was due to the surface being of a low roughness except for a number of inhomogeneties in the oxide layer and particles on the wafer surface which resulted in speckle. These dominated the LLS intensity distribution with orientation and resulted in the scattering intensity being dependant on the number and size of the scatterers as the beam scanned an annulus across the surface during the rotation. The variation of LLS intensity was therefore more dependent on the sampled position on the wafer than due to the directional orientation of the detected scattering. When the substrate was heated to approximately 600°VG (at time, t = 600s) the LLS intensity underwent a rise of a factor of approximately 2 x 10^3 over ~800s. The speckle pattern with orientation was also drowned out. The LLS intensity then levelled and reduced, with an increase in directionality, seen on the graph as a widening of the trace.

Thermal anneals on (001) GaAs substrates performed in an MBE chamber to remove the native oxide resulted in a sharp increase in LLS intensity a factor of about 10 (Smith et al. 1993), attributed to the development of pits due to supply of mobile Ga atoms from revealed holes in the oxide layer. Figure 5.1. show a much greater rise which is not abrupt but continues for around 800s. Cross-sectional TEM studies performed on layers

grown in our CBE chamber also show a dark line at the substrate epilayer interface assumed due to contamination. It is proposed that the morphology development observed by laser light scattering was due to contamination effects during the anneal. The rise appeared independent of the chamber pressure and it is suggested that the contamination was due to the desorption of previously deposited species from the cryopanel as a result of radiant heating from the substrate heater stage and the arsine cracker cell. Indeed when the substrate or arsine cracker cells were increased in temperature an increase in chamber pressure was observed.

To minimise substrate - surface contamination, prolonged outgassing of the cracker cell and substrate heater stage were carried out prior to the loading and annealing of the GaAs substrates. The substrate stage was held at 700°C overnight, with a Mo block in place of the substrate, and the cryopanel held at -60°C. The substrates were loaded with the substrate heater stage at 70°C, arsine cracker cell at 900°C and the cryopanel at -197°C. Substrate anneals carried out after such outgassing showed a sharp and relatively small (factors of 3 - 10) increase in LLS intensity.

Figure 5.2 shows the LLS intensity during a substrate anneal (of a substrate labelled M507) at ~600°C between times, t = 1105 and 3000s, performed after an outgassing procedure. As the substrate temperature was increased towards 700°VG the LLS intensity increased where there was no speckle, until at ~700°C the intensity underwent a step increase of approximately a factor of 3. This was followed by a slow partial recovery. The scattered light intensity still varied randomly with substrate orientation and position as the substrate was rotated. This suggests that inhomogeneties still dominated the scattering, but the rest of the surface was, although rougher than before, not oriented and the scattering was a function of probe position. The general trend of a step increase of a factor of three followed by a small recovery was similar to that reported in MBE (Smith et al. 1993).

The LLS intensity during the anneal of a substrate labelled M504 is shown in figure 5.3. The anneal was performed after an outgassing procedure. During the anneal the intensity rose with the characteristic of M507 (figure 5.2) except that the increase was not so sudden. Afterwards the intensity partially reduced but then slowly increased again to a value of around 300 times that before annealing. This suggests that the outgassing was only partially successful although the step change did occur, it was suppressed and followed by a slow intensity increase. The slow increase is not as great as in figure 5.1 and is delayed suggesting that the contamination was reduced to a level where the step change process occurs, and the outgassing did remove the most volatile contaminants from the cryopanel, since the rise was delayed. It does highlight that two different oxide removal processes can occur for clean and contaminated surfaces.

5.1.3 Summary of LLS results

The results of the laser light scattering studies are summarised in table 5.1. The 'outgassing procedure' column specifies the length of time, if any, that the outgassing procedure outlined in section 5.1.2 was used for. The previous growth column outlines the alloys that were grown in the previous growth run, but not thickness, to give some indication of the contaminants that were likely to have been present on the cryopanel during the anneal. Step change LLS development refers to any rapid changes that occurred at approximately 600°C, such as the step - increase observed in figure 5.2, and gradual LLS development features refer to slow LLS intensity changes over a time scale of minutes, factor intensity increases refer to the relative increase from the unannealed intensity level, and recovery (rec.) to a decrease in intensity towards the unannealed level. The overall growth features present are outlined in the right hand column as:

1, Rapid increases like that observed in figure 5.2;

2, Some recovery after a rapid increase;

3, A gradual increase in intensity as observed in figure 5.1, this may be after a rapid increase and recovery;

4, Some recovery after a gradual increase.

Sample label	Outgassing procedure time	layers grown on last substrate	Laser light scattering development features		Overall features present
			Step change	Gradual	
Without outgassing procedure					
M479	none	InGaAs, AlGaAs	none	>80x increase	3
M482	none	GaAs	none	~10x increase over 500s then small recovery plus directionality	3,4
M490	none	InGaAs	none	~10^4x increase over 1200s	3
M491	none	InGaAs	none	~10^3x increase over 600s then part rec. plus directionality	3,4
M492	none	InGaAs;S	none	10^3x increase over 700s	3,4
M500	none	GaAs;C, AlAs	~6x increase	part rec. then ~12x increase over 2000s	1,2,3
M501	none	InGaAs, AlAs	none	~10^4x increase over 700s then stable	3
M502	none	InGaAs, AlAs	~5x	part rec. then 100x increase over 1500s	1,2,3
M506'	none	GaAs	-	-	-
M517$^+$	none	GaAs, AlAs	none	~10^2x increase over 2000s	3
M518	none		none	~10^4x increase over 1000s, sharp 10 spike after 500s	3
M575	none	GaAs, AlAs	none	~10^2x increase over 1000s, started at 600°VG	3
With outgassing procedure					
M503	60 hours	InGaAs, AlAs	~6x increase	0.2x rec. then stable	1,2
M504	36 hours	InGaAs;S	~2x increase	part rec. then 4x 10^2x increase over 1200s	1,2,3
M505*	2 weeks	InGaAs;S	none	none	none
M507	12 hours	GaAs	~5x increase	~0.5x recovery	1,2
M515	12 hours	InGaAs, AlAs	none	4x 10^3x increase over 2000s with 3x increase spike	3
M523	24 hours	GaAs	~3x increase	partial recovery	1,2

M524	60 hours Mo only 300°VG	GaAs, AlAs	none	~10^3x increase	3
M543	18 hours	InGaAs	~4x increase	small rec.	1,2
M553	18 hours	GaAs, AlAs	~3x increase	none	1
M569	12 hours	GaAs;C	10x increase	none	1

* Anneal expected not to have removed native oxide

+ Anneal performed without As_2

' Semi-insulating wafer

Table 5.1: Laser light scattering results during the substrate annealing of 2" epi - ready (001) N+ substrates

From table 5.1 it can be seen that without outgassing previous to substrate loading into the growth chamber the anneal resulted in a range of behaviours, which do not appear to be dependant on the growth history of the chamber. The most universal and dominant feature was a gradual rise in LLS intensity (feature 3) of factors of 10^2 to 10^4 over a time period of approximately 1000s. Three of the substrates monitored then exhibited a decrease in intensity (feature 4) and a widening of the trace suggesting elongated islands developing (see section 5.2.2). The annealing of two substrates (labelled M500 and M502) resulted in a small rise followed by a recovery (features 1,2) before this gradual rise. This small rise is believed to be the characteristic rise of substrates annealed after outgassing, but inhibited due to contamination. The annealing of the substrate labelled M518 resulted in a large 10^4 times increase suggesting a large amount of contamination, and also a sharp 10 times spike in intensity which recovered in seconds attributed to substrate contamination by volatile species which then desorbed from the substrate surface.

Most substrates annealed after the outgassing procedure did not result in the gradual increase in LLS intensity. Of the three that did, the substrate labelled M504 exhibited a relatively small increase after the small rise, and the outgassing procedure for the

substrate labelled M524 involved only heating the substrate heater stage with the Mo block in place to 300°VG, which was not seen to be great enough to desorb contamination from the cryopanel previous to substrate loading. With the outgassing procedure the most common feature was the step change increase at approximately 700°VG (feature 1) as shown in figure 5.2. A decrease in intensity after this increase was sometimes observed.

During the annealing of a substrate labelled M505, no changes were observed in the LLS intensity. However a factor of 20 increase in intensity occurred during the first 25nm of growth of the GaAs buffer layer. This is believed due to the oxide layer not being removed by the anneal, and shows that LLS can determine whether the oxide layer is removed which should result in some intensity increase. Sample M517 was annealed without an As_2 flux. This resulted in a continuous increase of intensity but no directional development. Subsequent use of an As_2 flux resulted in a further increase which stabilised and the development of a 180° rotation period attributed to directional features. The result shows that the anneal should be performed under an As_2 flux to produce a good surface morphology.

Table 5.1 shows the outgassing procedure to have a fair success rate in eliminating the gradual rise attributed to substrate contamination due to desorption from the cryopanel of volatile species from radiant heating of the substrate heater stage.

A secondary ion mass spectroscopy study of six samples of those described in table 5.1 was performed by A. Chew of Loughborough consultants to identify substrate - epilayer contamination resulting from the anneal which were responsible for the large increase in LLS intensity. The analysis was performed using Cs+ bombardment and negative ion detection to optimise the sensitivity to C, O and S. Samples were left under vacuum overnight to reduce background levels of C and O. The samples were analysed at the

same rate so allowing a direct comparison of concentration and count rate. The data were taken sequentially and averaged so the interface concentration will be a lower limit.

Figures 5.4 and 5.5 show the SIMS profile for samples M501 and M503 respectively for substrates annealed without and with previous outgassing procedures respectively(see table 5.1). The substrate - epilayer interface is at the right of each graph, at time, t = 1200s on figure 5.4 and at time, t = 1900s on figure 5.5. The substrate - epilayer spike maximum concentrations were measured for carbon, oxygen, sulphur, aluminium and indium. These are shown in table 5.2 for the six samples analysed. The first layer grown on substrate in each case was a GaAs buffer. This buffer was not intentionally doped for samples labelled M500, M501, M502 and M506, and doped with sulphur at approximately 3x 10^{19} cm^{-3} for M503 and 1x $10^{19}cm^{-3}$ for M504.

Sample label	Spike concentration/ Atom cm^{-3}			Spike height/ Counts	
	C	O	S	Al	In
Without outgassing procedure					
M500	6 x 10^{19}	6 x 10^{19}	1 x 10^{18}	8 x 10^{2}	1 x 10^{2}
M501	3 x 10^{19}	9 x 10^{19}	6 x 10^{17}	4 x 10^{2}	9 x 10^{0}
M502	5 x 10^{19}	7 x 10^{19}	7 x 10^{17}	6 x 10^{2}	4 x 10^{1}
M506	9 x 10^{18}	1 x 10^{19}	3 x 10^{17}	6 x 10^{1}	no spike
With outgassing procedure					
M503	1 x 10^{19}	5 x 10^{18}	no spike	no spike	6 x 10^{0}
M504	4 x 10^{19}	5 x 10^{18}	no spike	no spike	3 x 10^{1}

Table 5.2: Summary of SIMS results on the substrate epi - layer contamination.

From table 5.2 it can be seen that the outgassing procedure results predominantly in the removal of Al and S contamination and a small decrease in O contamination. Al containing layers typically have higher S and O concentrations than GaAs due to the higher affinity of Al to these elements, so it appears that the main contaminant responsible for the large LLS intensity increase is Al. Al spikes are commonly observed in MBE, MOVPE and CBE grown substrate - epilayer interfaces profiled by SIMS (Joyce 1993). No difference was detected between the sample labelled M503 and the sample labelled M504, even though annealing of the sample labelled M504 resulted in a gradual LLS intensity rise (figure 5.3). The rise may have been due to levels of carbon in the samples being below the background level detected by SIMS.

5.1.4 Atomic force microscopy results

To investigate the morphological development responsible for the laser light scattering intensity changes during the pre - growth anneal two samples were annealed and the resulting surface morphology observed by atomic force microscopy without growth of an epilayer. Atomic force microscopy was performed in ambient conditions within one hour of removal from the ultra - high vacuum system to minimise native oxide growth and surface contamination. Adjacent wafers, from the same boule, were investigated to improve conformity of results.

Figure 5.6 shows an AFM plot of the surface morphology of an as received epi - ready wafer. The morphology was composed of islands approximately 30nm in diameter and approximately 1nm in height. A number of depressions were present between the islands

Figure 5.7 shows the surface morphology of a substrate (labelled M569) annealed with overnight outgassing previous to substrate loading. The morphology was dominated by a near random distribution of shallow pits up to 7nm in depth, of density approximately

$10^{14}m^{-2}$, and size approximately 50nm shown as dark areas in figure 5.7. These pits were formed during the substrate cleaning and their origin is discussed in section 5.1.5. The island structure seen in the epi - ready substrate was still present around the pits.

Figure 5.8 shows the surface morphology of a substrate (labelled M575) annealed without outgassing previous to substrate loading. A much larger lateral scale dominated with no large density of pits, or small (approximately 40nm diameter) islands. The morphology was of islands of size approximately 1μm in diameter and up to 3nm in height. A small number of the largest islands also contained faceted pits, approximately 100nm in diameter and up to 25nm deep, at their apex.

An Auger electron spectroscopy (AES) study was undertaken on the two annealed substrates after ~1 hour under ambient conditions. The Al and other contaminant levels were below the background level for both substrates loaded into the CBE growth chamber with and without previous outgassing of the chamber. All that was detected was Ga and As above the instrumental and chamber background detection limits. This does not show that there was no Al present but that if any only a few monolayers at most were present.

5.1.5 Discussions

The SIMS results show that the main effect of the outgassing procedure is to drastically reduce the levels of Al and S contamination and slightly reduce the O level at the substrate - epilayer interface. The main culprit of the large rise in LLS intensity during the anneal and change in morphology without the anneal is thus Al, since Al is known to getter S and O and its presence would increase the adsorption of S and hinder the desorption of O. The contamination of Al was predominantly due to desorption of previously deposited Al containing compounds from the cryopanel surface. With a heated Mo block in place,

altering the substrate orientation caused increases in chamber pressure, so it is believed the heating and desorption only occur from a localised area of the cryopanel. The heating of the cryopanel leading to the contamination is predominantly due to radiant heating from the substrate heater stage and is mainly from radiation from the heaters themselves, as the substrate is only absorbent to part of the black body radiation output spectrum from the heaters. Annealing of substrates of higher band-gap compounds such as InP, or substrates with a lower doping level, would be expected to result in more contamination since they are less adsorbing to the heater radiation and would increase the thermal load on the cryopanel.

With a successful outgassing procedure the LLS and AFM results show a gradual small increase in LLS intensity as the substrate is heated between ~550°C and ~600°C. This increase is consistent with the slow desorption of reduced oxide. The oxide removal is slow because either the Ga diffusing to the surface to react with the (involatile) native oxide (to result in the volatile Ga_2O), or volatile Ga_2O reaction product having to diffuse through the layer after reaction at the substrate oxide interface. The oxide thickness reduces with time until holes are revealed through the oxide layer. These holes will occur at the areas of the oxide layer that were thinnest before the anneal. The height variation for an oxide of thickness 1 - 2nm thick was only ~1nm, suggesting that the depressions, up to 7nm in depth, observed after annealing (with the outgassing procedure), are not present before the annealing in the substrate - oxide interface. This is supported by a much reduced pit density observed after the desorption of oxide from a deliberately re-oxidised epilayer (Smith et al. 1993), since the oxide would be of much more even thickness, and the majority of the oxide would reduce and desorb by the above process before holes are revealed.

The step increase in LLS intensity appears to occur as holes in the native oxide layer, which is not of uniform thickness, appear. The increase in LLS intensity is consistent

with the model proposed by Smith *et al.* (1993) where exposed gallium atoms surface migrate to the native oxide at the edges of the holes and reduce the native oxide to a volatile oxide which desorbs. The holes thus become pits as they supply Ga. The locations of the pits will be related to the morphology of the initial oxide, and their size related to the oxide thickness. Once the holes are revealed due to variations in the initial native oxide layer the reaction is activated due to the much faster surface diffusion of Ga from inside the pit to the pit edge than the diffusion through the oxide layer. The small island morphology still remains as shown on figure 5.7 although it probably was not present on the underlying GaAs substrate previous to oxide desorption. This is suggested due to the hole development. The holes form at depressions where more than two islands meet. As the hole enlarges Ga is reacted from the bare GaAs surface, and the rate of lateral enlargement will be dependant on the oxide thickness, thus the holes will enlarge most rapidly along the intersections between adjacent islands and slowest into the islands, as shown schematically in figure 5.9. The island intersections will tend to be exposed before areas further into the islands and will provide Ga to the centres of the islands as shown in figure 5.9c . Thus the areas of thinner initial oxide thickness will be lower that those of thicker. The morphology of the epi - ready substrate, due to inhomogeneities in the native oxide layer thickness, is exaggerated on the substrate surface during the anneal because of the four atoms of Ga required to reduce one molecule of Ga_2O_3 to Ga_2O. The points at which the holes were first revealed will be deep pits due to the longer time of exposure before all oxide is removed. After the oxide desorbs a decrease in LLS intensity is sometimes observed due to thermal annealing resulting in partial smoothing of the surface.

Without a successful outgassing procedure the deposition of Al onto the substrate surface with the presence of O resulted in the development of islands. The observation of Al contamination at the substrate - epilayer interface without chamber outgassing previous to substrate loading is supported by laser reflectometry intensity oscillations observed from

the interface on growing GaAs on a GaAs substrate with phase (i.e. growth of GaAs resulted in reflectivity oscillations with an initial increase in reflectivity) suggesting a material of lower refractive index (Joyce, private communication). Samples held at 600°C after growth of an epilayer did not result in any increase in LLS intensity even after growth of epilayers containing Al, so the roughening was dependent on the presence of the oxide layer also. Aluminium has a much greater binding energy with oxygen and S, and the presence of Al on the surface would act as a getter for these contaminants, and result in poor morphology. Also it appears that the presence of Al prevents the native oxide removal by the above mechanism of hole formation and Ga surface migration and reaction with the native oxide, since the step change, observed in LLS intensity with the outgassing procedure, is not observed in the worst cases. It is not obscured by the greater increase in intensity due to the islands but simply does not occur. In some cases the step increase does occur followed by a gradual increase, but the step increase is always smaller and less abrupt than when occurring alone. The presence of Al or other contaminants inhibits the pit formation by a number of possible mechanisms: possibly by reducing the Ga surface diffusion to the hole edge to react with the native oxide; or to inhibit the reaction; or to provide another reaction which dominates.

The large increase in LLS intensity appears due to another process occurring than the surface migration of Ga from revealed holes to reduce the native oxide. The results are consistent with a model in which a thin Al containing film forms on the surface and reacts with the native oxide substituting some of Ga for Al. The oxide is then no longer pure Ga_2O_3 but contains Al. After much of the oxide desorption the AlGaAs resulting substrate surface contains large O and S impurity concentrations then roughens with time as does the growth of AlGaAs with large ($>10^{18}cm^{-3}$) O impurity levels. The LLS intensity increase occurred at various times during the anneal due to the amount of volatile Al containing species on the cryopanel and their volatility. If less volatile or buried species were only present then it would have taken the substrate heater longer to desorb

them. This would have resulted in the increase being delayed, and the pit formation process not completely inhibited. It may have also resulted in a lower LLS increase because of a reduced level of contamination and the contamination occurring when less oxide was present. A small density of faceted pits up to 25nm deep were observed on some of the largest islands perhaps due to a migration process similar to the pit formation without the Al contamination.

AFM has shown that the mean height of the roughness was not considerably different with or without the outgassing procedure. The dramatic difference between final LLS intensity with and without outgassing was due to the nature of the roughness. Without the outgassing procedure annealing resulted in an island morphology with a mean size of approximately one micron. Using the smooth surface approximation (Church et al. 1979), the LLS geometry used would result in a maximum sensitivity to roughness of period 1.31 microns and the intensity would be proportional to the height squared of the Fourier component of the roughness with that period. The mean island size was near this value and thus the LLS was very sensitive to development of these islands. Orientation dependence was due to a variation in island periodicity resulting in a larger component at that period which the LLS is sensitive to. With the outgassing procedure annealing resulted in a near random distribution of pits. The pits arrangement had no dominant periodicity, and thus from the shot model (Church et al. 1979), the LLS intensity was the sum of the scattering from each individual pit. The overall LLS intensity resulting from the vertical depth of the pits was much less than for the development of islands of similar vertical height, but of period corresponding to the sensitivity of the LLS geometry.

5.2 Growth of GaAs and AlGaAs

5.2.1 Morphology changes during the growth of GaAs and AlGaAs

The morphological development of GaAs and AlGaAs epilayers grown on GaAs substrates was found to be dependent on the morphology of the substrates. The LLS intensity during the growth pre-growth anneal and subsequent growth of GaAs, AlAs and also InGaAs (which will not be discussed here) is shown in figure 5.10. During the GaAs and AlAs growth the substrate temperature was 510°C, group III flux was 1.5 x 10^{15} atoms/cm^2/sec, and the group V flux was 6 x 10^{15} As_2 dimers/cm^2/sec. The onset of GaAs growth resulted in a small increase followed by a decrease in scattered light intensity over about 30nm. The increase was not observed in all traces and may have originated from initial surface roughening due to small levels of contamination or oxide on the surface lowering the substrate surface energy and resulting in some areas of Volmer -Weber 3D growth. However the increase is small relative to other effects observed so any island development probably wasn't dominant. Alternatively the increase may have been as a result of surface roughening from a growth transient, or may have been due to a change in refractive index, due to a temperature fluctuation or change in reflectivity. The decrease was observed on most growths (after chamber outgassing), although some which exhibited a partial recovery of the step change during annealing (e.g. M523) did not. The decrease whether during growth or during the annealing was due to the filling of the pits described in section 5.1.4. The pits were not observed by AFM on any sample after growth. This dip is followed by a steady rise and widening of the trace during GaAs and AlAs growth as islands a few monolayers high develop on the surface, elongated in the $[\bar{1}10]$ direction. These islands were of typical dimensions 350 x 250 nm as shown by AFM, figure 5.11. The oscillations in intensity during the AlAs layer growth and subsequent GaAs were due to interference, not any change in surface morphology.

When annealed without the outgassing procedure, or without sufficient outgassing to reduce the contamination significantly, the substrate already contained islands on the micron scale up to tens of atoms in height. Figure 5.12 shows the LLS intensity during the anneal of M524 during the anneal and subsequent growth of GaAs and AlAs epilayers, without a sufficient outgassing procedure. The first few monolayers of epilayer growth resulted in a slight increase followed by a decrease in scattered light intensity over the first ~25nm of growth. This was presumably due to the first few monolayers adding to the islands, followed by some smoothing, including the filling of the pits observed. However the growth did not completely smooth the surface and the decrease was followed by a slow increase, and an increase in island directionality with further development of a $\sin^2(\varphi)$ characteristic with substrate orientation φ, due to island elongation in the $[\bar{1}10]$ direction. The islands formed during the anneal were thus of too large a scale to smooth out during GaAs and AlAs epitaxial growth.

The scattered light intensity from a surface, at a constant angle from the normal at which light is incident, as the surface is rotated with respect to the detector is a function of the scattered light intensity from individual scattering centres, the number of centres and the spacial distribution of the centres. The large scale (radar equivalent) model (section 3.3.2) states that the scattering from each centre is dependent on on the size of the 'facet' oriented with a normal half way between the incident beam and the detection direction, taking account of the angular reflection spectrum which itself is dependent on the facet size. However, the elongated islands discussed above have, on a large scale, no facets oriented at ~11°, since their height is only a few nm and their lateral dimensions of the order of a micron. Thus it will be assumed that the scattering is from surface steps, and the scattering is proportional to the circumference of the island (or step upon it) oriented within a small angle (~1°) from the detector in the plane of the surface. If $(r_{max} - r_{min})$ $r_{min}) << 1$ the elongated islands lateral radius, r, can be approximated to $r = r_{min} + ((r_{max}$

- r_{min}) $\sin^2(\varphi-\pi/4)$, where r_{min} is the island radius in the [110] direction, r_{max} is the island radius in the $[\bar{1}10]$ direction and φ the angle of the detector from about the [100] direction. The width of the steps oriented with a normal to the line direction within a small angle of φ will be proportional to the local radius of curvature of the segment oriented normal to the scattering, and the scattering from each island will be approximately proportional to $r_{min} + ((r_{max} - r_{min}) \sin^2(\varphi+\pi/4))$. The number of scattering centres, N, will be constant with rotation, since the probe area is constant, but the period of the centres will vary, resulting in variation of the diffraction of the light scattered between the centres. If the distribution of centres was random then the scattered light intensity would be the sum of the scattering from each centre and thus proportional to $1/(r_{min} + ((r_{max} - r_{min}) \sin^2(\varphi+\pi/4))$. However the distribution will not be random since the islands are touching and there will be some periodicity. The separation of the islands, and the distribution of islands in the detector direction (φ) will be a function of the radius in the direction φ. The light scattering at an angle θ from the normal will be a function of the peridicity at a particalar lateral wavelength (given by equation 3.14) and the number of scattering centres. It will therefore be a function of the mean island spacing, and thus a function of $r_{min} + ((r_{max} - r_{min}) \sin^2(\varphi-\pi/4)$ and N. The function will be dependent on the periodicity of the islands. The laser light scattering from the surface will therefore be a complex function including $\sin^2\varphi$.

5.2.2 Laser light scattering interference oscillations

Intensity oscillations are seen in both LLS and normal incidence laser reflectometry (also known as laser interferometry and DOR) during growth of layers of differing refractive index. The intensity oscillations in LLS and laser interferometry were compared by simultaneously monitoring of the growth of an AlAs λ/4 thick layer followed by a thick (>400 nm.) GaAs layer, shown in figure 5.13. The growth of the AlAs layer was terminated after half an interference oscillation in the laser interferometry trace and GaAs

growth was started. The interference oscillations have the same period, since the light diffusely reflected and transmitted within the structure and then detected by the scattered light detector will be only a few degrees from the normal, and thus will have similar path lengths to the normal. The LLS oscillations are of a lesser amplitude, possibly due to destructive interference between light scattered in transmission through the growing surface, scattered reflection from the interface, and scattered in transmission through the growing surface on leaving the structure after specular transmission through the surface and specular reflection off the interface. Smoothing of the surface may have resulted in the ratio of diffuse reflection from the surface to that at the interfaces being less than in the DOR trace, which would result in a reduction of amplitude. However this would also result in a decrease of the mean level which was not observed.

Large changes in surface morphology were observed as large changes to the scattered light intensity. These were observed during oscillations as changes in both the mean level of the oscillation and the amplitude of the oscillation. The change in surface scattered light intensity from the surface resulted in the mean level of scattered light intensity being altered, since a change in 'apparent substrate reflectivity' was detected by LLS. This change in 'apparent substrate reflectivity' results in a change to the ratio of scattered light detected from the surface and interface, and the change in mean level will also result in a different oscillation amplitude, thus exaggerating any instantaneous scattered intensity change. If the mean level were to cross the value of the underlying interface then the oscillations would go out of phase with that previous.

5.2.3 Discussions

The micrometre scale islands formed during substrate anneal without chamber outgassing previous to substrate loading were not smoothed during growth. However features on a smaller scale of below 100nm , such as the pits which evolved during anneals with

chamber outgassing were smoothed during the first tens of monolayers of growth. The smoothing of these pits is consistent with that reported in MBE, along with the initial small transient increase during the first few monolayers (Smith *et al.* 1993). They however found the slow increase in LLS intensity which followed, to be due to the development of a ridged, aligned surface steps, whereas this study found the development of two dimensional islands a few monolayers high.

The LLS results suggest that the growth occurs initially in a layer by layer manner by the nucleation of 2D islands accompanied by smoothing of small scale features. These 2D islands elongate due to the higher lateral growth rate in the $[\bar{1}10]$ direction than the $[110]$ direction. This anisotropy in growth rate is due to differences in adatom diffusion, probably originating from the aligned As_2 dimer pairs in the $[\bar{1}10]$ of the (2 x 4) surface reconstruction or incorporation efficiency on the different oriented surface steps as observed in MBE growth of GaAs (Shitara et al. 1992). The similarity of using TEG to elemental Ga in MBE suggests that Ga, not TEG or a metalorganic dissociate compound such as DEG, may possibly be the diffusing and surface step incorporating species in CBE. However Isu et al. (1992) has shown that the activation energy of the diffusion length in CBE, and thus the diffusion length, are dependant on the group V source, As_2 in this study and in the reported MBE results, and not on the group III source although the surface diffusion length was longer than using atomic Ga. It thus seems that the anisotropy is wholly due to the arsenic surface coverage, which may effect both the relative diffusion length and the sticking coefficient at surface step edges, since the orientation of the step edge will effect the surface composition and charge of the step. This is supported by LLS results such as figure 5.12 which shows elongation during both GaAs and AlAs growth at approximately the same rate.

The large scale islands formed during the pre-growth anneal without chamber outgassing previous to substrate loading, were not completely smoothed because they were of a

larger lateral scale than the pits. The scale was large enough that, after the initial smoothing the surface diffusion length of the arriving species was not greater than the step separation. An energy barrier to adatom migration down the surface steps may have also contributed. The dominant growth mode during GaAs and AlAs epitaxy on the island dominated surface was probably step flow but the step separation was great enough to prevent significant smoothing. As the steps moved, due to growth they would eliminate in the troughs but 2D islands nucleated on the tops of the islands to maintain them. Orme et al. (1993) suggested that there was competition between step flow and nucleation which favours nucleation at the top of the islands when the top surface is greater than the diffusion length or there is a step edge barrier. A density of surface steps is required for step flow growth. The growth of GaAs and AlAs in this study resulted in maintaining the island height independent of height at the same lateral size, strongly suggesting the presence of a step edge barrier stopping the motion of admolecules off a terrace to incorporate in a lower step. The barrier could not have been wholly responsible since smaller lateral features such as the pits were smoothed in the first tens of monolayers. If the wafer was sufficiently off-cut from the (001) plane to provide a large number of aligned terraces the large islands may have been smoothed since the islands on the substrate or after some growth may have had the form of variation in terrace width. The elongation of the islands was for the reasons put forward in the last paragraph.

LLS is thus most sensitive to the lateral scale of roughness which is dominant in CBE growth of GaAs and AlAs. RHEED oscillations (previously taken by Dr. T. Joyce, not shown) suggest 2D growth but LLS and AFM have shown the presence of islands a number of monolayers high. RHEED is sensitive to roughness on the atomic scale, but not on the micron scale where islands may be present as was suggested by Orme et al. (1993). LLS is thus shown to be a useful technique for the monitoring of GaAs and AlAs epitaxy. Interference oscillations during the growth of multilayer structures can be observed as in laser interferometry with the same period, demonstrating LLS as a feasible

technique for measurement of growth rate. The amplitude of the oscillations is not only dependent on the refractive index difference between layers, but also on the development of surface topography. Thus care should be take in attempting to calculate compositions from LLS interference oscillations.

5.3 Low compressively strained layer growth: $In_xGa_{1-x}As$ (x<0.25) on GaAs

It is well known that a 'cross-hatch' pattern develops on the surface of strained epitaxial layers which have achieved significant relaxation by the introduction of misfit dislocations (Olsen, 1975). The critical thickness d_c, for which it is energetically favourable for misfit dislocations to be present can be approximated to the empirical relationship $d_c = (0.2 \pm 0.1) / \varepsilon_0$ nm (Dunstan *et al.*, 1991). The onset of significant relaxation occurs as predicted by the empirical relationship $d_{cr} = (0.8 \pm 0.1) / \varepsilon_0$ nm, where h_{cr} is the 'significant relaxation critical thickness' for a layer of misfit ε_0. This relationship was determined from double - crystal X-ray diffraction studies of $In_xGa_{1-x}As$ layers grown on GaAs by a variety of techniques (Dunstan *et al.*, 1994). This relaxation starts at a well defined thickness approximately 4 times the 'critical thickness, that the first misfit dislocations appear.

5.3.1 Laser light scattering results

LLS was used to study the growth of $In_xGa_{1-x}As$ ($x \leq 0.25$) layers grown on GaAs by CBE. Substrate rotation with a period of 6 s was used during normal data acquisition at a rate of around 20 data points per second, resulting in a data point every 3° or so in angular orientation. A typical trace for the growth of InGaAs on GaAs is shown in figure 5.14. As soon as InGaAs growth commences the islands elongate further in the $[\bar{1}10]$ direction as shown in an expansion of the trace, figure 5.15a. At a thickness of ~110nm,

the cross-hatch emerges, resulting in sharp peaks of LLS intensity when the substrate is aligned within a few degrees of the <110> directions (figure 5.15b).The onset of the cross - pattern measured from such traces is shown with the critical thickness and the onset significant relaxation relations in figure 5.16. The onset of the cross - hatch pattern coincides with the onset of the significant relaxation and suggests a strong link between them.

5.3.2 Atomic force microscopy results

The cross-hatch patterns appeared to the eye and in NOM as sharp lines in both directions, but both are not truly representational methods. AFM was used to quantitatively study the surface topography of the cross-hatch. Figure 5.17 shows an AFM plot of the surface of a 170nm thick $In_{0.1}Ga_{0.9}As$ layer (about 1.5 times the thickness for the onset of significant relaxation). This shows the cross-hatch to consist of directional troughs and ridges a few monolayers high running in the $[\bar{1}10]$ direction. Figure 5.18 shows an AFM plot of a 100nm thick $In_{0.2}Ga_{0.8}As$ layer (approximately 2 times the thickness for the onset of significant relaxation) showing alignment in both the $[\bar{1}10]$ and $[110]$.directions.

5.3.3 Discussions

Celii et al. (1993) suggested that the cross-hatch is due to the formation of atomic steps on the surface due to the generation of dislocations. However the AFM studies of the surface topography show that the pattern is not composed of slip lines running in the <110> directions, but of aligned ridges on the surface. Dr. R. Beanland shown that the spacing was an order of magnitude greater than the misfit dislocation spacing (Beanland and Boyd, 1995).

It is most probable that the cross-hatch pattern is primarily caused not by the introduction of a large density of surface steps produced by dislocation glide, although this may have some effect, but by a locally varying strain field at the surface which will alter the local growth rate when dislocations are present (Fitzgerald,1991). Once started the cross hatch would auto-accelerate somewhat due to elastic strain relaxation in the hillocks further increasing the growth rate at their apex relative to the troughs. Since the onset of the cross-hatch coincides with the onset of significant relaxation and not the critical thickness, at least as detected here, it seems likely that the cross-hatch requires a large number of dislocations to form, perhaps due to variations in dislocation spacing. However it has been found (Beanland, 1992) that at the onset of significant relaxation around 10% of dislocations exist above the InGaAs - GaAs interface. It is suggested that these dislocations existing above the interface have a greater effect on the local surface strain field and thus the development of the surface cross-hatch pattern. It has been calculated that the minimum thickness for a dislocation generation source involving an internal dislocation to operate is approximately $4h_c$ (Beanland, 1992).This is that measured as the onset of significant relaxation (Dunstan *et al.* 1994) and the surface cross-hatch pattern by this study. It thus is suggested that these internal dislocations play a large role in the significant relaxation and the development of the cross-hatch. LLS is thus demonstrated as a valuable technique for monitoring the growth of InGaAs on GaAs, and was used to grow layers just above the thickness corresponding to significant relaxation.

5.4 High compressively strained layer growth: InAs on GaAs

The development of surface topography during the initial stages of InAs (on a thin unrelaxed layer of $In_{0.1}Ga_{0.9}As$) on GaAs growth was monitored in real time using LLS. Figure 5.18 shows the development during growth at 0.028nm/s growth rate, from the flux set-point and a group V/ group III flux ratio of 50. The growth rate was kept low so

that a large number of data could be acquired per monolayer, but this may not have been necessary. At this line pressure an offset in flux is suggested, from measuring InGaAs compositions using this value, which may have resulted in the growth rate to be around 0.8 times that quoted above, and thus thicknesses in figure 5.19 may be around 25% too great. The growth rate was not monitored, but the validity of LLS is not affected. The breaks in the data were instrumental. Growth resulted in no change of scattered light intensity for 1nm of growth followed by a rise by a factor of 5 over the proceeding 1.5nm. This was followed by a broadening of the trace with angular orientation and a gradual rise. The initial 1nm of growth was pseudomorphic. The increase over the next 1.5nm was due to the surface forming islands. The gradual rise and increase in directionality was due to coalescence of adjacent islands to form larger directional islands which develop in preference to the original islands. This was shown by Nabetani *et al.* (1995) to be due to misfit dislocation introduction reducing the strain in the large islands. The presence of the two sizes of islands is shown by AFM in figure 5.20, of the final surface after the growth. Small approximately 40nm diameter islands are seen 2nm in height, along with a number of large directional island of various sizes but typically 100nm diameter and 6nm in height. Smooth areas are shown between some islands No change in LLS intensity was observed after growth presumably to the slow growth rate.

LLS is shown to be very sensitive to the development of the 3D islands during the growth, showing continuous changes during each monolayer deposition, and would be suitable for stopping growth at the point when separated small islands are present, before coalescence. These islands have been suggested to be a potential method of forming self organised quantum dots or disks.

5.5 Summary of chapter

LLS has been demonstrated to be a valuable in-situ monitoring technique since it is relatively simple to set up, and is compatible with most growth techniques. It gives valuable information on the surface topography at a scale which usually dominates growth, and which is related to surface processes. Orientation information is achieved by substrate rotation during normal data acquisition. Interference oscillations are also exhibited for epilayers of differing refractive index, as in specular laser interferometry (DOR), making LLS suitable for monitoring the growth of optically active structures.

It has been shown that pre-growth annealing epi-ready substrates can result in the development of an island morphology that is maintained during growth. The islands are around 1μm in lateral diameter and a few nm in height, and are associated with substrate-epilayer contamination due to desorption of previously deposited species from the cryopanel as a result of radiant heating from the substrate stage. By outgassing the substrate heater stage and the arsine cracker cell for a few hours before substrate loading the interface quality can be improved to that seen under clean MBE conditions. Surface pits are then observed as in MBE up to 6nm in depth but less than 100nm across. These pits fill during growth of GaAs to leave a surface dominated by islands a few monolayers in height and around 1μm across. Growth of GaAs leads to an initial reduction in scattered light intensity due to smoothing but the islands remain and elongate, observable by LLS as a broadening of the trace due to a $\sin^2(\varphi)$ intensity relation with substrate orientation (of angle φ).

Growth of $In_xGa_{1-x}As$ ($x \leq 0.25$) epilayers on GaAs result in the development of a 'cross-hatch' pattern of ridges aligned along the <110> directions, at the onset of significant relaxation. The scattering is caused by the ridges, not the dislocations themselves, and they are identifiable by LLS as sharp spikes when, during rotation, the

scattered light detector is aligned along each <110> direction. This demonstrates LLS as a suitable technique for detecting the presence of significant relaxation, although direct correlation to the level of relaxation was not produced. It is suggested that the directional ridges are due to the presence of a laterally varying strain field altering the local growth rate, primarily due to misfit dislocations lying above the GaAs - $In_xGa_{1-x}As$ epilayer interface.

Laser light scattering has been demonstrated sensitive to the pseudomorphic to island growth transition during high misfit (7.2%) InAs on GaAs heteroepitaxy. The transition results in an increase in scattered light intensity after ~1nm of a factor of around 5 over 1.5nm. Coalescence of the islands is observed as a more gradual increase. LLS is thus suitable for monitoring the formation of self organised islands, also referred to as quantum dots or discs when buried in GaAs or AlGaAs.

correlation to the level of relaxation was not produced. It is suggested that the directional ridges are due to the presence of a laterally varying strain field altering the local growth rate, primarily due to misfit dislocations lying above the GaAs - $In_xGa_{1-x}As$ epilayer interface.

Laser light scattering has been demonstrated sensitive to the pseudomorphic to island growth transition during high misfit (7.2%) InAs on GaAs heteroepitaxy. The transition results in an increase in scattered light intensity after ~1nm of a factor of around 5 over 1.5nm. Coalescence of the islands is observed as a more gradual increase. LLS is thus suitable for monitoring the formation of self organised islands, also referred to as quantum dots or discs when buried in GaAs or AlGaAs.

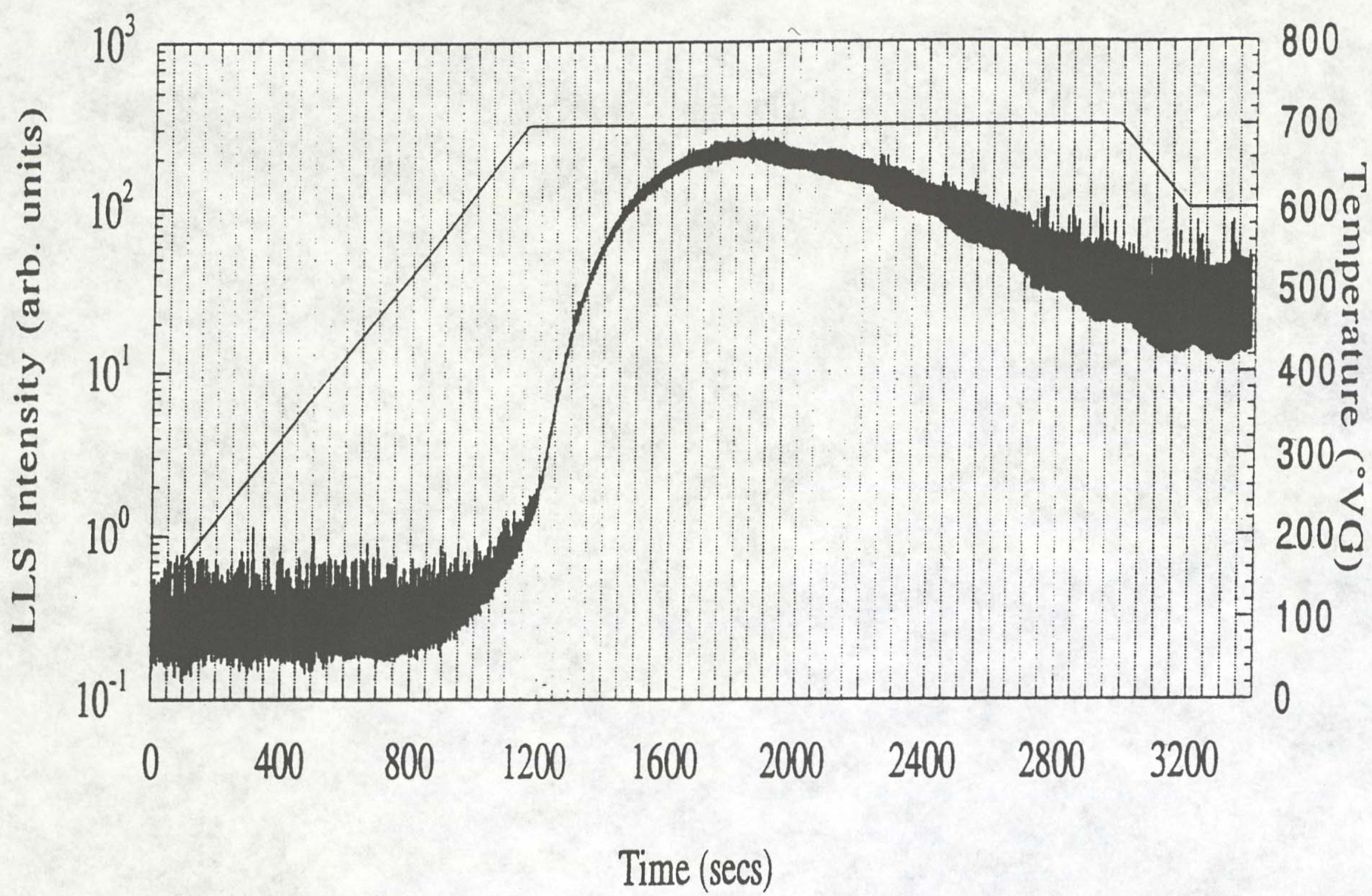

Figure 5.1: Plot of LLS intensty with time for a substrate anneal, without an outgassing procedure.

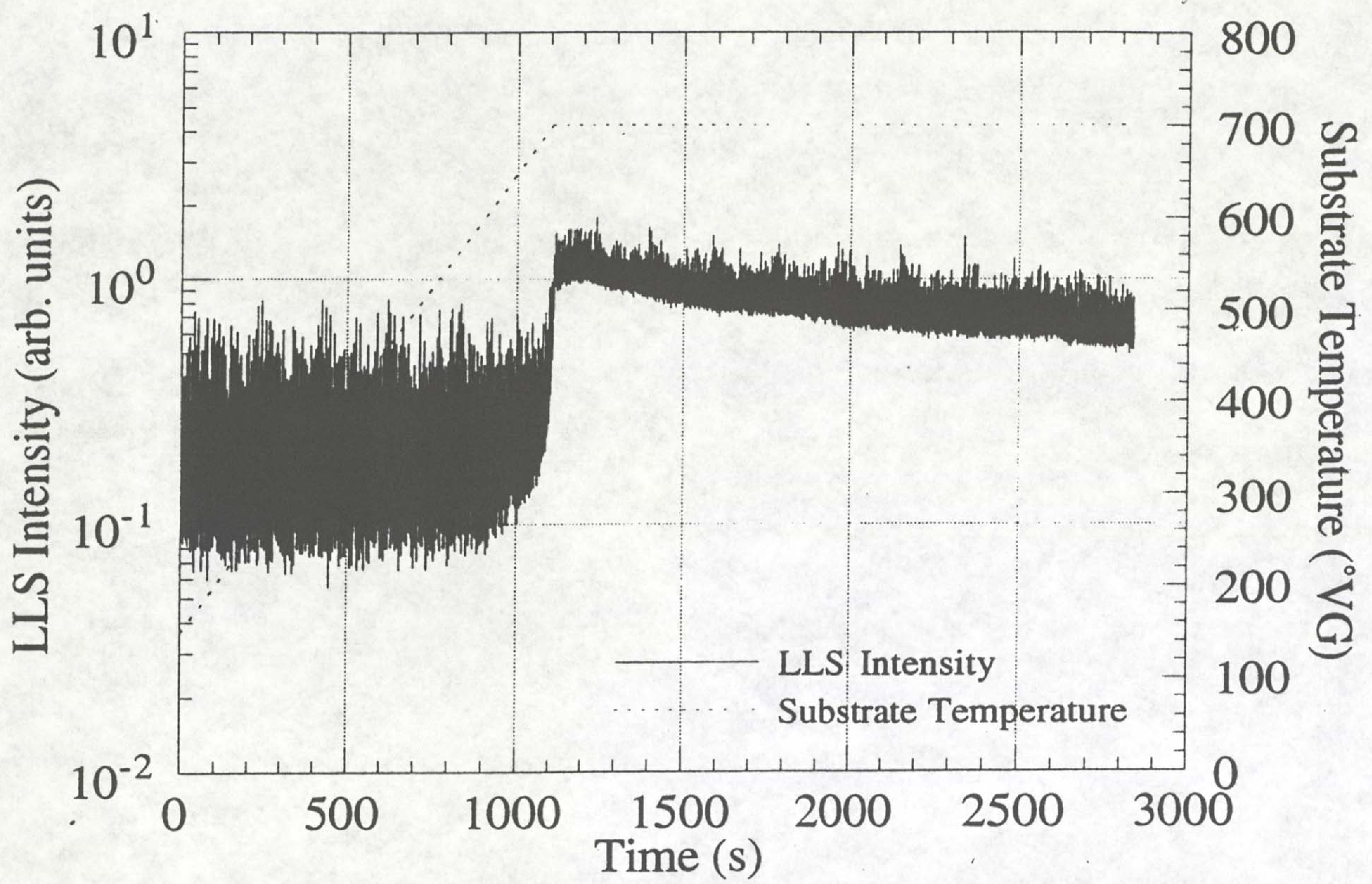

Figure 5.2: Plot of LLS intensity with time for a substrate anneal, with an outgassing procedure.

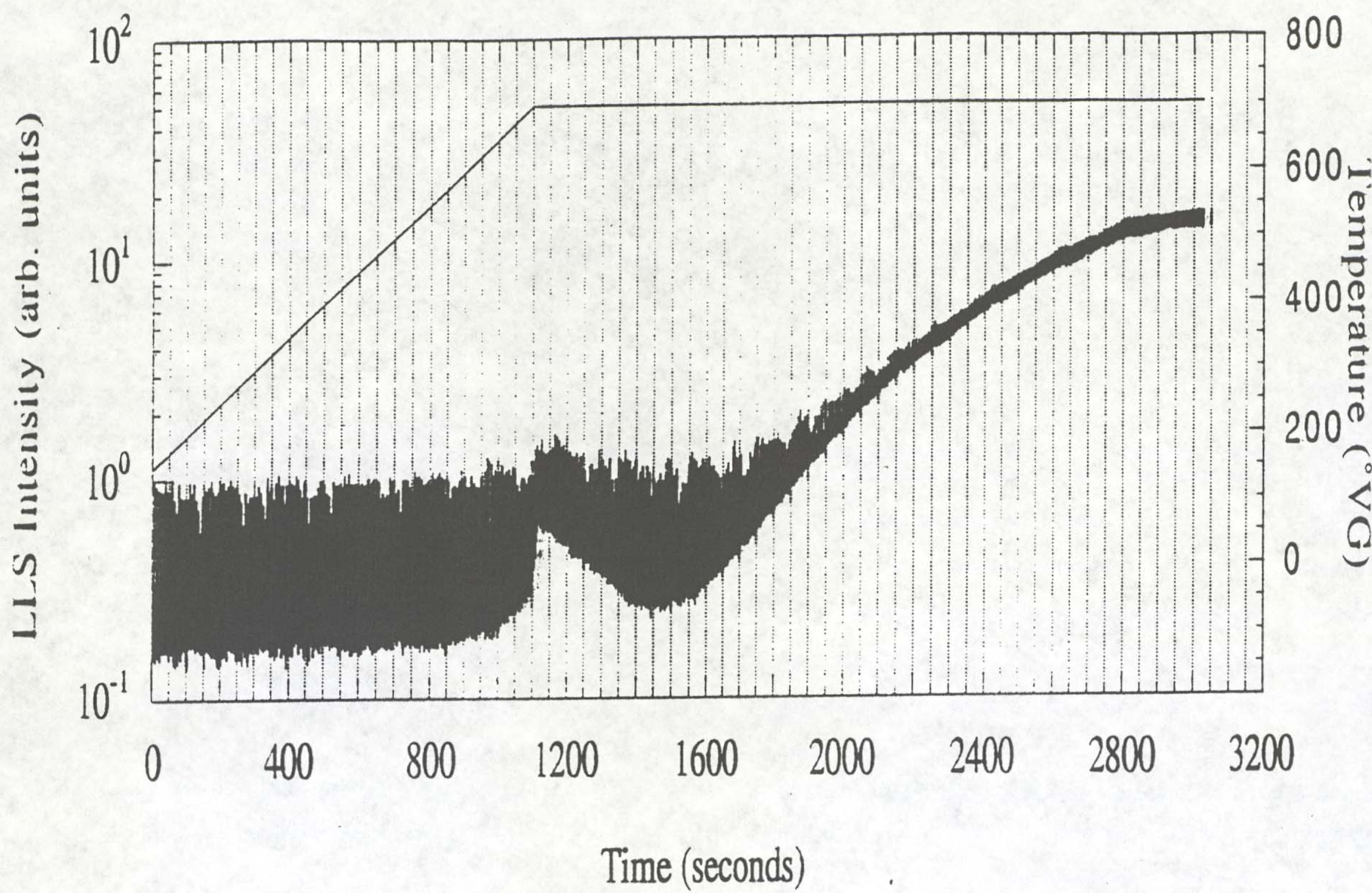

Figure 5.3: Plot of LLS intensity with time for a substrate anneal, with an unsuccessful outgassing procedure.

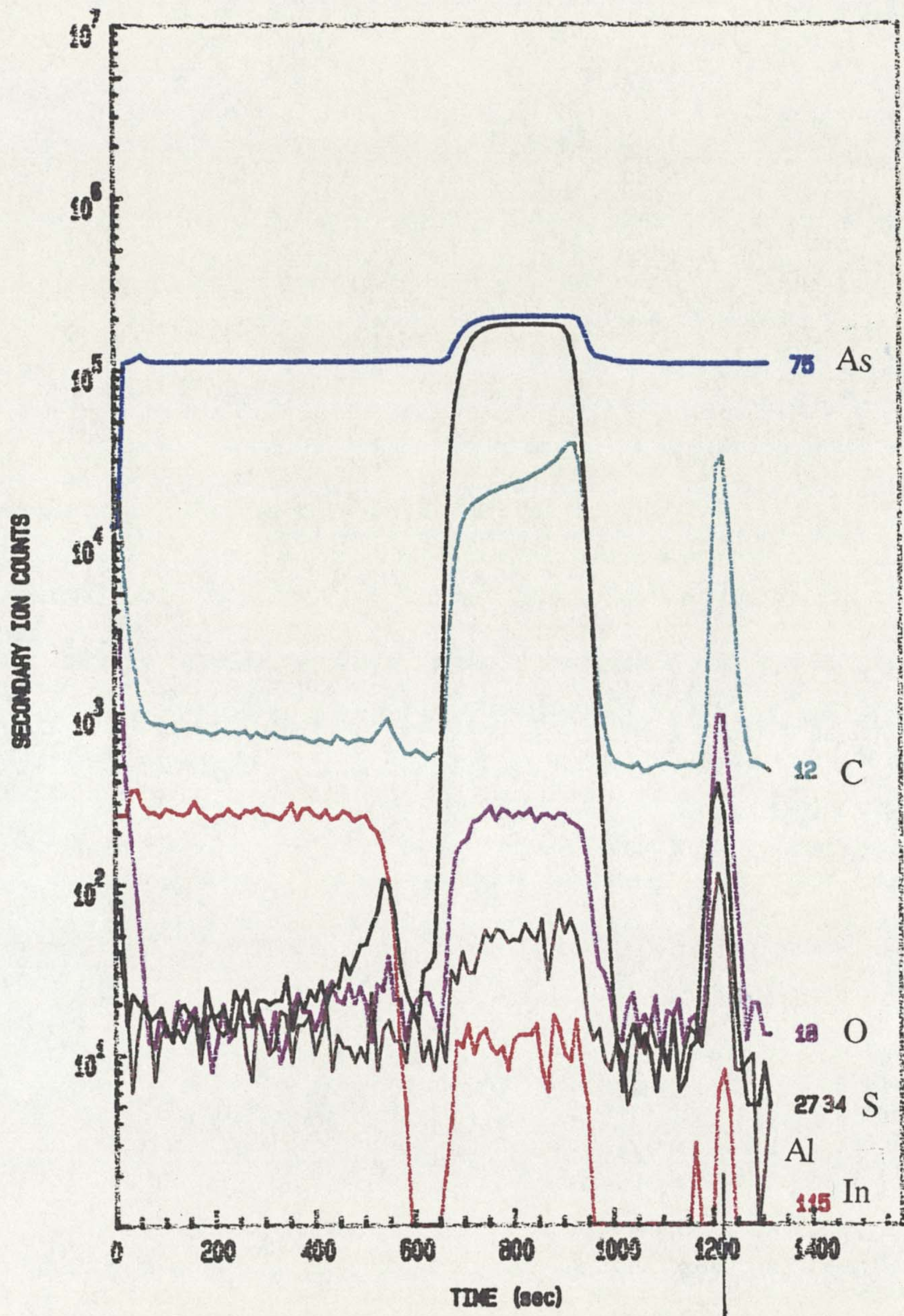

Figure 5.4: SIMS profile of sample M501, showing contamination interface spikes.

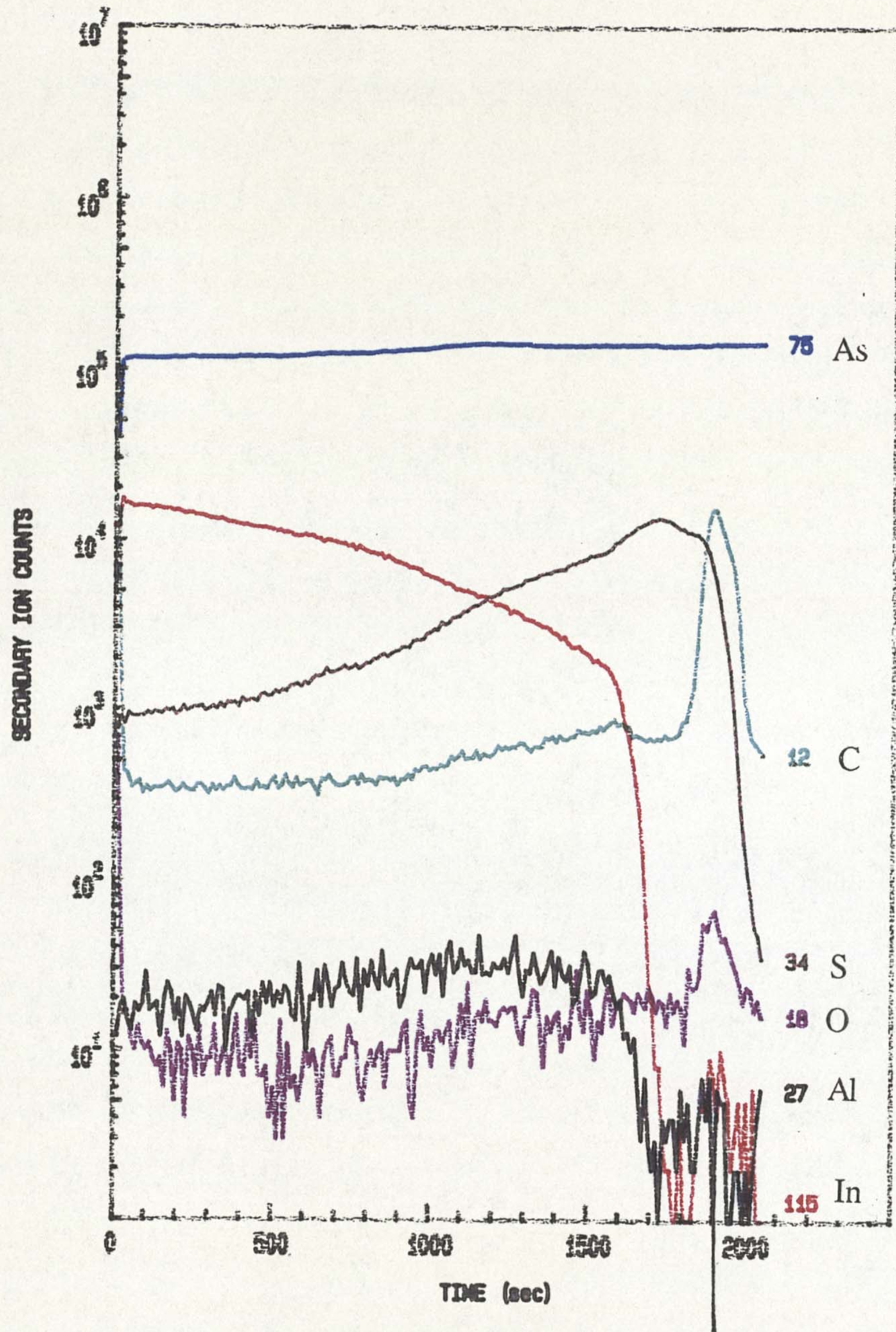

Figure 5.5: SIMS profile of sample M503, showing lower levels of interface contamination with respect to M501.

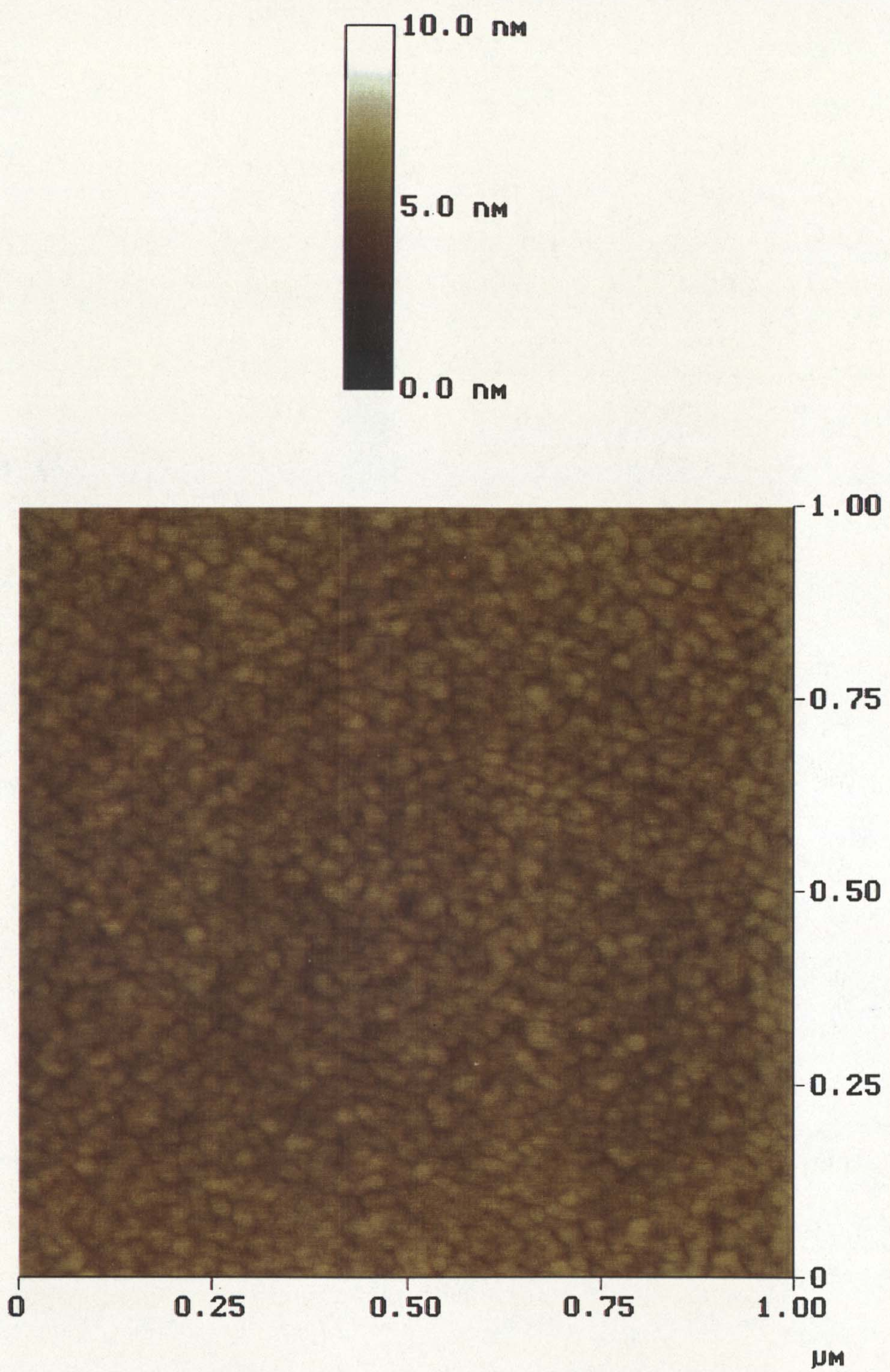

Figure 5.6: AFM of the surface morphology of an 'as received' epi-ready (001) GaAs substrate. The maximum roughness was 1.5nm in height.

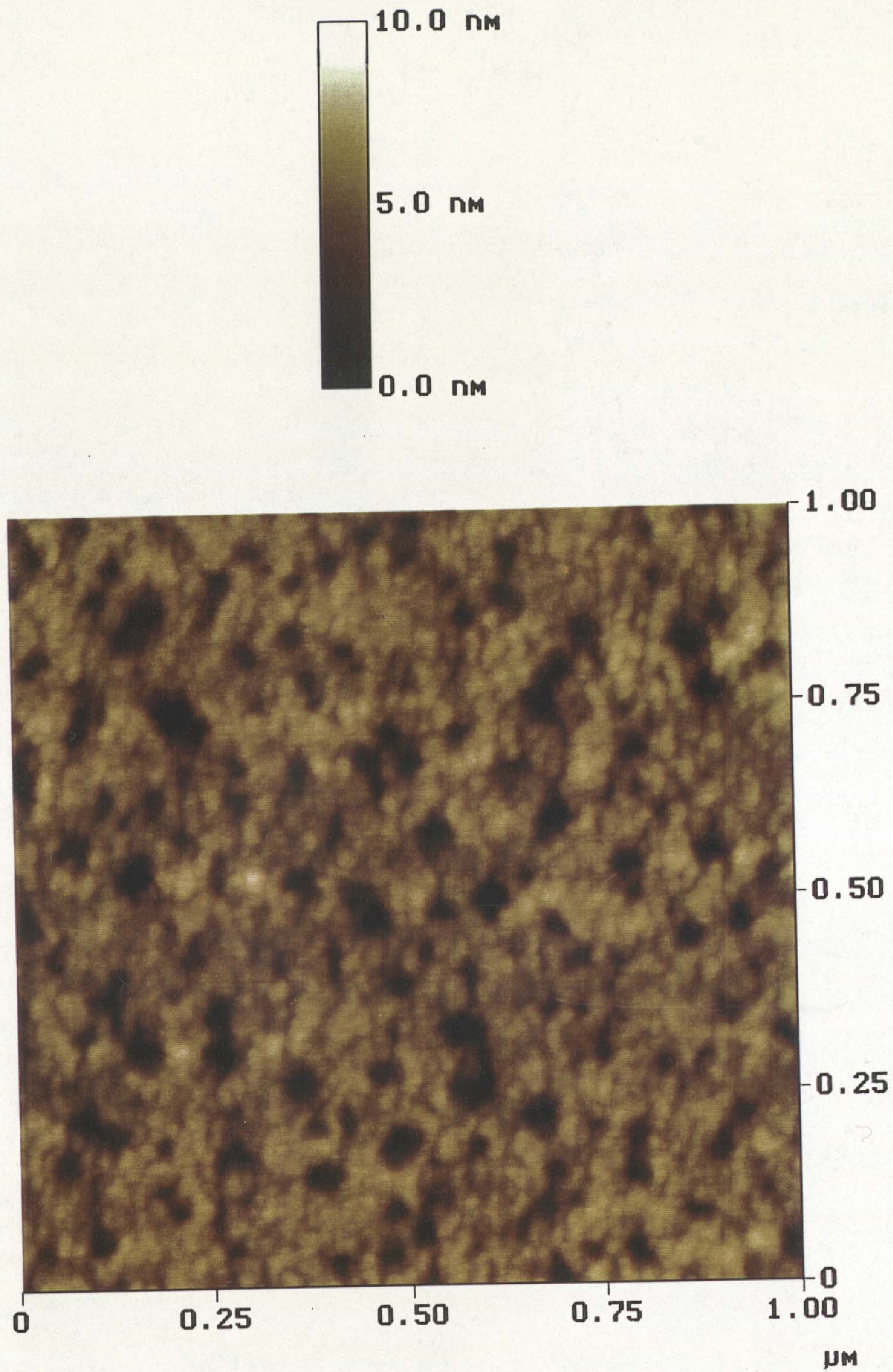

Figure 5.7: AFM of the surface morphology of a GaAs substrate after annealing in the CBE chamber with the outgassing procedure employed. The maximum roughness was 7nm in height.

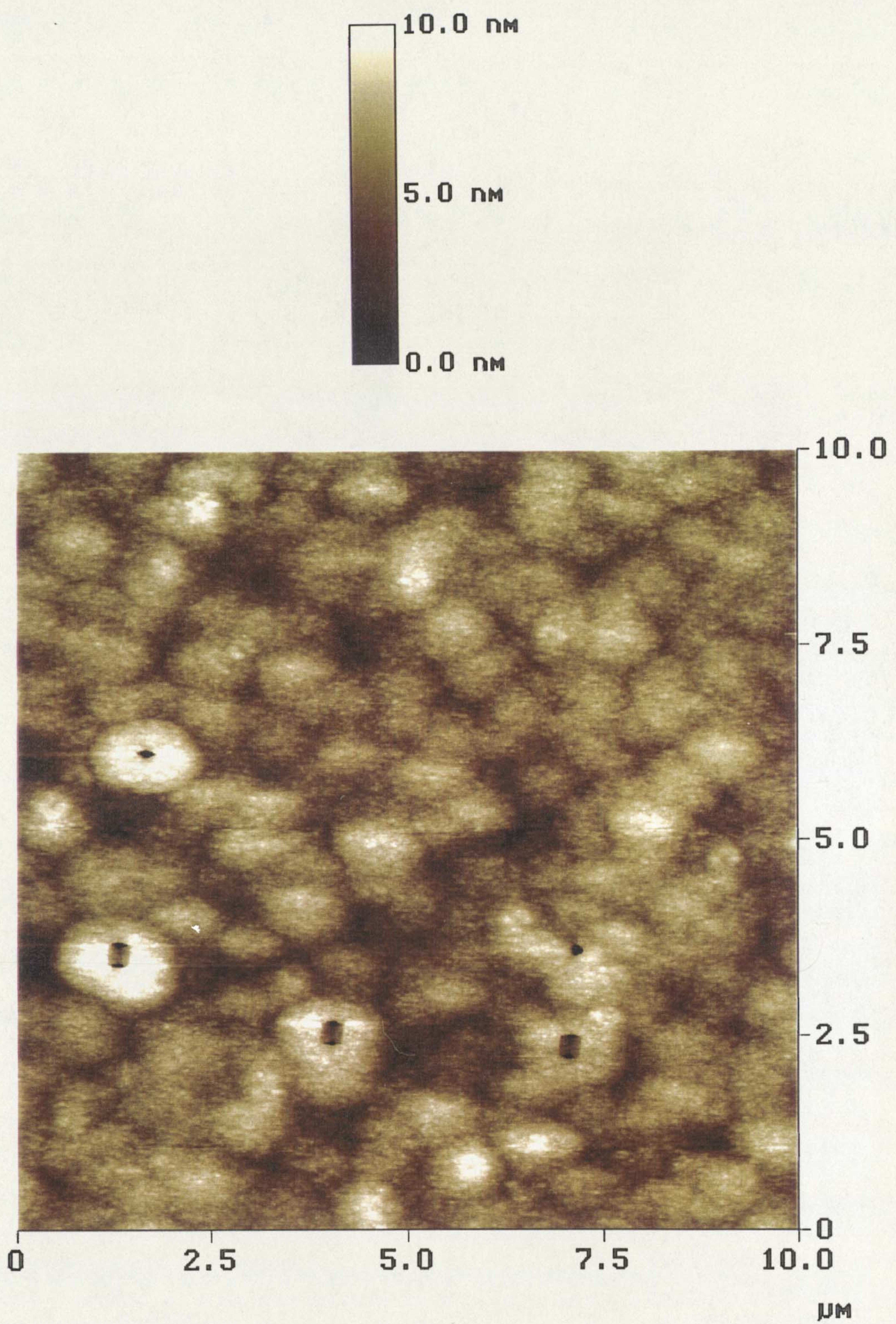

Figure 5.8: AFM of the surface morphology of a GaAs substrate after annealing in the growth chamber without the outgassing procedure.

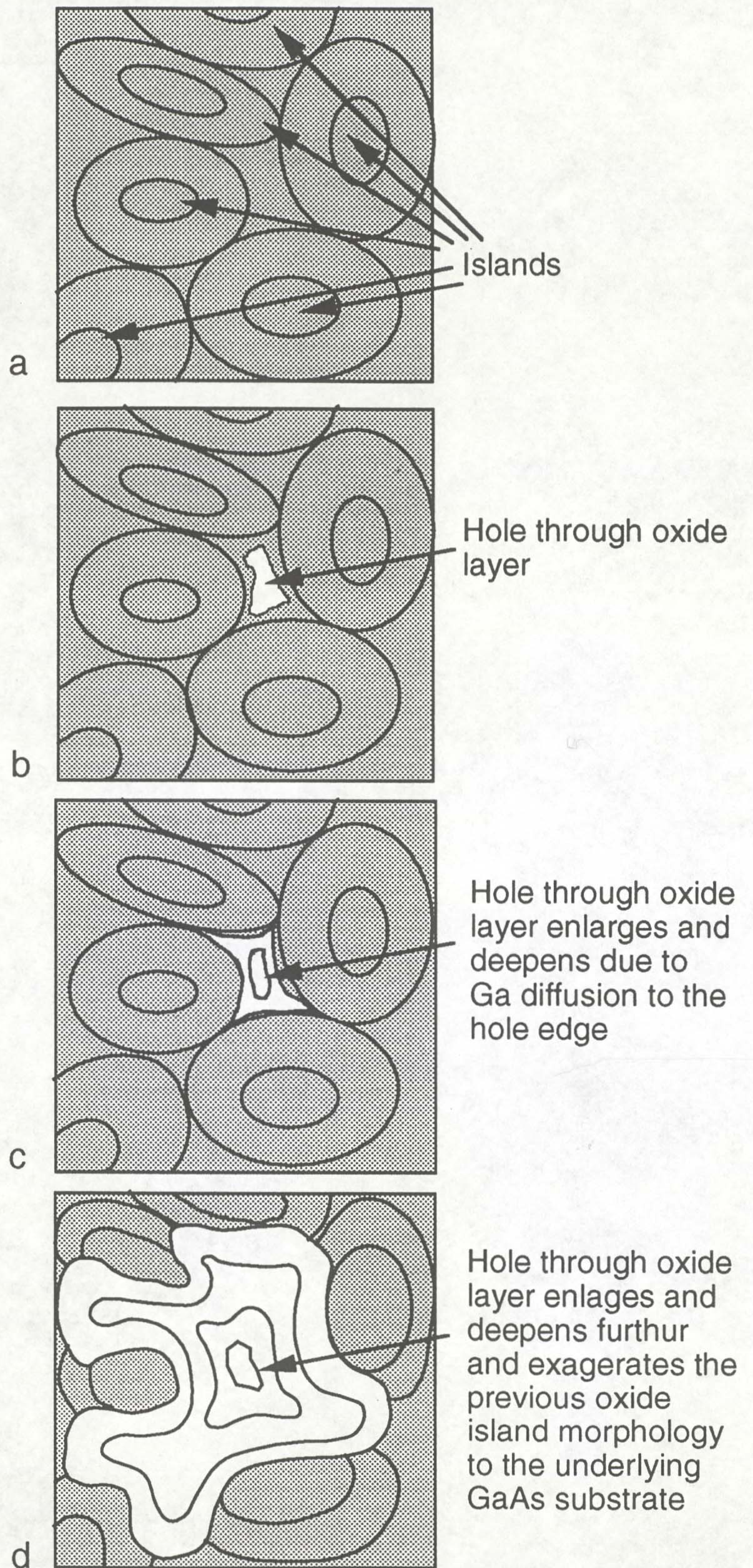

Figure 5.9: Sequence of schematic diagrams showing the development of surface morphology during the oxide removal occuring during GaAs substrate annealing after the chamber outgassing procedure.

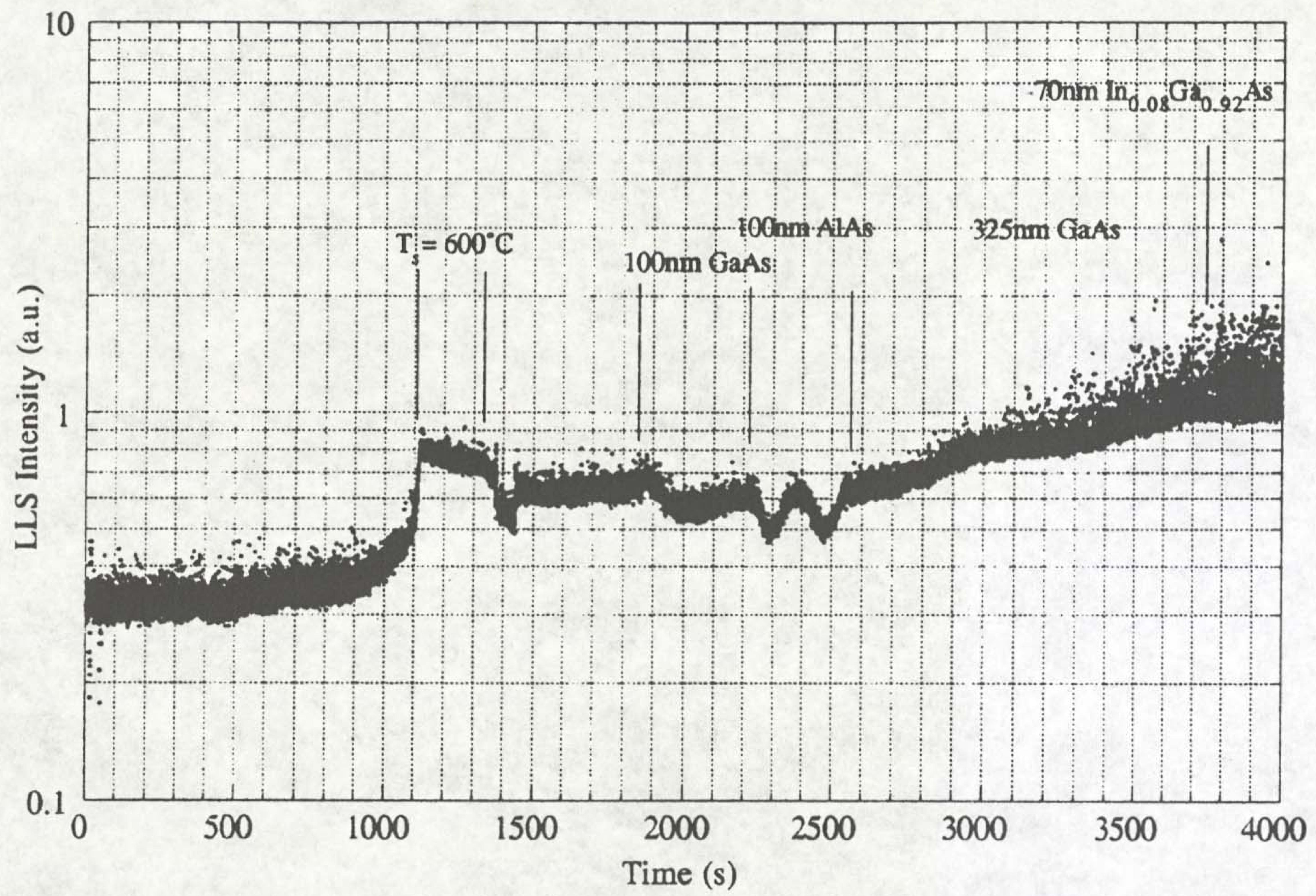

Figure 5.10: LLS intensity variation during the pre-growth anneal and subsequent growth of GaAs and AlAs, on a GaAs substrate loaded after the chamber outgassing procedure.

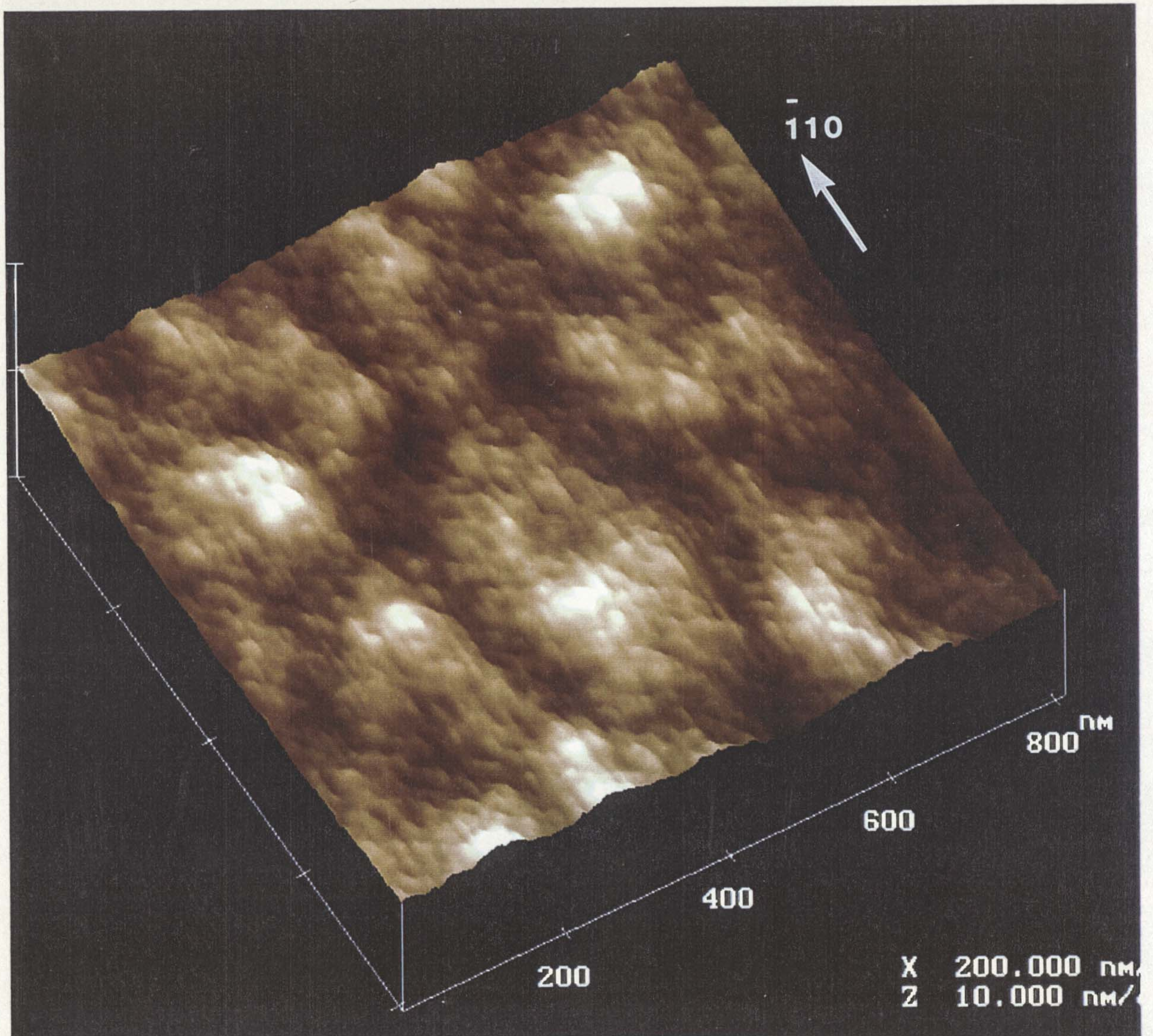

Figure 5.11: AFM of the surface morphology of a GaAs epilayer grown on GaAs by CBE. The islands are ~1.5nm in height.

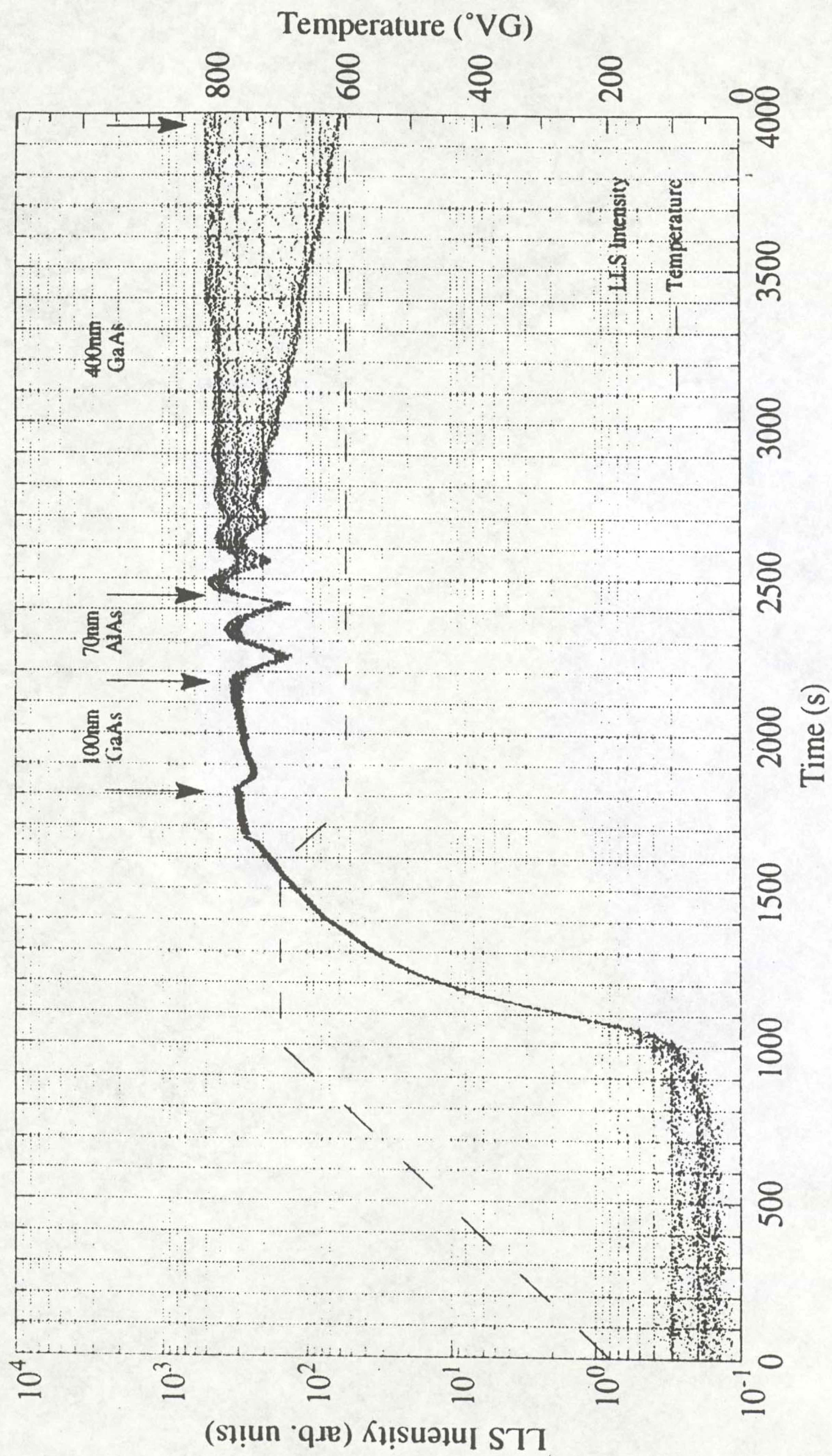

Figure 5.12: LLS intensity variation during the anneal and subsequent growth of GaAs and AlAs, on GaAs without a successful outgassing proceedure.

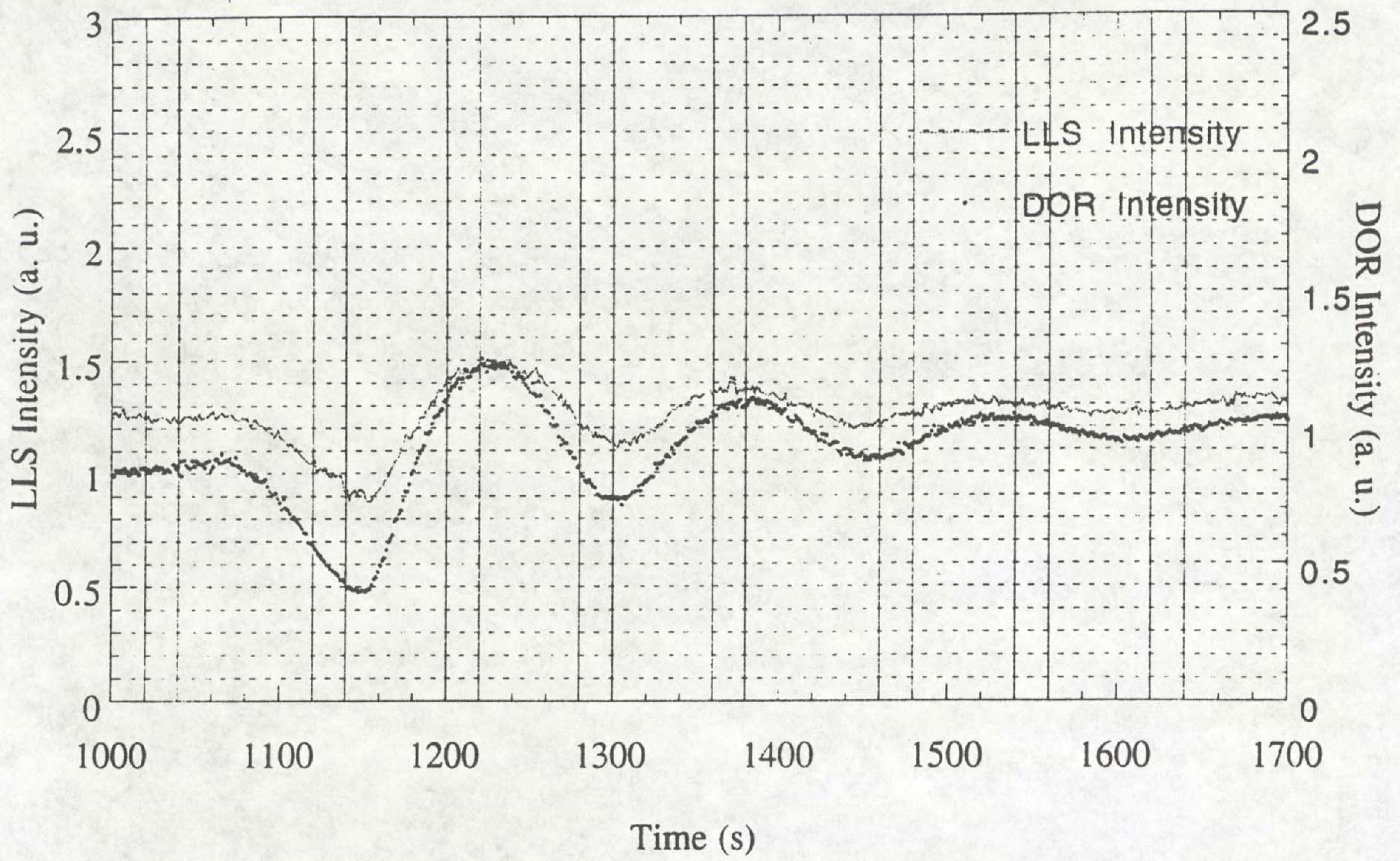

Figure 5.13: Intensity oscillation in diffusely and specular reflected light during the growth of AlAs and GaAs.

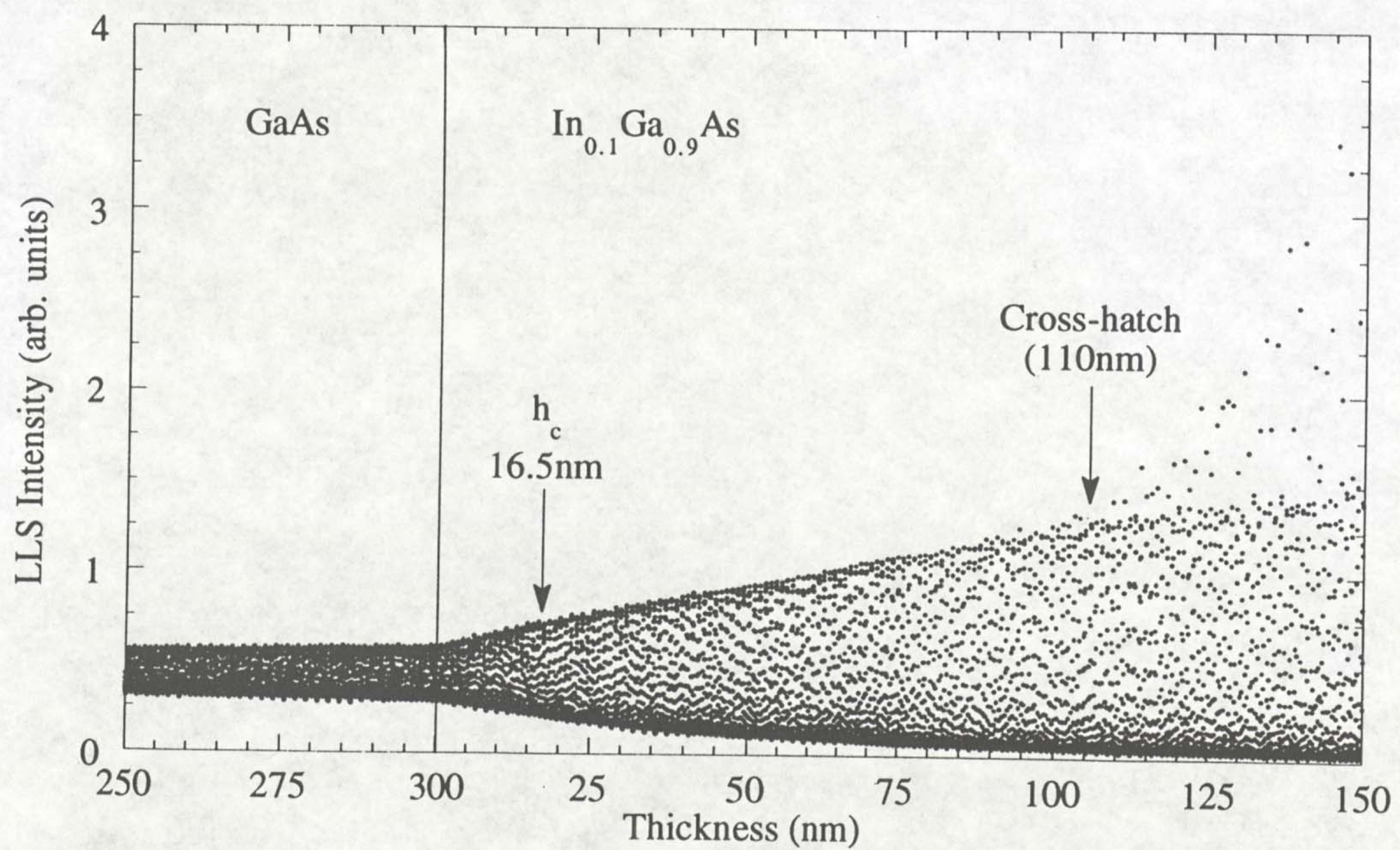

Figure 5.14: LLS intensity variation during the growth of $In_{0.1}Ga_{0.9}As$ on GaAs.

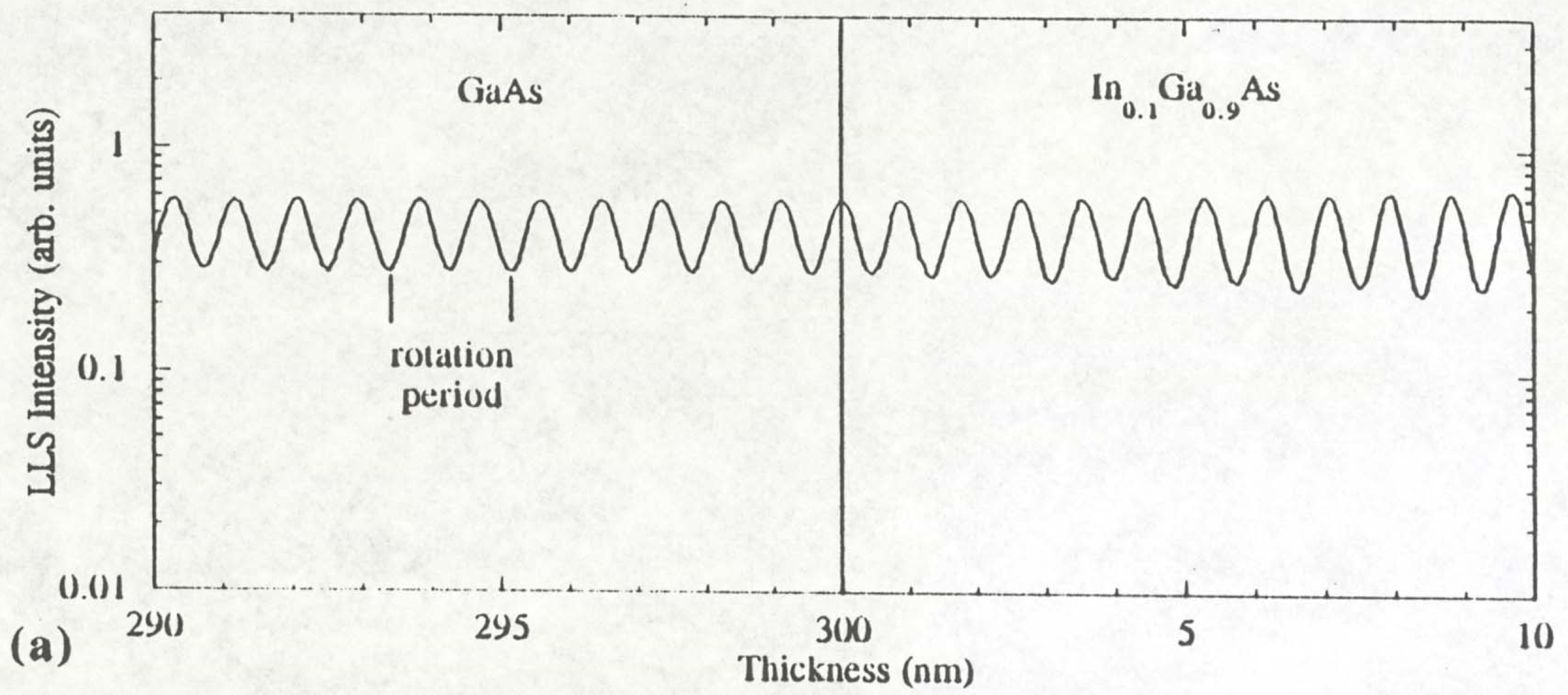

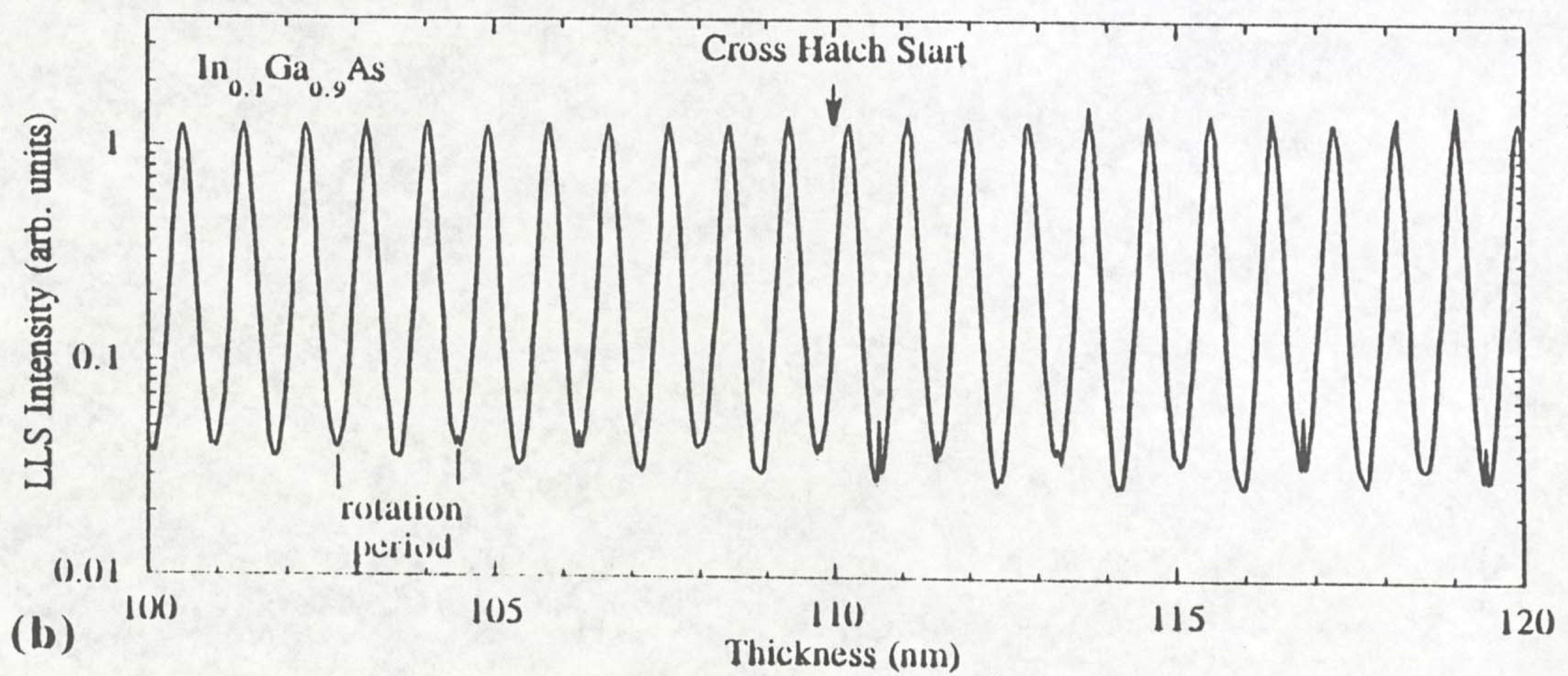

Figure 5.15: Expansion of the LLS trace in figure 5.14, during InGaAs on GaAs heteroepitaxy (a) at the onset of InGaAs growth, and (b) At the onset of significant relaxation.

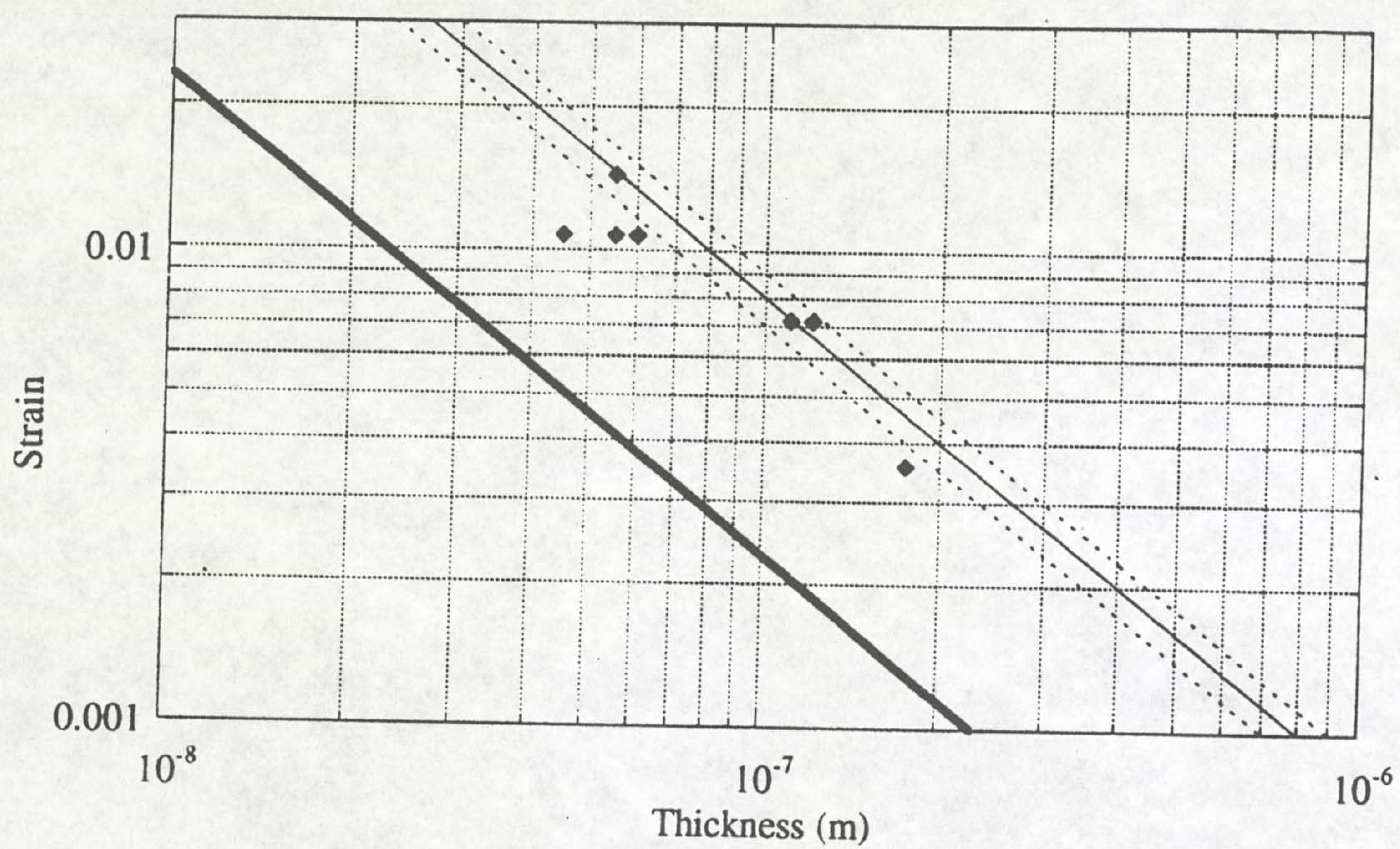

Figure 5.16: The onset of the onset of the cross-hatch as identified by LLS, compared to estimates of the critical thickness for dislocation introduction and the critical thickness for significant relaxation.

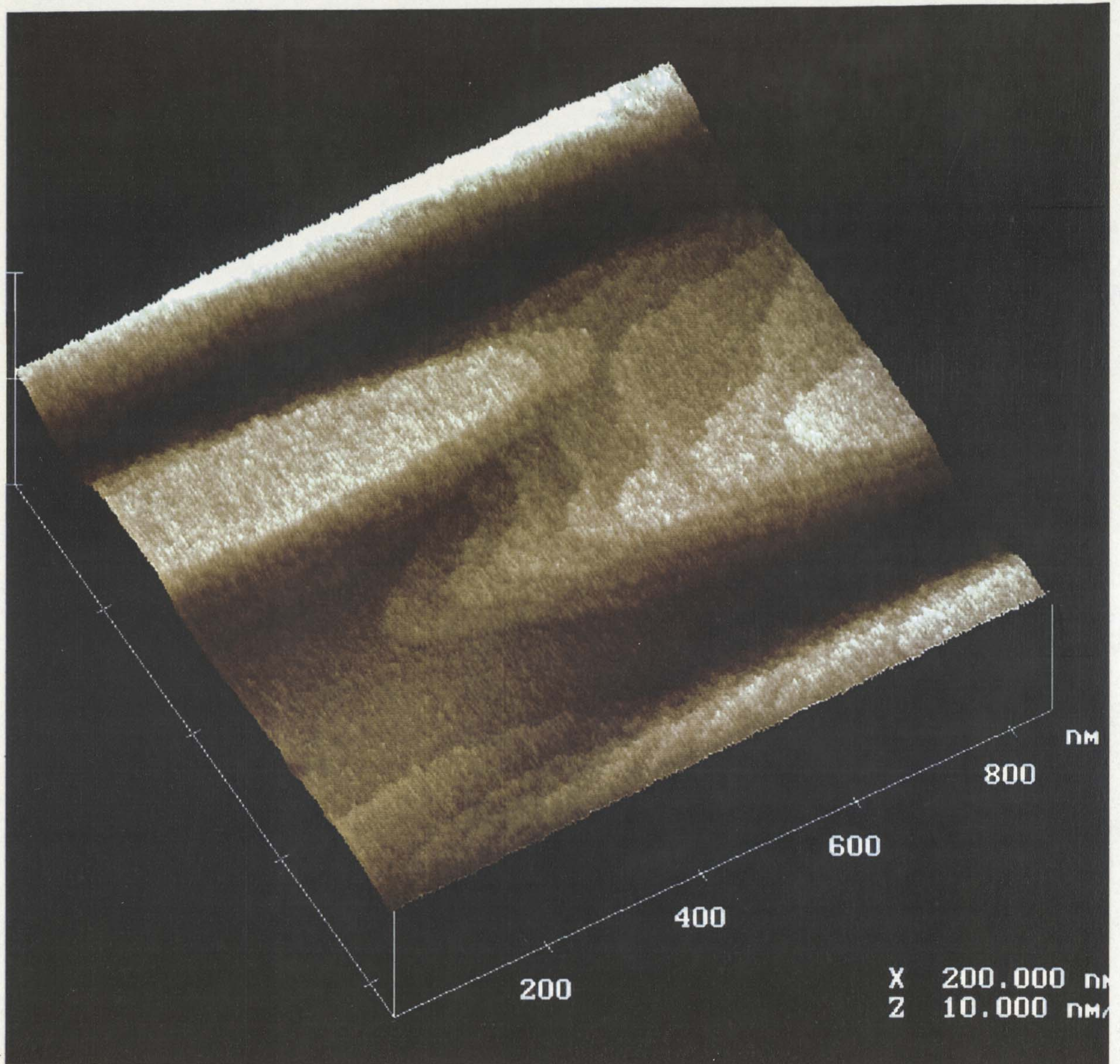

Figure 5.17: AFM of the surface morphology of a 170nm thick $In_{0.1}Ga_{0.9}As$ epilayer grown on a GaAs substrate by CBE.

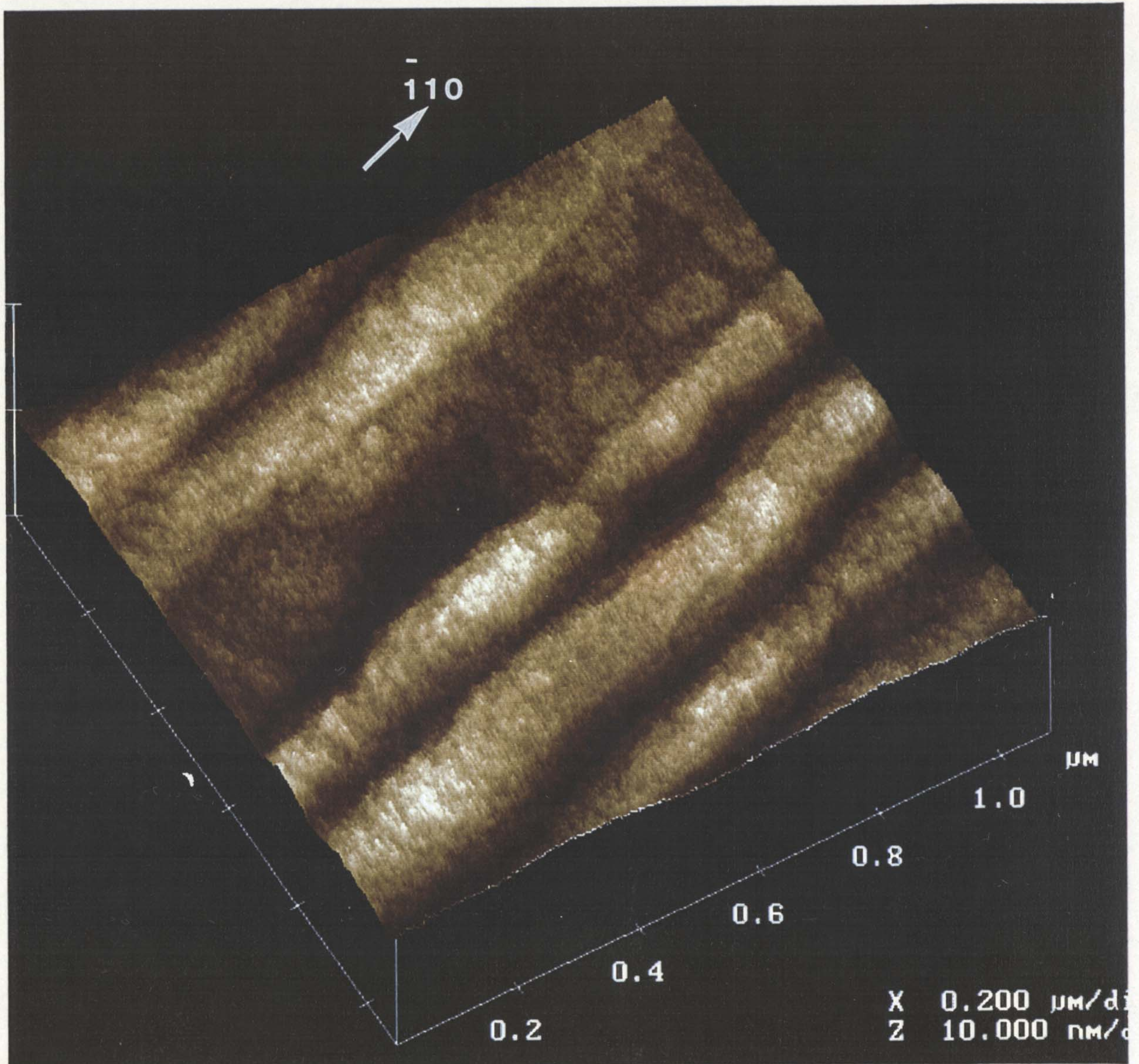

Figure 5.18: AFM of the surface morphology of a 100nm thick $In_{0.2}Ga_{0.8}As$ epilayer grown on a GaAs substrate by CBE.

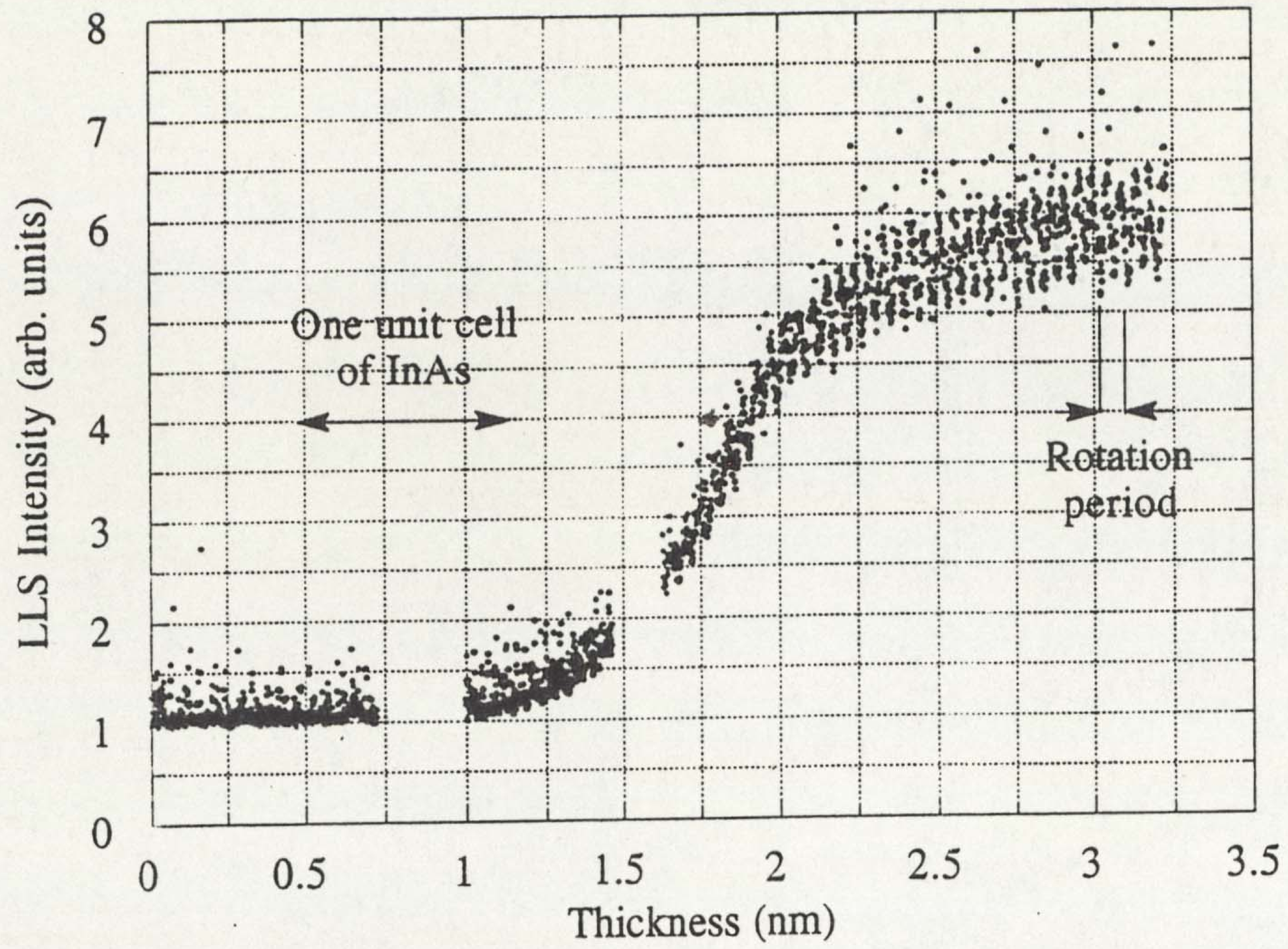

Figure 5.19: Variation in scattered light intensity during the growth of InAs on GaAs by CBE.

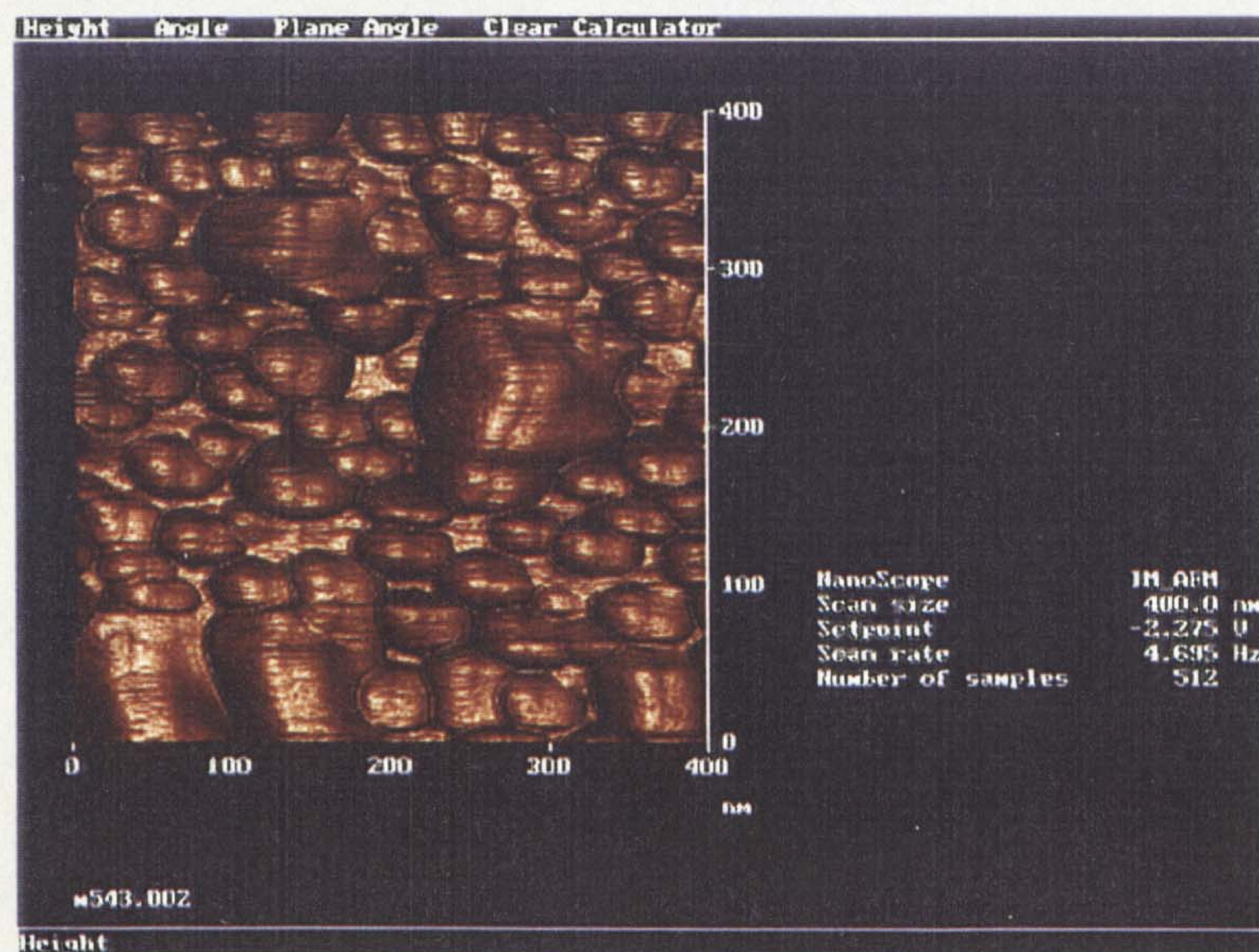

Figure 5.20: AFM of the surface morphology of a ~3nm thick InAs epilayer grown on a GaAs substrate by CBE.

CHAPTER SIX
LASER MODIFIED CHEMICAL BEAM EPITAXY

6.1 Low temperature laser assisted growth of GaAs

6.1.1 General growth rate results

6.1.2 Modelling of growth rates to temperature rise

6.1.3 Chopped beam results

6.1.4 Effect of group V-III flux ratio

6.1.5 Growth rate and Carbon incorporation profile

6.1.6 Morphology results

6.1.8 Discussions

6.2 High temperature laser inhibited growth of GaAs

6.2.1 Growth rate results

6.2.2 Morphology results

6.2.3 Discussions

6.3 Summary of chapter

This chapter investigates the use of Ar^+ laser irradiation to locally effect the growth rate and dopant incorporation of GaAs grown by chemical beam epitaxy using TEG and pre-cracked arsine as precursors. Low temperature laser assisted growth of GaAs is achieved by growing at a substrate temperature below that of the maximum (~490°C for TEG and As_2) and increasing the growth rate towards the maximum unassisted rate in the laser irradiated area. High temperature laser inhibited growth is achieved by growing at a temperature at or above that for the maximum unassisted growth rate and causing a local decrease in growth rate by laser irradiation. Here the effect of irradiation on the growth rate, structure, surface morphology and dopant incorporation are presented with the aim of achieving selective area growth. The origin of the modifications are discussed since they are important in predicting the effect of laser irradiation during GaAs epitaxy with TEG and pre-cracked arsine, and for further studies using other precursors and compounds.

In this chapter the laser powers quoted (W_L) are those of the laser output and not of the power incident on the substrate. The quoted laser power densities (intensities) are also calculated from the laser output power. The incident laser power (W_I) and power density will be lower due to losses in reflection from the two directing mirrors and the focusing mirror and in transmission through the CBE reactor viewport. Each will result in an estimated 8% reduction in power (from the reflectivity of glass) although transmission through the view-port may reduce the intensity by a greater degree due to coating by metalorganics within the chamber. The incident power and power density will thus be about 0.72 x those quoted.

6.1 Low temperature laser assisted growth of GaAs

6.1.1 General growth rate results

The unassisted growth rates were determined by laser reflectometry using the Ar+ laser at 12mW power, which had a negligible effect on the growth. The growth rate of GaAs is shown in figure 6.1, using the room temperature refractive index of GaAs (Aspnes *et al.* 1986), and normalised to the maximum unassisted growth rate. The maximum unassisted growth rate, at a substrate temperature of 490°C, was found to be 0.54nms^{-1} under the conditions used (4torr TEG and 700torr pre-cracked arsine), which is in agreement with that determined by cleaved edge TEM measurements. From figure 6.1 is observed that the unassisted growth rate undergoes an increase of over a factor of ten as the substrate temperature is raised from 320°C to 430°C.

Laser reflectometry was used to measure the growth rate of GaAs as a function of substrate temperature (T_s), laser power (W_L) and precursor beam pressures. Figure 6.2 shows laser reflectivity traces for laser assisted growth at a substrate temperature of 357°C, along with unassisted traces at 357°C and 490°C. Laser irradiation is shown, in figure 6.2, to increase the growth rate (observed by a reduction in oscillation period) and increase the damping of the oscillations. The specular reflected beam profile remained well defined for the first three or four interference oscillations, thereafter it progressively broadened, finally becoming an annulus. The reflected beam broadening and the damping in reflected intensity were due to the local nature of the enhancement (discussed further in section 6.1.5).

The laser assisted growth rates were measured using the same laser as which produced the enhancement, and thus represent an incident power averaged growth rate over the whole laser irradiated area. The damping in amplitude of the oscillations in figure 6.2 was

due to the variation in thickness over the laser irradiated area which increases with time. An attempt to to extract the variation in thickness from the damping was unsuccessful. Laser assisted growth rates were determined from the first four turning points in the interference oscillations, when the reflected beam was still well defined, and the damping small, indicating that the laser height profile would not have a dramatic effect on the measured growth rates. Indeed the oscillation period remained constant for the first four turning points. Laser assisted growth rates, normalised to the maximum unassisted growth rate, are given as a function of laser power for four different substrate temperatures in figure 6.3. At the two higher substrate temperatures an increase in growth rate is observed which strongly resembles that of increasing temperature (figure 6.1), this relative enhancement was found to be independent of the TEG flux, as shown by comparing open and closed circles in figure 6.3, both at 357°C but under TEG line pressures of 2torr and 4torr respectively. However at the two lower substrate temperatures a sharp knee in growth rate with laser power is apparent, and the maximum unassisted growth rate is not recovered for the available laser power, 2.5W. Indeed the growth rate appears to saturate at 0.7 x the maximum unassisted growth rate. This suggests a non - thermal element to the enhancement.

6.1.2 Modelling of growth rates to temperature rise

To determine the dominant process involved in the laser enhancement it is first necessary to find the temperature rise within the laser effected area, since any other contribution will be from this elevated temperature. It was not possible to directly measure the temperature rise in the laser effected area within the CBE chamber, since no accurate techniques were available. Thus in this section the measured assisted growth rates of section 6.1.1 are modelled on a purely pyrolytic assumption and the modelled temperature rise compared with that predicted by a thermal conduction model.

Using profilometry the laser enhanced region was found to be an ellipse of major and minor axis widths 0.2cm by 0.015cm (see section 6.4), corresponding to an area of 2.36×10^{-3}cm^2, and equal in area to a disc of radius 0.027cm (270μm). The mean power density from the laser is thus 424Wcm^{-2} for 1Watt laser power (ignoring window and mirror losses).

The time independent solution to the thermal conduction equation [3.1] using values of incident power W_I = 0.72Watts, substrate reflectivity R=0.4, constriction radius r_c= 0.027cm, and thermal conductivity $K_s = (366/T^{1.2})$ watt/cm K estimates the maximum temperature rise within the laser region ($\Delta T_{max.}$) per Watt laser output power to be 26°C/Watt (0.061°CWatt^{-1}cm^2) at T_s=313°C increasing monotonously to 29°C/Watt (0.068°CWatt^{-1}cm^2) at 400°C.

The laser assisted growth rates discussed in section 6.1.1 (figure 6.3) are shown converted to substrate temperatures with corresponding unassisted growth rates, against laser power in figure 6.4. The growth rates were converted using the results in figure 6.1, taken in the same way on unassisted growth. Linear fits were taken for each set of data, and the gradients of each are shown in the key. The linear fit to the assisted growths from the substrate temperature of 357°C and 4torr TEG are shown applied to laser enhancement from each substrate temperature. Figure 6.4 shows that the laser assisted growth rate is almost exactly superimposed on the unassisted growth rate verses substrate temperature curve (figure 6.1) if the temperature rise is 44°C/Watt (0.10°CWatt^{-1}cm^2) for the two higher substrate temperatures. This value is above the theoretically modelled temperature rise of ~27°C/Watt (0.064°CWatt^{-1}cm^2). The theoretically modelled value of temperature rise was only an estimate, however, and assumed infinite substrate dimensions. The substrates used were 5cm diameter and only 400±20μm thick. This thickness is comparable to the minor axis of the irradiated area, and since radial heat conduction was assumed, could result in the surface temperature being 60% higher in the

laser effected area than the equation predicted. The finite dimensions will also result in heating of the entire wafer. In particular the laser irradiated area may have been over-estimated, since it was the area of enhancement that was measured which may be larger (if the growth rate enhancement were pyrolytic) due to thermal conduction. This shows the modelled temperature rise to be within the error of the estimation.

At the two lower temperatures this temperature rise would also account for most of the observed enhancement. However, the knee in growth rate with laser power (observed in figure 6.3) brings the apparent temperature above that of the purely pyrolysis growth rate fitted to the two higher temperatures, This could not be accounted for by the measurement technique since power averaging should smear the growth rate with laser power curves, and indicates that another process is involved alongside pyrolysis in the enhancement at the two lower temperatures. At the two lower temperatures and high laser powers the growth rate from the fitted thermal enhancement is not obtained. This may be due to measurement technique which power averages over the entire laser irradiated area which would mean the readings include parts of the laser area not enhanced to the peak growth rate, exaggerated by the knee observed at lower powers and would result in a lower mean growth rate than expected.

6.1.2 Chopped beam results

The indication from the results shown in figure 6.4 that photo-thermal effects dominate at the higher temperatures was investigated with the laser operated in a chopped beam mode with a mark : space ratio of 1:1. The growth rate, for constant time - averaged laser power, should be frequency dependent. If the dominant mechanism is thermal, at high frequencies the growth rate is expected to be that associated with the laser operating at half power. This is because the average power would be half that of the CW level, and the temperature oscillation about the corresponding temperature would tend to zero with

increasing chopping frequency. At low frequencies the growth rate should tend to that of half way between the full power CW assisted growth rate and the unassisted growth rate, since in the low frequency limit half of the growth time would be spent at a temperature corresponding to the CW full power level, and half at the unassisted substrate temperature. The transition would be expected to occur at frequency related to the rise and fall time of the temperature within the laser effected area. Solution to the time dependant heat conduction equation, taking the heating geometry to be a constriction in half space, indicates the transition to low frequency occurs at about 10Hz (Farrell, 1995.). Sugiura, Iga and Yamada (1988) measured the fall time in the substrate temperature around the laser area to be 100ms using a computer controlled pyrometer, in agreement with the solution. At 2Hz chopping frequency, they measured the average temperature rise to be 4°C in the 'laser on' state (at a power density of 200Wcm^{-2}) and less than 0.2°C in the 'laser off' state, however their measurements represented an average temperature rise over an area that may have exceeded the laser heated area.

If the enhancement were purely photolytic then the transition from low to high frequency limit would be dependent on the reacting species lifetime on the surface compared with the 'laser off' (space) time interval. Above this transition frequency the species arriving onto the substrate would remain until the 'laser on' interval. During growth the photon count would remain constant and the growth rate would be constant with frequency at the half CW laser power level. Below this transition the species would desorb during the 'laser off' interval and the growth rate would tend, over an order of magnitude in frequency, to the low frequency limit of half way between the unassisted rate and the full power CW rate. The species lifetime for the adsorbed TEG molecules under low temperature CBE growth conditions is not accurately known. Evidence of growth rate saturation due to reaction site blocking by As_2 dimers ethyl radicals and adsorbed TEG suggest that all TEG may adsorb and remain on the surface in low temperature CBE until a fraction of one monolayer covers the surface, this fraction being dependent on the

group V - group III ratio and the substrate temperature. This suggests, that for the conditions used in laser assisted CBE, the lifetime would be around 0.1 - 0.5s and a transition frequency from high to low frequency behaviour starting somewhere between 2 - 5Hz. Clearer evidence comes from the effect of repetition rate of pulsed ArF excimer laser irradiation on the growth rate, where although the enhancement originates from pyrolysis a large temperature rise of a few hundred degrees occurs for a very short time interval, due to the 10ns pulse length. This is comparable in effect to the case of a chopped beam with a very low duty ratio and a photolytic decomposition mechanism. Farrell et al. (1992) showed that the growth rate decreased from its maximum at repetition rates below 10Hz, suggesting that for photolysis the transition from high to low frequency behaviour, with a mark space ratio of 1:1 should start at approximately 5Hz. The decrease occurred slowly over an order of magnitude of repetition rate, as is expected, and was found to be independent of the group III flux, indicating that the lifetime is not purely controlled by surface site blocking. A mixed photolytic and photo - thermal mechanism would be expected to have transitions at the two frequencies with the level between the transitions being related to the ratio of the two processes.

The variation of growth rate with chopping frequency was previously reported by Sugiura, Iga and Yamada (1988). They found no change in growth rate with chopping frequency between 2 - 300Hz and concluded a photolytic enhancement with a negligible photo - thermal component. The data was not presented, however and it is not known if the conditions were chosen to give a measurable change in growth rate between the two frequency limits, due to the growth rate measurements being made by a stylus profilometer. The data presented in the paper on the temperature dependence of the laser assisted growth rate, does show some scatter in values. Furthermore, a transition corresponding to the species lifetime would have to be identified to show a significant photolytic component.

This study used a substrate temperature of 357°C and a CW laser power of 1.5W, since from figure 6.3 there is a significant difference in the growth rate between that at 0.75W, and that corresponding to half way between the 1.5W assisted rate and the unassisted rate. The results, shown in figure 6.5, show a variation in growth rate with chopping frequency. At the highest frequency available (300Hz) the growth rate agrees with the 0.75W CW rate, and there is a clear trend towards the low frequency limit at the lowest frequency available (15Hz). This transition is near the predicted photo - thermal transition frequency, and occurs over less than an order of magnitude in frequency, clearly showing that a photo - thermal contribution is dominant for substrate temperatures above about 350°C.

6.1.3 Effect of group V-III flux ratio

The effect of (pre-cracked) arsine pressure on the growth rate, measured by laser interferometry, at substrate temperatures below that corresponding to the maximum growth rate (at 490°C) is shown in figure 6.6. The growth rate undergoes a decrease on increasing the arsine pressure above that roughly corresponding to a 1:1 V:III flux ratio. This is believed to be due to the arsenic dimers blocking reaction sites for adsorbed TEG molecules. Below the peak arsine flux the reflectivity decreased rapidly upon growth due to poor morphology. The effect of a high arsine over-pressure is to produce a reduction of up to 50% in the growth rate from that at a unity flux ratio. Flux calculations show the growth rate peak position to be above the 1:1 V:III ratio by an offset in arsine pressure, which may be due to a certain coverage required to maintain an arsenic rich surface, or due to an actual offset in the arsine pressure gauge. This does suggest, however, that caution should be assuming the sole importance of the V:III ratio and not the actual flux under all conditions used, since the effect of the group V pressure alone and the interaction between the group V flux and temperature, may be significant.

The effect on laser assisted growth is expected to be similar if a thermal mechanism is dominant, and by reducing the arsine pressure towards a group V:III flux ratio of 1:1 the growth rate will be increased both inside, and away from, the laser irradiated area. Measurable laser enhanced growth was found to occur at a substrate temperature of 275°C as shown in figure 6.7, using an arsenic flux of 250torr and a TEG flux of 4torr, corresponding to a group V/III ratio of 1.7:1. Figure 6.8 also shows laser assisted growth rates from 313°C at an arsine flux of 250torr (and TEG flux of 4torr), alongside laser assisted growth rates from 313°C and at an arsine flux of 700torr (and TEG flux of 4torr and thus a V:III ratio of 4.8:1), previously shown in figure 6.3. A reduction in arsine flux resulted in an increase in growth rate at all laser powers used, but relatively less so at high powers. A reduced arsine over-pressure thus resulted in a reduction in relative growth rate selectivity from inside and away from the laser effected area. This suggests that under most conditions a high arsine pressure is advantageous for selective area laser assisted CBE. The step in growth rate with laser power is also less pronounced at lower arsine flux, suggesting the step, and therefore perhaps any photochemical components present under these conditions, are arsine flux dependant.

6.1.4 Growth rate and Carbon incorporation profile

The local nature of the laser assisted growth rate enhancement will result in a variation of thickness across the substrate in the region of the irradiated area. Whether this enhancement results in an abrupt, flat topped, profile or a rounded profile is of importance to the characteristics of a device incorporating laser assisted layers. The profile of the enhancement will also have a direct effect on growth rate and other measurements.

The laser beam directly from the laser had a top hat profile, due to the multi-mode operation, but at incidence was expected to have been rounded somewhat due to the

focusing. The growth rate (and thus thickness) profile will arise from this and the growth dynamics, the surface diffusion of adsorbed surface species for photochemically assisted growth, and the local nature of the heating for pyrolytically enhanced growth. For a laser induced pyrolytic growth mechanism (which the results in section 6.1.1 suggest for Ar+ laser assisted CBE) the local growth rate depends on the local surface temperature. The local temperature rise is not proportional to the laser intensity at that point, but will depend on the size and power distribution of the laser - irradiated - area and its position. This may result in a laser - assisted - area greater than the laser - irradiated - area and when the size of the laser - assisted - area is used instead of the laser - irradiated - area in the thermal conduction model the maximum temperature rise at the peak of the enhanced region will be estimated below the actual value. This and the arguments presented in section 6.2 may have been what led authors (e.g. Sugiura, Iga and Yamada, 1989) to propose a photolytic origin for the laser enhancement. Our measurements give a measure of the average of growth rate, intensity averaged over the entire irradiated area, which may be more reliable as a comparison and more useful in predicting the characteristics of devices incorporating laser assisted layers.

The specular reflected beam profile was monitored with time during laser assisted growths using a video camera, focused on a screen in the path of the reflected beam, and connected to a video recorder. The profile remained well defined for around 200nm (corresponding to three to four interference oscillations), thereafter it progressively broadened, finally becoming an annulus (due to the area within the laser irradiated area, at normal incidence ($\pm\sim1°$) reducing below that at orientations a certain range of angle away). This demonstrated the local nature of the growth as the variation in thickness over the laser irradiated area.

The broadening of the reflected beam was due to the large scale height profile of the laser - irradiated - area. Interpreted by the large scale scattering model (section 3.3.2) the

angular profile of the reflected beam was double the (intensity proportioned) angular profile of the surface. The beam visibly broadened when the sides of the laser area became inclined to half the angular width of the original beam at the monitor screen. After around 300nm growth rings were observed due to interference, since the incident radiation was of narrow wavelength spread. Quantitative results of the height profile were not obtained because of the focusing of the beam, the intensity variation, and the low wavelength spread. Also the laser - irradiated - area was expected to be smaller than the laser - effected - area, which would result in only the central area being profiled. The broadening was, however, not significantly effected by the sub-micron surface morphology, which would dominate scattering to higher angles.

The broadening in the reflected beam profile would reduce the signal to the photodiode, since not all the beam would be collected after considerable broadening. This signal loss and the oscillation damping, observed in figure 6.2, indicated a variation in thickness across the region monitored by laser reflectometry. The growth rate results presented in sections 6.1, 6.3 and 6.4 were determined from the first four turning points in the interference oscillations, that is from the first ~120nm of assisted growth where, judging from the reflected beam profile and the interference oscillations (e.g. figure 6.2), the profile would be quite level and they will therefore give a good representation of the mean growth rate over the laser irradiated area.

The height profile of a laser assisted growth, at 357°C and 2W is shown in figure 6.8, measured by stylus profilometry. From this the laser irradiated area was estimated. The enhancement is not flat topped along the minor axis but roughly Gaussian, consistent with that expected by heat conduction and a pyrolytic mechanism to the enhancement..

Enhancement from the two lower substrate temperatures resulted in a step in the height profile, and a more planar central area. A Nomarski optical micrograph, Figure 6.9a,

reveals a very pronounced laser effected area, grown at 313°C, 4torr TEG, 700torr arsine, and 2W laser power. Atomic force microscopy of the step, figure 6.9b shows it to be a height increase of 70nm over a lateral distance of 2μm, where the peak height was 200nm. This step is more pronounced than would be expected from the beam profile and thermal conduction and confirms the growth rate step with laser power observed in figure 6.3, supporting the presence of a non-thermal element in the enhancement under these conditions. It also shows that flat topped enhancements with steep sides are possible with laser assisted growth, which would be desirable for selective area growth.

CBE growth of GaAs using TEG and arsine results in unintentionally p-type doped layers. The p-type background doping is due to carbon incorporation from the TEG molecule (Joyce *et al.* 1993). Using SIMS the carbon incorporation was found to increase when the substrate temperature is reduced below 450°C from around 1 x $10^{17}cm^{-3}$ to 8 x $10^{18}cm^{-3}$ at 357°C, as shown in figure 6.10. This is in agreement with Joyce *et al.* (1993) who showed an increase to 3 x $10^{18}cm^{-3}$ at a substrate temperature of 425°C and no variation in carrier concentration in the range 450 - 650°C.

Laser irradiation during growth may locally alter the carbon concentration, which may be useful in itself and also in identifying the salient mechanism for the growth rate modification. If the enhancement were purely pyrolytic in low temperature laser assisted CBE, then the growth rate enhancement should be accompanied by a carbon incorporation decrease which should be consistent with the increase in growth temperature. However, if the dominant mechanism were photolysis it is unclear whether the carbon incorporation would decrease due to a raised decomposition efficiency or increase due to another reaction pathway than the β - elimination process. Iga *et al.*(1989) showed that the carbon incorporation, measured by SIMS, increased from $10^{17}cm^{-3}$ to $10^{19}cm^{-3}$ in the non-irradiated areas as the substrate temperature is reduced from 500°C to 400°C but to be maintained at $10^{17}cm^{-3}$ in the irradiated area (0.5W laser power, 400μm

diameter beam), which they used to support a photolytic mechanism. However, in an earlier study Yamada, Iga, and Sugiura (1989) reported a lower reduction at 390°C from 5 x $10^{19}cm^{-3}$ to 2 x $10^{19}cm^{-3}$ (150mW laser power, 100µm diameter beam) which is similar in terms of equivalent temperature to that which would give rise to the reported growth rate enhancement.

In this study a substrate temperature of 357°C, and 1W laser power were used, since these are conditions which will give the clearest insight into the dominant mechanism. The carbon concentration was measured by SIMS. A parallel light source illuminating the sample and a CCD camera were used to locate the laser area (similar to the Makyoh method of whole wafer sample investigation (Nemeth-Sally *et al.* 1993), which enabled SIMS to be performed after 400nm of laser assisted growth, to maintain good morphology and improve the accuracy of the SIMS measurement. The data was taken for a 250µm square and afterwards electronically gated to take data from the centre 50µm of the laser - effected - area. AsC- ions (mass 87a.m.u.) were detected in place of C- ions (mass 12a.m.u.) since this was found to result in a lower SIMS background level. Laser irradiation resulted in a reduction in carbon incorporation from 8 x $10^{18}cm^{-3}$ to 5.3 x $10^{18}cm^{-3}$ as shown in figure 6.10. Assuming a purely pyrolytic reduction it can be seen, from figure 6.10, that this corresponds to a temperature rise of 28±5°C. This is what was estimated from the thermal conduction model and strongly supports the presence of a significant pyrolytic element for laser enhanced CBE from a substrate temperature of 357°C. Across the 250µm etched area the carbon incorporation varied roughly Gaussian with the same dimensions as a height profile, further supporting the conclusion of a thermal carbon incorporation reduction.

Using a lens configuration it was possible to use diffracting optics to grow patterns of lines or spots. Using a double slit in the path of the beam with the conventional focusing arrangement rows of lines were produced or the line could be split into a row of spots.

Using a square grid, an array of up to 16 spots approximately 200μm in diameter and of separation 2mm. Unfortunately it was not possible to image the whole array since the small height of the features (~300nm) required the use of Nomarski which had a maximum field of view of around 5mm. The dimensions and separation were limited by the chamber design involving a 0.3m distance between the substrate and viewport. It demonstrated the feasibility of using diffractive optics to laser write patterns on the surface in a production CBE system. Sugiura *et al.* (1989) demonstrated that patterns could be written using diffractive optics to produce concentric rings, scanning to write lines, and a holographic interference method (employing interference of two laser beams) to produce corrugations of pitch 0.85μm using a CBE system modified specifically for this purpose.

6.1.5 Morphology results

The morphological development of laser assisted GaAs CBE is difficult to quantify, since the surface morphology of unassisted GaAs epitaxy is not purely dependent on the growth conditions, but is dominated by the initial substrate morphology, which was shown in section 5.1 to vary dramatically between growths due to surface contamination. One further problem was that to accurately locate the centre of the laser effected area required a laser affected area with a large height profile requiring several hundred nanometres of growth at high laser power, or a laser area with a differing morphology to the non-irradiated area . Laser assisted CBE of GaAs was found to usually result in rougher surfaces in the irradiated areas than away, in contrast to that expected based purely on an increased growth temperature within the laser affected area, although it must be remembered that more material was deposited within the laser affected area than in unaffected areas.

After 400nm of GaAs grown at a substrate temperature of 313°C, and a laser power of 2W laser irradiation resulted in an increase in height of growth islands from 10nm mean height away from the effected area to 20nm mean height in the centre of the laser - affected - area, very narrow features were also observed aligned along the [110] direction. At the step edges of laser assisted areas grown at a substrate temperature of 313°C the surface morphology was observed to be very undulated, with islands coming up from the substrate level to height of the top of the step, as shown in figure 6.10b, perhaps due to an increased photochemical element present under the conditions around the area of the step. It is not expected that the laser power density or temperature profile would vary such, and it appears to be due to the kinetics of the assisted growth process at the edge of the selective area.

Laser assisted growth from a substrate temperature of 357°C, 2.5W, and for 400nm assisted layer thickness (calibrated from previous laser interferometry measurements, see figure 6.3), resulted in the development of a ripple pattern of height approximately 6nm, as shown in figure 6.11. The morphology away from the laser consisted of 2nm height islands 400nm in diameter. The ripples are roughly aligned in the <110> directions with a lateral period of 190±10nm. This ripple pattern was only observed at substrate temperatures at or above 357°C, at laser powers above 1.5W, and after laser assisted growth on a wafer cleaned after the outgassing procedure outlined in section 5.1.

Ripple structures have previously been reported for pulsed laser assisted growth (e.g. Farrell et al. 1993), pulsed laser annealing (Cullis, 1985), and pulsed laser etching of semiconductors (Kumagai et al. 1991). In each case the ripple pattern had a similar lateral period to that shown in figure 6.11. With the exception of the ripple structure developed during the excimer laser CBE of GaAs, which like the Ar+ assisted growth was crystallographically aligned, the observed ripple patterns were oriented to the polarisation of the incident laser beam. The non-epitaxial growth periodic ripple patterns were

attributed to interference of the incident laser with a stimulated surface wave (Sipe et al. 1983). All these structures were developed by UV radiation, and the period of the ripple structures were similar to the wavelength of the incident light. Due to the similarity in dimensions with wavelength, a surface wave was thought to be responsible for the ripple structure in the excimer laser assisted CBE growth.

The period of a surface - wave induced ripple structure is $\lambda/(1\pm\sin\theta)$, where λ is the wavelength of the incident light and θ is the angle of incidence (Oron and Sorenson, 1979). The ripple pattern shown in figure 6.11 exhibited a period of $\lambda/(2.7\pm0.2)$ from a near normal laser incidence, and was crystallographically oriented, and hence is unlikely to have been developed by interference between the incident beam and a stimulated surface wave.

It is suggested that the ripple pattern was due to strain induced by the temperature rise in the laser effected area. The maximum temperature rise in the laser irradiated region at 2.5W laser power and from a substrate temperature of 357°C is calculated to be about 70°C from the heat flow equation, and modelled on growth rate enhancement to be about 110°C (see section 6.1.2). Using a model based on the yield strength of GaAs (Hussien et al. 1989), plastic deformation should take place for laser induced temperature rises of about 80°C at 357°C. The conditions used therefore are around the critical temperature rise for the onset of plastic deformation. The ripple pattern is, however, more periodic and less crystallographic than the 'cross-hatch' observed in low misfit InGaAs which has undergone significant plastic relaxation (see section 5.3), and laser inhibited growth at substrate temperatures and powers resulting in temperature rises significantly above the estimated critical temperature rise for the onset of plastic deformation (Hussien *et al.* 1990). Also a cross-sectional and plan-view TEM investigation of the laser irradiated area did not detect misfit dislocations, although it was also unsuccessful for laser inhibited CBE (see section 6.2).

Growth of strained layers, such as high misfit InGaAs on GaAs, often results in initial development of three-dimensional islands and later, in thicker continuous layers, the development of crystallographically aligned periodic ripple patterns, due to elastic strain relief in the developed surface corrugation. In the case of Ar^{+} laser assisted CBE of GaAs the laser assisted GaAs epilayer is grown on GaAs, and both the epilayer and the underlying GaAs will be compressively strained due to thermal expansion as a result of the laser induced temperature gradient. Thus the laser imposes a strain before growth commences and the laser deposited material is in this respect in identical to the underlying substrate. The laser assisted layer will not nucleate as a conventional strained epilayer but its growth will be analogous to conventional continuous strained layer growth. It is suggested that Ar^{+} laser assisted CBE under these conditions develops a ripple pattern in a similar way to continuous strained layer growth (after the initial three dimensional island nucleation phase) and elastic strain relaxation results from the development of a ripple pattern. The lower compressive stress required to produce the ripple pattern, with respect to InGaAs on GaAs, may be due to the different surface energy and growth dynamics.

Laser light scattering was used to monitor the development of the ripple pattern (using no rotation, and thus giving no angular information). This was performed at an angle of 23° corresponding to a maximum sensitivity to roughness of lateral period 1.2μm (section 3.3.3), not the period of the ripple pattern. For roughness of 1.2μm lateral period the measured intensity is proportional to the height squared(see section 3.3.3). The LLS intensity during growth of 400nm of laser assisted growth at a substrate temperature of 357°C and a laser power of 2W is shown in figure 6.12. The LLS intensity increases roughly exponentially after about 150nm of growth. This is consistent with the development of a strain induced surface corrugation. Once three dimensional islands develop these reduce the local stress at their apex and increase it at their base, due to

elastic strain relaxation. This lateral strain variation results in a local growth rate increase at the apex and a local growth rate reduction at the base. This then initiates further ripples alongside, resulting finally in a periodic array of ripples. The periodic array of ripples once present will thus auto-accelerate in height, as observed in figure 6.12, due to the lateral strain variation and resulting lateral growth rate variation. The development will be energetically favourable if the strain energy relieved is greater than the increase in surface energy due to the ripple development. The lateral period of the ripple pattern was similar to the size of islands observed in the unirradiated material suggesting that the surface diffusion length of adsorbed species is important in the period (or existence) of the array, as is expected since the strain variation does not effect the overall growth rate, but only the relative incorporation across the surface. The dimensions are also expected to be dependent on the strain and material properties such as the Young's Modulus.

The periodic ripple pattern was not observed for assisted growth on substrates with larger (~1μm diameter) islands which formed during substrate cleaning because of a lack of chamber outgassing prior to substrate loading. These islands will themselves undergo elastic deformation and the development of a smaller scale periodic ripple pattern will not be favourable. This elastic strain relaxation may be a cause of the morphology deterioration observed during most laser assisted growths. It is suggested that at substrate temperatures below 357°C the ripple pattern did not develop at the maximum available power (2.5W) due to the reduced strain per watt of power, a reduced diffusion length of adsorbed species, and different growth kinetics occurring at laser assisted growth from the reduced substrate temperature.

Elastic strain relaxation could, at least in part, also be responsible for the very pronounced ripple structure reported (Farrell et al. 1993) in pulsed excimer laser assisted CBE growth of GaAs, where the periodic temperature rise can be several hundred degrees.

6.2.6 Discussions

Figure 6.13 shows the temperature dependent unassisted growth rate, found by laser interferometry, with that reported by other workers. An offset in substrate temperature is shown applied to the results by other workers. This is justified since substrate temperature measurements, although self consistent will not be absolutely correct due to the measurement technique (see section 4.3). The data are also shown normalised to the maximum measured in each set to account for the different beam fluxes used. With the normalisations each set of data is reasonably comparable.

The laser assisted growth rates found in this study, by laser reflectometry are shown in figure 6.14 as a function of temperature for three laser powers, along with the unassisted growth rate. An Arrhenius plot (not shown) did not show a constant activation (i.e. a straight line of log(growth rate) against log(1/substrate temperature)) energy either for unassisted and assisted growth. This shows that the growth rate is not limited by a single reaction but by a number depending on the growth conditions. Thus activation energies were not calculated or used in evaluating the growth kinetics.

Shown in figure 6.15 are the results of other studies into the temperature dependence of laser assisted growth, normalised identically to their respective unassisted curves. All studies do show a reasonable consistency in appearance. With the exception of Sugiura *et al.* (1988) all show a shift in temperature from the unassisted curve, and similar shape to the unassisted curve above ~380°C, but a different shaped curve below ~380°C.

Since different spot sizes were used in each study an indication of the dominant process in laser assisted CBE may be found. If the enhancement were purely thermal then a power over radius relationship would be expected whereas if purely photolytic decomposition of adsorbate molecules were responsible then a power over radius squared

(power density) relationship would be expected (see section 3.1). The results shown in figures 6.14 and 6.15 are not consistent with either, which may be due to differences in estimating the spot size and enhancement (the other studies used stylus profilometry which is expected to give a less accurate measure of the maximum growth rate, as opposed to the incident power averaged growth rate for laser interferometry). However all studies are more consistent with a power over radius relationship than power over radius squared (or simply power). In particular Yamada et al.(1989), Dong et al. (1995) and the results from this study at 1W are all similar in appearance and similar in power over radius, but differ in laser power over radius squared by a large degree. The data from Sugiura et al. (1988), from which the photolytic mechanism was proposed does not agree with either relationship, but is somewhat closer in terms of power over radius, and shows considerable scatter. Thus comparing all studies does strongly suggest a dominantly photo - thermal mechanism to laser assisted CBE. At low temperatures (350°C and below), where a step change in growth rate with laser power was observed in this study, deviation from this relationship is apparent in all studies, usually with an increase in growth rate from that expected, showing some non thermal element is contributing.

6.2 High temperature laser inhibited growth of GaAs

6.2.1 Growth rate results

The growth rate of GaAs, using TEG and pre-cracked arsine as precursors, measured using RHEED and post growth cleaved edge TEM layer thickness measurements shows a temperature dependence above approximately 500°C (Joyce *et al.* 1992) shown in figure 2.1. This is in agreement with work performed by other workers (e.g. Robertson et al. 1988). Above approximately 670°C the growth rate decreases rapidly with increasing temperature, attributed to desorption of Ga and adsorbed TEG molecules. Between 500°C

and 670°C a slower decrease in growth rate is observed, attributed to desorption of adsorbed TEG molecules (Robertson et al. 1988).

The aim of laser inhibited growth is to produce local decrease in GaAs growth rate, by locally heating the substrate. In this study substrate temperatures of 500 - 650°C were used since these are the conventional CBE growth temperatures and conventionally result in the most favourable surface morphology and structure. The growth rate reduction was expected to be great enough to be of use in changing layer composition for device fabrication.

Using laser reflectometry (laser interferometry) to measure the temperature dependent growth rate of GaAs between 500 -670°C has not been as successful as at other temperatures. The increase in refractive index with temperature resulted in the growth rate to appear to continue to increase to 550°C then to be almost level until over 670°C. Using a linearly temperature dependent refractive index the growth rate does agree with Joyce *et al.* (1992). Laser interferometry measurements made during laser inhibited growth, in the range of 500 - 625°C and up to 2.5W laser power, showed no consistent change in period and without knowledge of the exact temperature in the laser irradiated area were meaningless. Further work (Dugdale, 1996) from substrate temperatures above 650°C, where the growth rate decreases much more rapidly with temperature, a growth rate decrease was measured, consistent with a local temperature rise of ~35°C per watt of laser power.

Between 500 - 625°C local growth rate inhibition was confirmed with post growth Nomarski optical interference microscopy. Although the exact amount was not measured.

6.2.2 Morphology results

The development of surface morphology during laser inhibited growth was monitored from scattered light (LLS), and characterised by post growth Nomarski optical-interference microscopy (NOM) and atomic force microscopy (AFM). The LLS scattering intensity variation during the growth of laser inhibited layers grown at a substrate temperature of 600°C, 2W laser power, 2torr TEG and 700torr AsH_3 was monitored . The intensity increased on growth but then later decreased, perhaps due to the periodicity of the roughness changing. The final intensity is only slightly higher than that observed away from the laser affected area indicating that the height of the surface roughness was only slightly increased by laser irradiation.

Nomarski Optical interference Microscopy of laser inhibited layers showed a cross-hatch pattern. Figure 6.16 shows the surface morphology of a layer grown at 600°C and 2.25W. Islands with a wide period distribution of around 3mm in the [-110] and 0.7mm in the [110] are observed as shown in figures 6.16b and 6.16d of average height 10nm away from the laser area increasing to 20nm in the laser area, measured by AFM. Figure 6.16a also shows striations in and around the laser area. These were observed to extend up to 6mm from the centre of the laser area in this sample. Figure 6.16b taken near the centre of the laser area, and at higher magnification shows a ripple pattern where clearly the positions of the ripples are defined by lines in the <110> directions. Figure 6.16b taken a few mm below the laser irradiated area shows a low density of defined striations predominantly in a direction emanating from the laser irradiated area. This cross hatch pattern was observed in all laser modified growths above 550°C and 0.5W laser power and at 500°C and 2.5W laser power, but not in laser assisted layers from below 400°C even at the maximum available laser power, 2.5W. At higher laser powers and/or substrate temperatures the pattern in the laser area more

resembled that observed in $In_xGa_{1-x}As$ / GaAs hetereoepitaxy (e.g. Beanland, 1992). This is in rough agreement with the Hussein et al. (1989) model. However, when the cross-hatch pattern was observed it always extended a number of mm from the centre of the laser irradiated region and did not at low powers just occur in the centre, inconsistent with the Hussein *et al.* (1989) model which predicts a plastic deformation region extending from the centre a distance within the strained area dependent on the laser power and substrate temperature.

The cross-hatch pattern was not detectable on samples which were annealed by the laser under the same conditions except for no TEG flux for the same length of time. This suggests that the cross-hatch was growth dependent and thus due to lateral strain variations inducing a lateral local growth rate variation, and not directly due to surface steps created by the dislocation glide. However the 'cross hatch' lines were along the <110> directions and very straight which suggests that, if they were strain driven that they mostly ran along the [110] and [-110] directions on a plane or interface parallel and near the surface which is not expected as the strain field should decrease slowly throughout the substrate thickness.

The thermal expansion coefficient of GaAs, $\beta(T)$ changes with temperature by the relationship $\beta(T) = (5.69 + 0.0015T)\ 10^{-6}$ per K above 400K (Brice, 1989). 2W laser power, from a substrate temperature of 600°C will result in a local temperature rise of the order of 70°C and thus a local strain of 5×10^{-4} or 0.05%. The density of threading dislocations arising from the substrate is typically below $10^4 cm^{-2}$ in high quality GaAs grown by the horizontal Bridgeman technique. If each misfit dislocation arising from the bending over of these dislocations were to move to the edge of the wafer, the maximum strain that can be relieved is also 0.05% for 5cm GaAs substrates. So most of the strain induced by the laser irradiation could feasibly be relieved by movement of threading dislocations and without the introduction of additional dislocations. Low misfit InGaAs

epilayers grown on GaAs substrates of a thickness which results in this level of strain relaxation often contain lower threading dislocation densities than their substrates over most of the substrate area due to the threading sections moving to the edge of the substrate. Thus it may be that plastic deformation is not always undesirable as was stated by Hussein *et al.* (1989) but may in fact reduce the dislocation density in the irradiated region.

An etch pit study was conducted to measure the threading dislocation density as a function of radius from the laser irradiated region on a 500nm thick laser inhibited epilayer grown at a substrate temperature of 600°C and 2W laser power . 500nm was etched by a $Cr0_3$ etchant. The 'cross hatch' pattern was further defined out to a distance of ~5mm. These lines were often terminated by an etch pit from a threading dislocation. However the etch pit dislocation density was constant with radius at a density of 3±1 x $10^3 cm^{-2}$ the same as that away from the laser effected area. Thus the laser irradiation may have resulted in relaxation but not by dislocation multiplication or surface half loop generation and the crystalline quality will not be effected. The 'cross hatch' was found to have a spacing of approximately 10µm, corresponding (assuming one dislocation per line) to a strain relaxation of 0.005% around 10% of the induced strain. This residual strain, once irradiation stops is expected to have little effect on the electrical properties of the layer.

6.2.3 Discussions

NOM demonstrated a local decrease in growth rate for laser modified CBE above 490°C. Other work (Dugdale, 1996) at higher substrate temperatures (>625°C), where the growth rate decreases more rapidly with increasing substrate temperature found that laser interferometry could be used to measure the local growth rate inhibition, and this inhibition was consistent with a temperature rise of ~35°C per watt of laser power, in

rough agreement with that shown in laser assisted CBE below 490°C. Thus it is concluded that the inhibition in growth rate is photothermal, and could be modelled using a heat flow equation, although allowance for the finite substrate dimensions should be made.

Laser irradiation resulting in a temperature rise of approximately 20°C by this model (e.g. Lax, 1977) or more at the substrate temperatures of laser inhibited CBE (>490°C) results in plastic deformation. This is consistent with the criteria for plastic deformation presented by Hussien *et al.* (1990). This further demonstrates the thermal effect of the laser irradiation. However the plastic deformation in the laser affected area was only by the movement of threading dislocations arising from the substrate, and present before epitaxial growth, and the change in lattice constant only around 0.005%. Thus device operation is unlikely to be altered by the plastic deformation. The plastic deformation extends up to 6mm from the laser irradiated area. Dislocation segment which have bent over parallel to the surface result in a lateral strain variation during irradiation which results in local growth rate variation during laser modified CBE above 490°C, and the development of a surface 'cross-hatch' pattern.

6.3 Summary of chapter

In summary it has been shown that there are two temperature regimes for Ar^+ laser assisted CBE using TEG and pre-cracked arsine as precursors. Above 350°C, there is strong evidence for the enhancement being dominantly photo-thermal ; a good fit between laser power and temperature rise at a temperature rise of 44°C/W within error of the modelled temperature rise of 28°C/W; variation with growth rate with chopping frequency at the frequency predicted from a time dependent heat flow equation; carbon incorporation reduction consistent with the thermal model; strain effected morphology at high (>1.5W)

laser powers; and growth rate dependence on laser spot radius more consistent with a power / radius relationship than a power density relationship.

The growth rate enhancement is by a factor of up to 20 depending on laser power / radius, substrate temperature and group V : group III flux ratio.

A surface ripple structure, partially aligned along the <110> directions, is observable in the laser affected area at high laser powers and substrate temperatures between 360-450°C. This is consistent with thermally induced elastic strain in the laser affected area resulting in variations in local growth rate. The development of the ripple structure is followed in real time using diffusely reflected light from the Ar+ laser and it is shown that the ripples start to appear after ~150nm of growth. Unintentional carbon incorporation is also reduced in the laser affected area, consistent with a local temperature rise.

Below a substrate temperature of 360°C a step change in the growth rate with laser power is observed. This step change indicates a deviation in the origin of the enhancement from purely photothermal. The position and sharpness of the step change in terms of laser power and the GaAs growth rate are dependant on the group V: group III flux ratio, indicating that the As_2 surface coverage has an important role in the growth kinetics of both unassisted and laser assisted CBE. A decrease in V:III ratio results in increased growth rates at lower laser powers and the step change moving to lower laser power and becoming broader. Laser assisted CBE at substrate temperatures (~313°C), and high (>5:1) V:III flux ratio, where the step change is greatest result in the greatest growth rate selectivity with high laser power. These conditions resulted in selectivity of around 20 times and well defined features grown with laser assistance.

Laser reflectometry, also known as dynamic optical reflectometry (DOR) and laser interferometry, is demonstrated to be suitable for monitoring the growth rate of laser assisted CBE of GaAs.

Laser modified CBE of GaAs at substrate temperatures above 490°C result in a growth rate inhibition. This is consistent with the photothermal effect observed below 490°C. However measurement was not obtained by laser interferometry due to the inhibition being small (<10%) and the temperature dependence of the refractive index. Above 490°C laser radiation, at laser powers required to produce an inhibition observable by Nomarski interference microscopy, also result in the development during growth of a surface 'cross-hatch' pattern of ridges aligned along the <110> directions, extending up to 6mm from the laser irradiated area. Such 'cross-hatch' patterns are believed to be associated with dislocations parallel to the surface, and indicate that thermally induced plastic deformation has occurred. An etch pit density study of one such sample revealed no net change in threading dislocation density in the region with respect to areas away from the laser area. However a number of those present were at the end of etched ridges, associated with segments parallel to the surface. It is suggested that the plastic deformation has occurred by the movement of threading dislocations already present from the underlying substrate without the nucleation of additional dislocations. This is consistent with the calculated thermal strain and density of threading dislocations originating from the substrate. The plastic deformation is thus not a significant problem in Ar+ modified CBE, and under the correct condition may possibly reduce the local threading dislocation density.

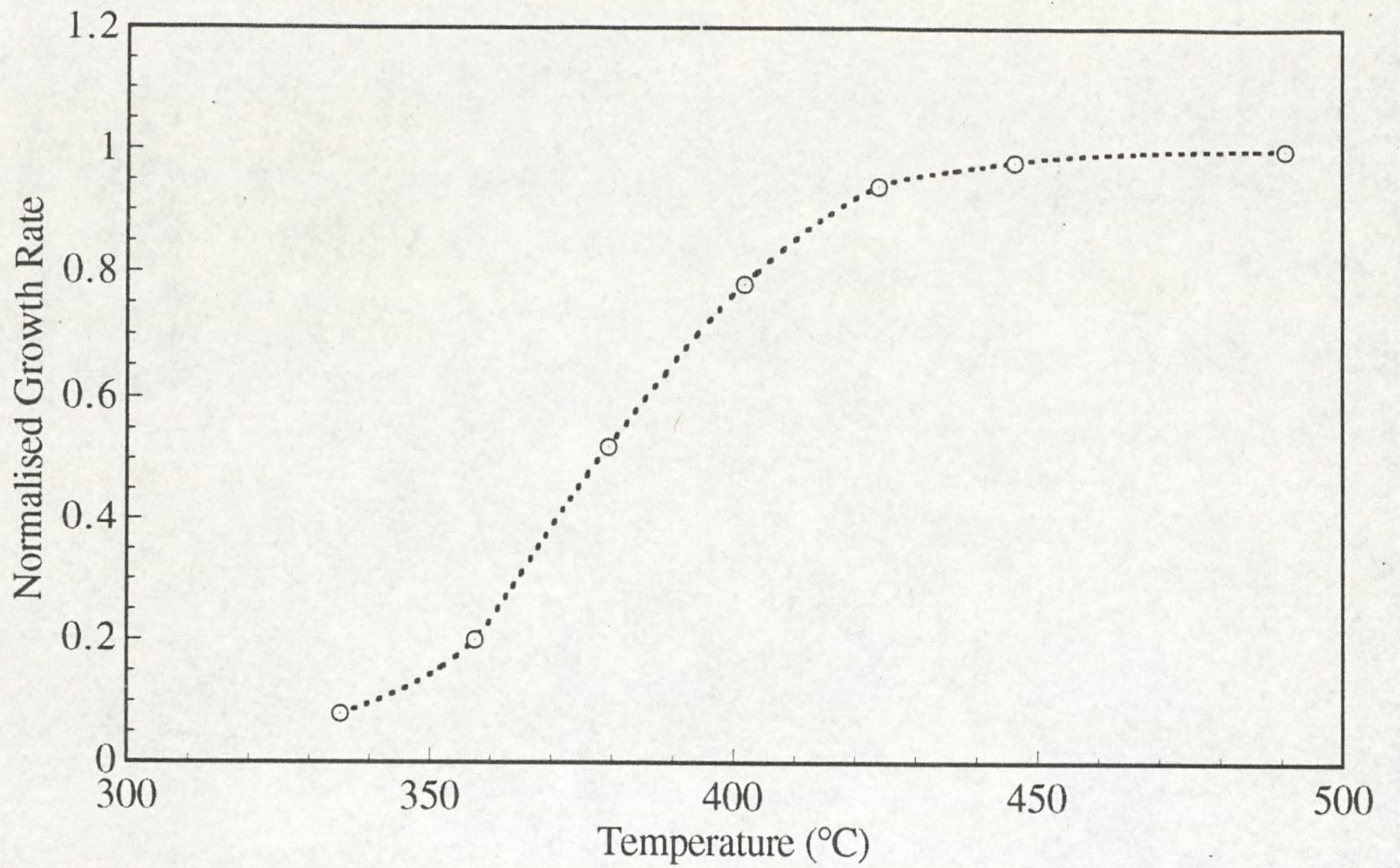

Figure 6.1: Temperature dependence of the growth rate of GaAs, using 4Torr TEG and 700Torr pre-cracked arsine, measured using laser interferometry.

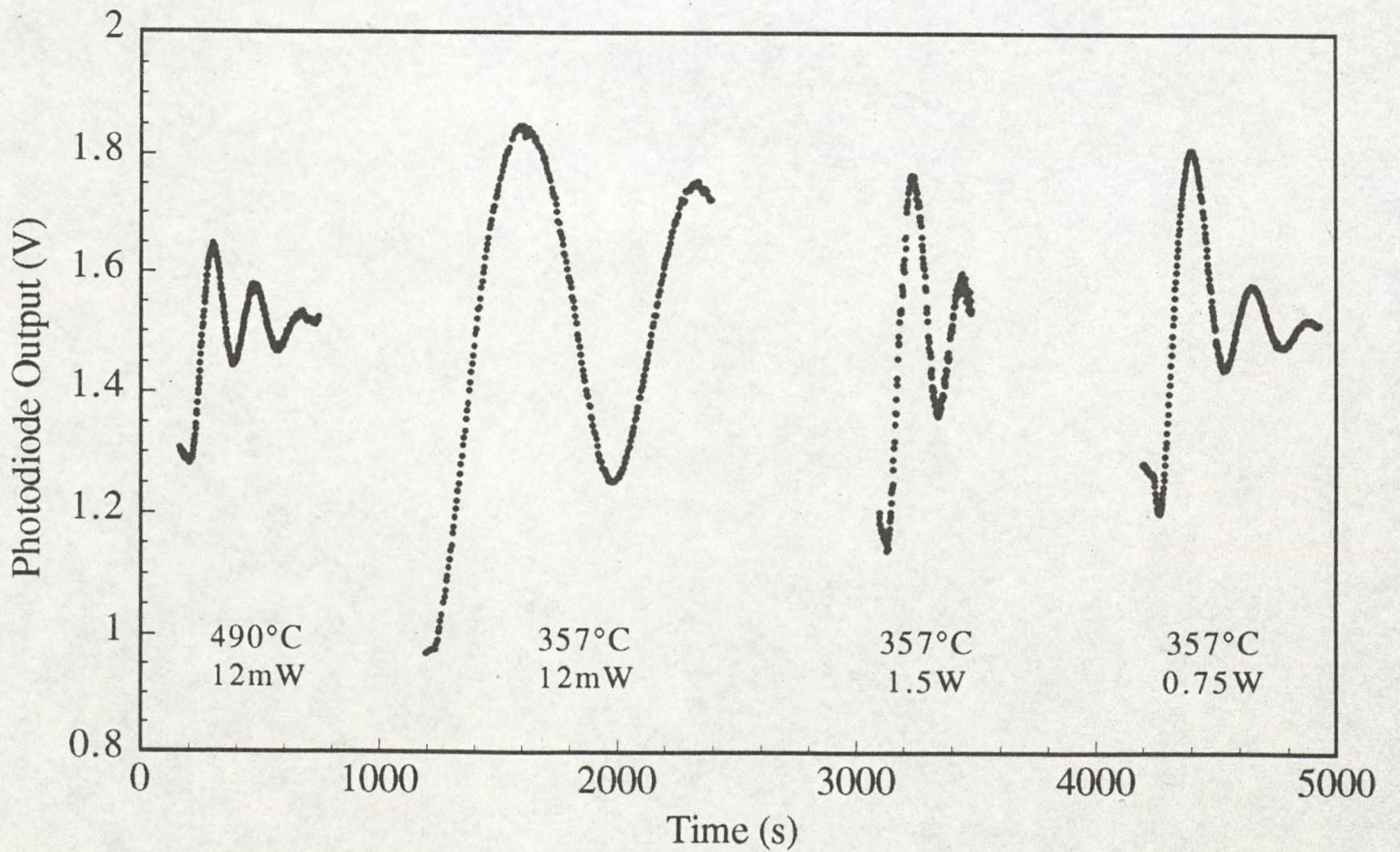

Figure 6.2: Laser interferometry traces for the growth of unassisted GaAs at the normal growth temperature (490°C) and laser assisted and unassisted GaAs at 357°C.

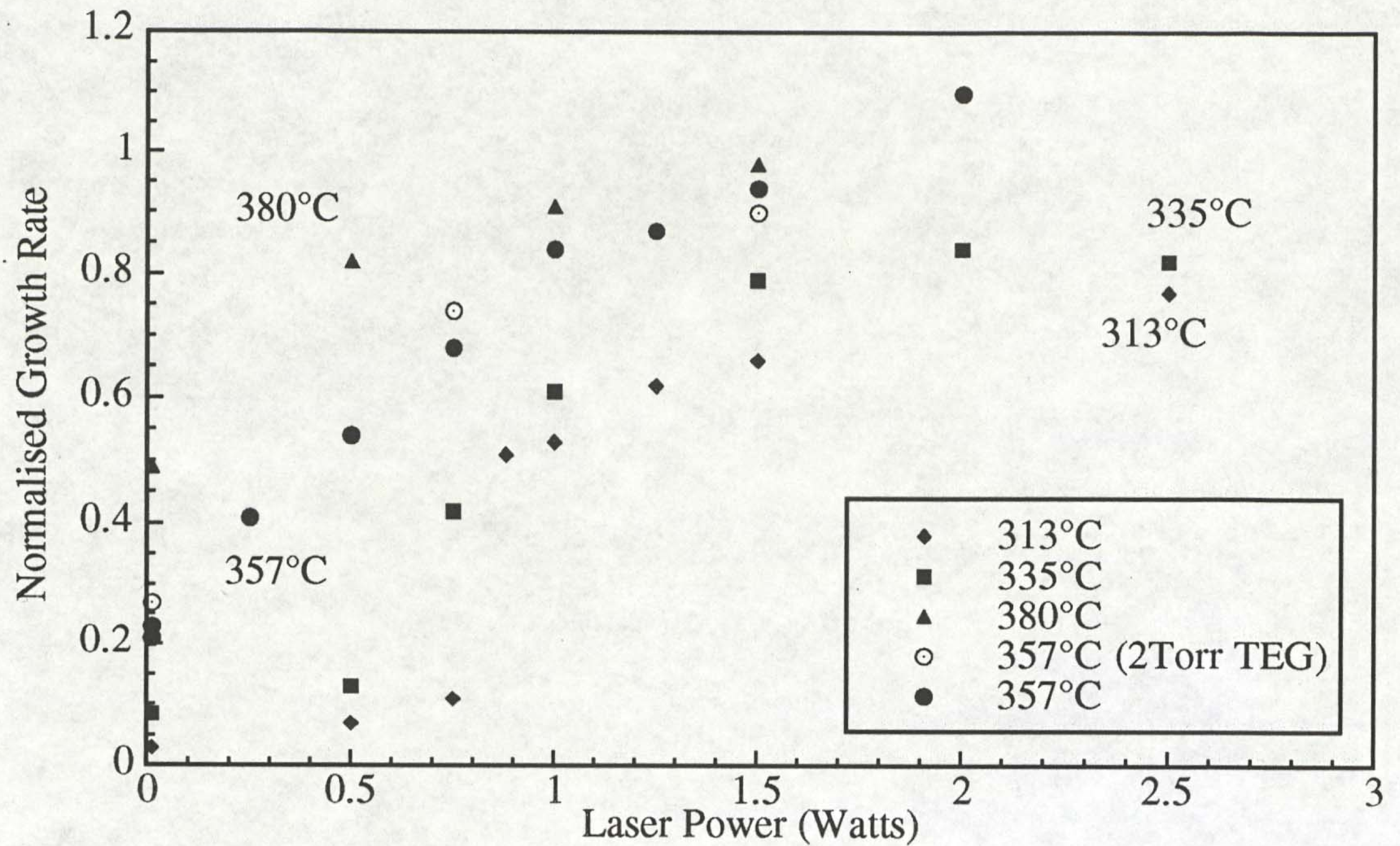

Figure 6.3: Laser assisted growth rates of GaAs, determined by laser reflectometry, using 4Torr TEG (except open circles, 2Torr TEG) and 700Torr precracked arsine. All data is shown normalised to the maximum unassisted growth rate of 0.54nm/s (except open circles, 0.27nm/s).

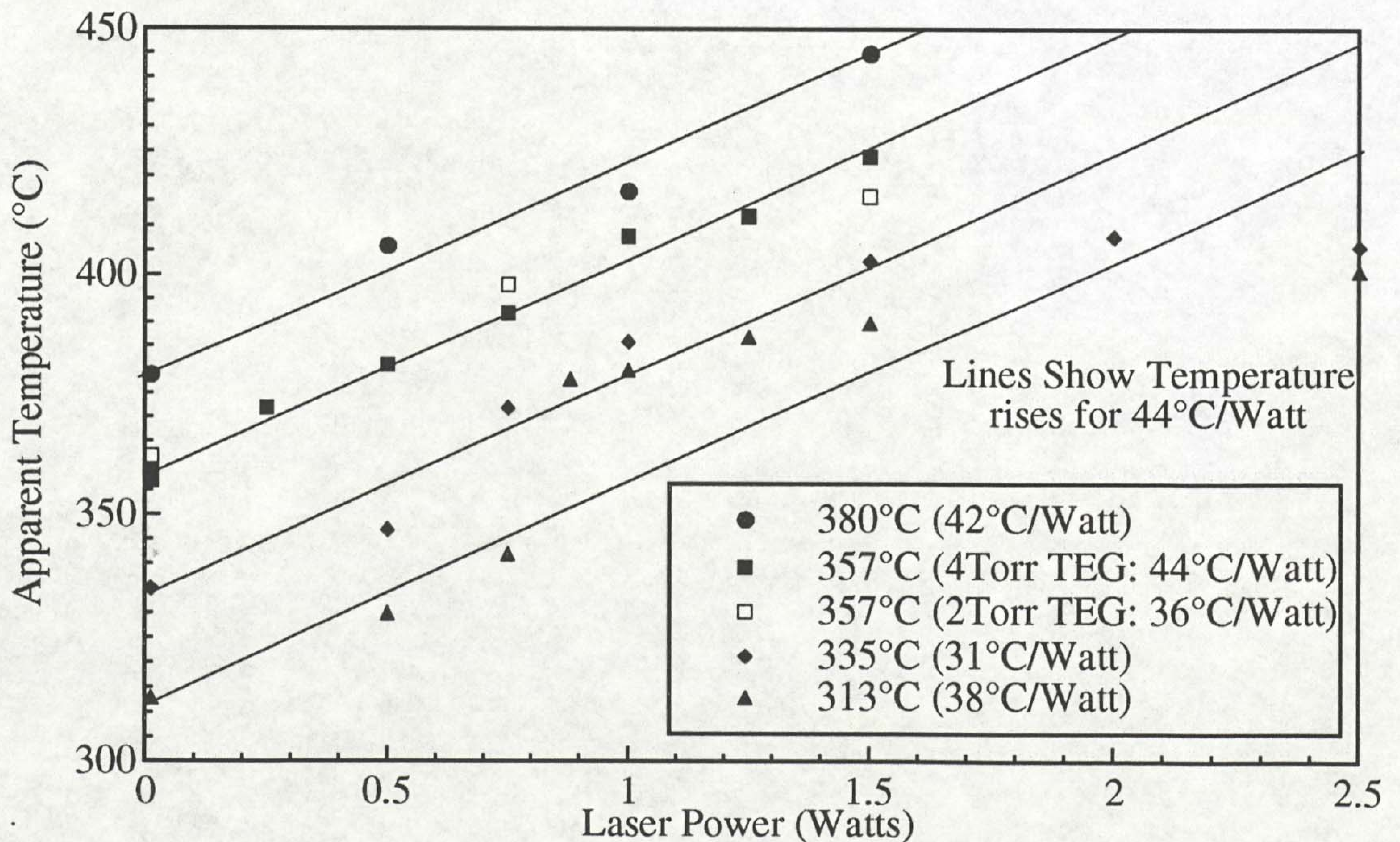

Figure 6.4: Apparent substrate temperatures for laser assisted growth of GaAs, assuming a purely photo-thermal enhancement. This was achieved by taking the growth rate from figure 6.4 and converting it to the corresponing substrate temperature with the same growth rate for unassisted growth from figure 6.1. Linear fitted laser induced temperature rises from the substrate temperature used are shown in the key.

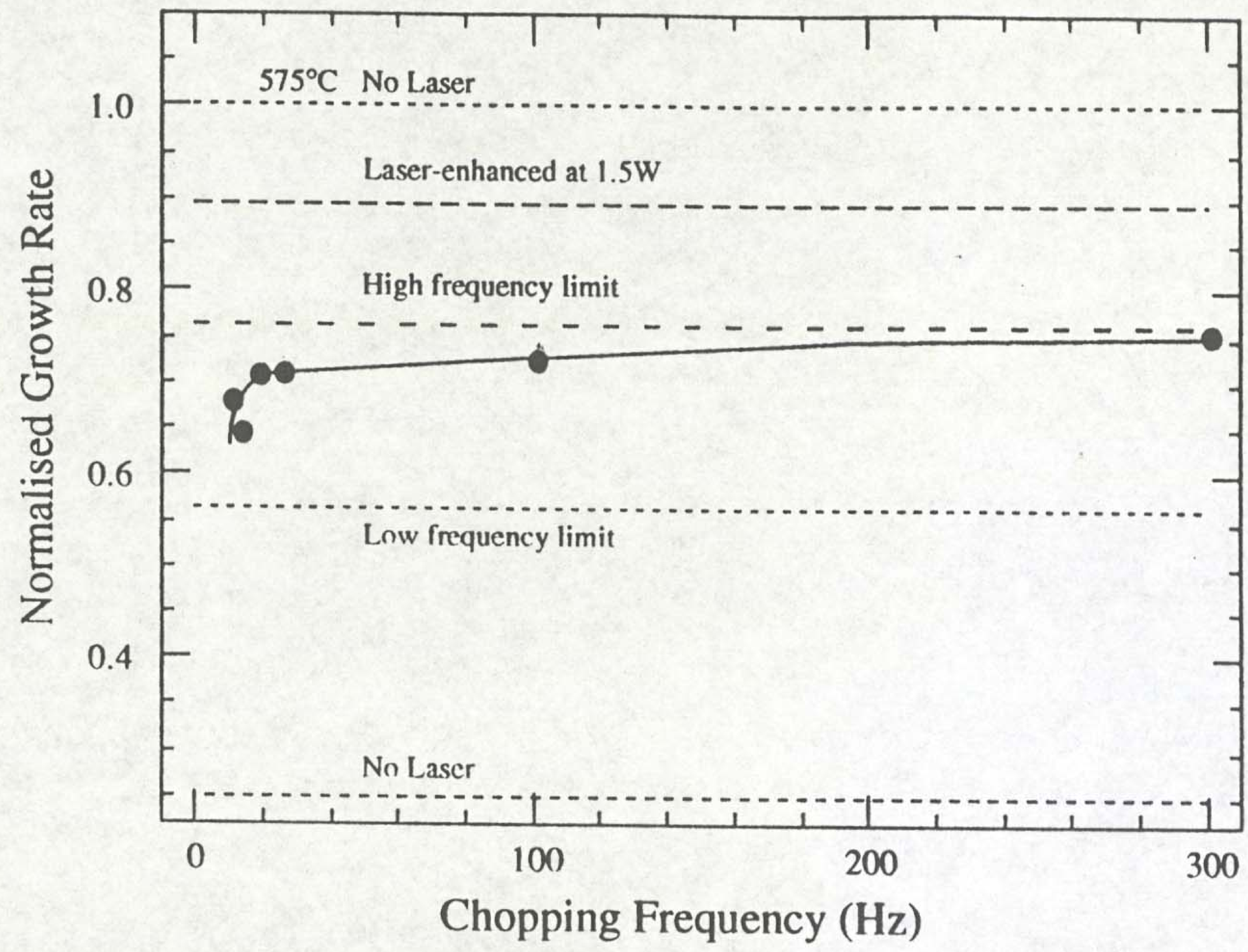

Figure 6.5: Effect of beam chopping frequency on the growth rate of laser assisted CBE at 357°C.

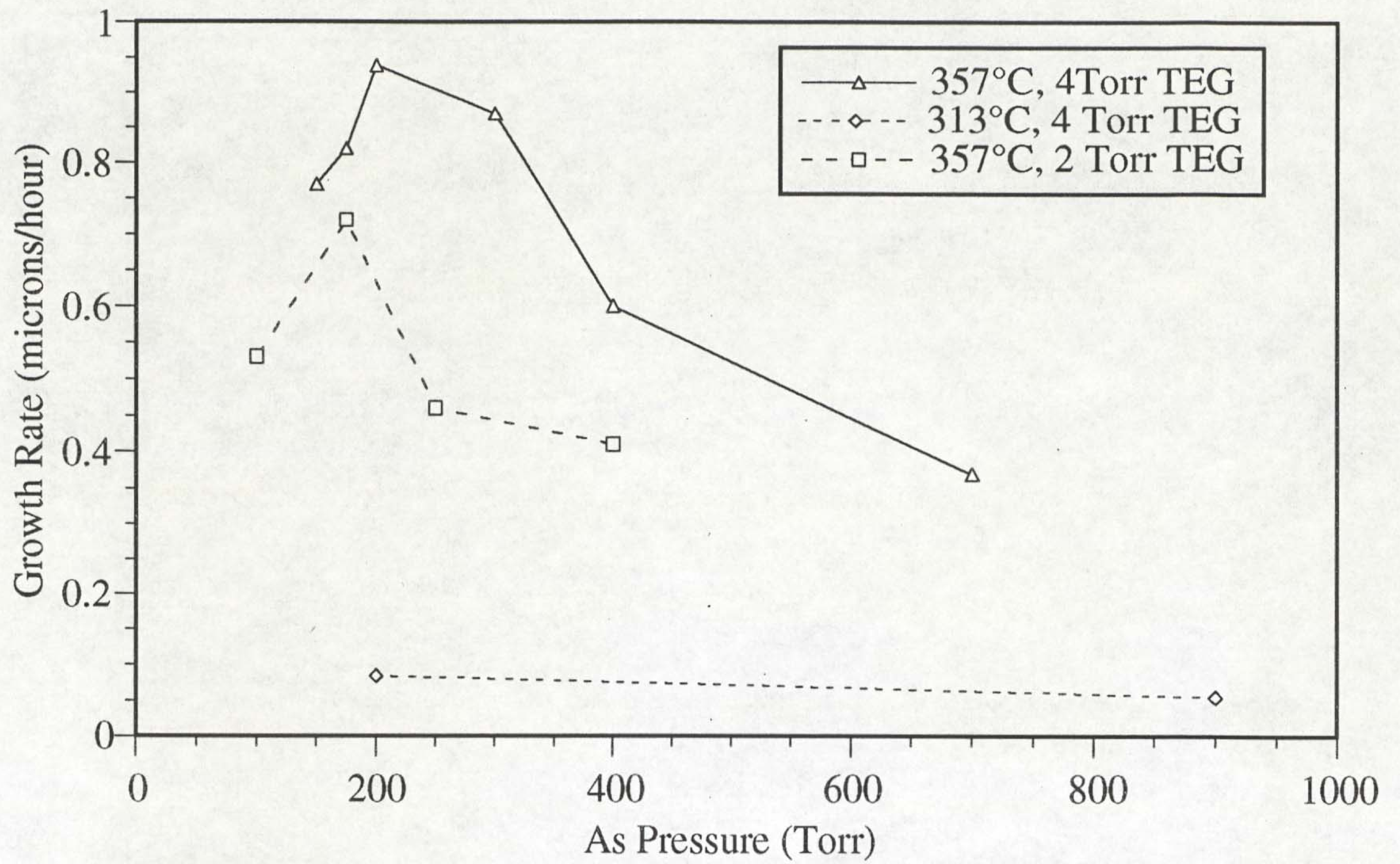

Figure 6.6: Effect of Arsenic line pressure on the growth rate of GaAs at 313 and 357°C.

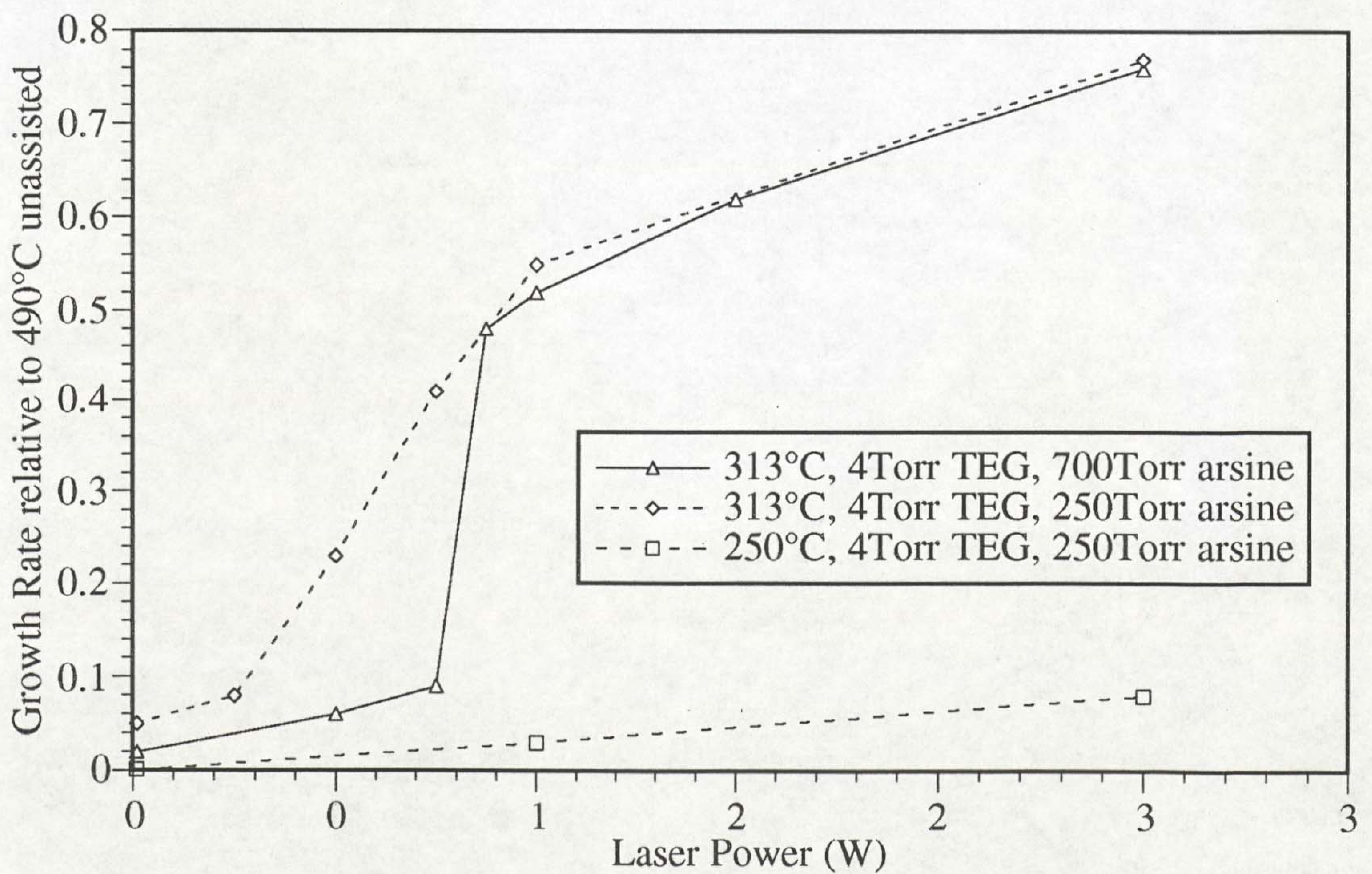

Figure 6.7: Arsine line pressure effect on the dependence of growth rate on laser power for laser assisted CBE.

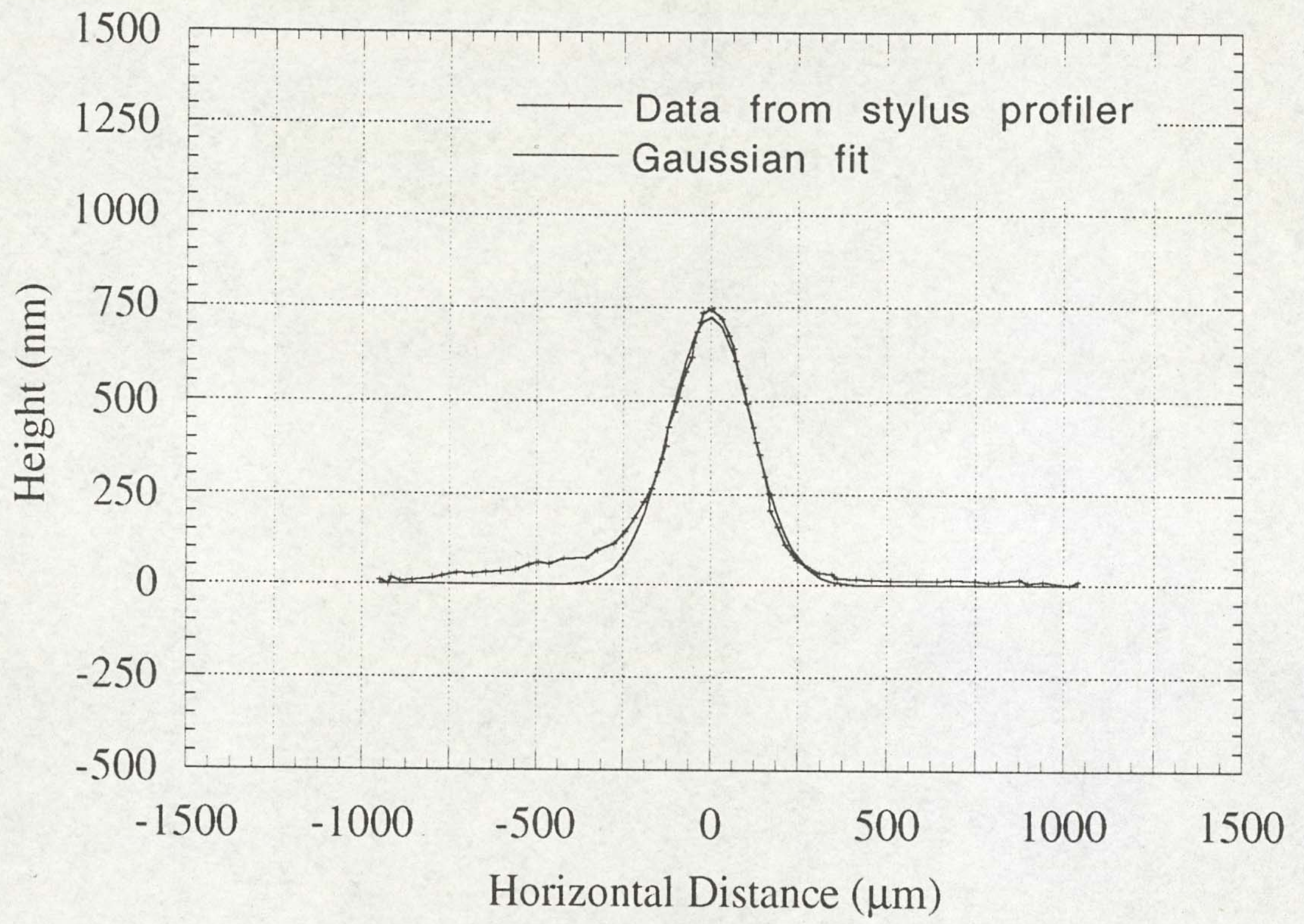

Figure 6.8: Height profile of a laser assisted feature grown at 357°C and 2W laser power, measured by stylus profilometry.

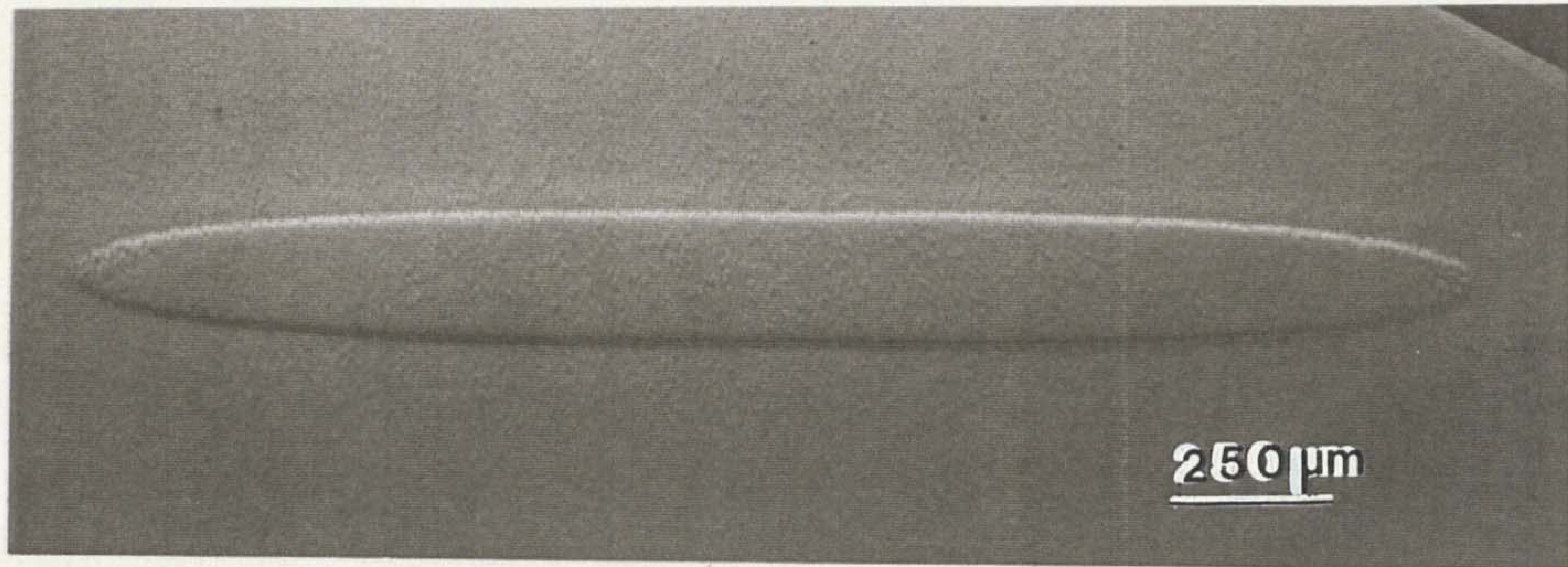

(a)

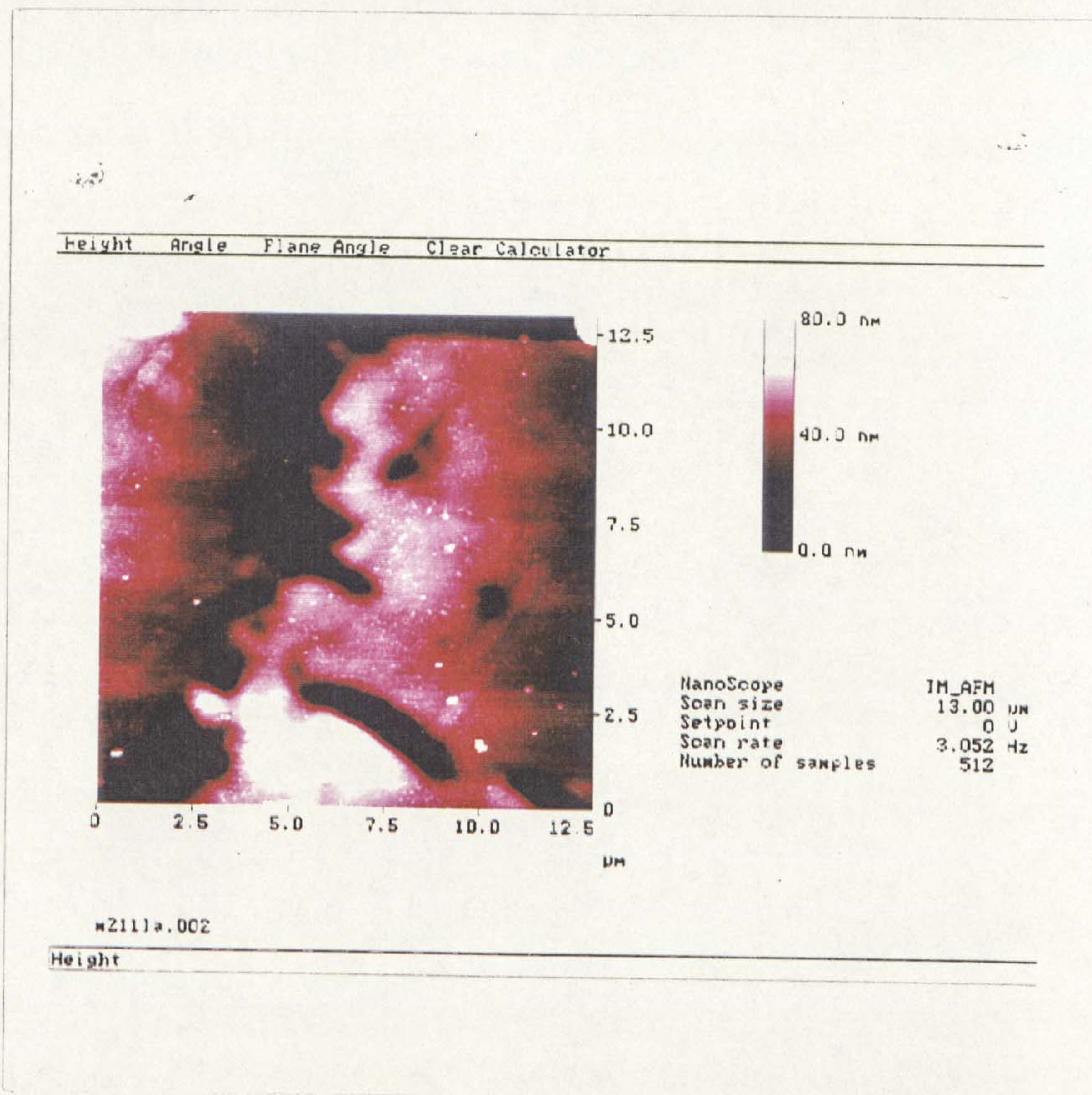

(b)

Figure 6.9: (a) Nomarski optical micrograph of a laser assisted feature (200nm high) grown at 313°C and 2W laser power. (b) AFM plot of the edge of the feature in (a).

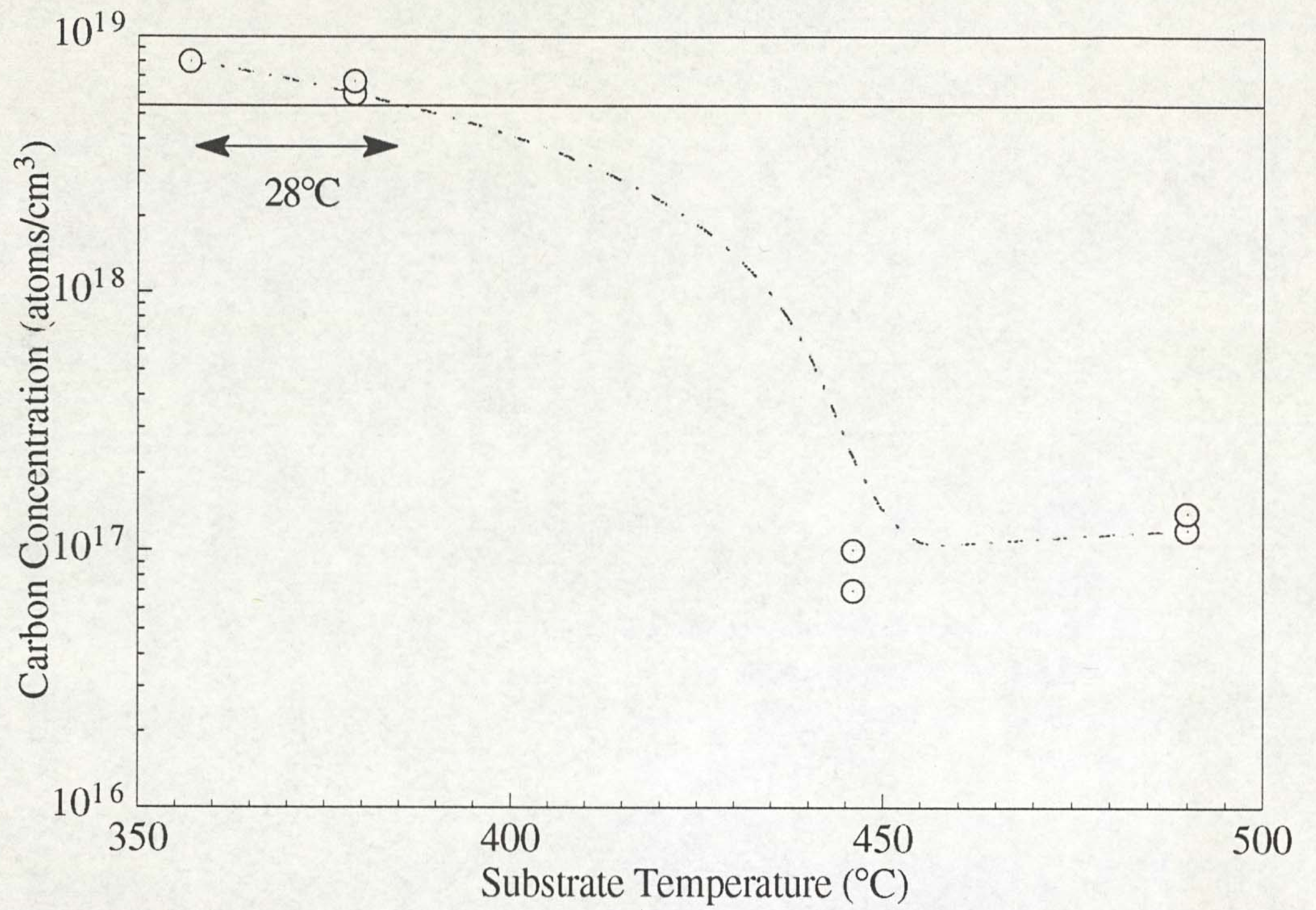

Figure 6.10: C-concentration from SIMS for laser assisted at 357°C and unassisted CBE between 357-490°C. The solid line indicates the C concentration for laser assisted growth at 357°C and 1Watt laser power.

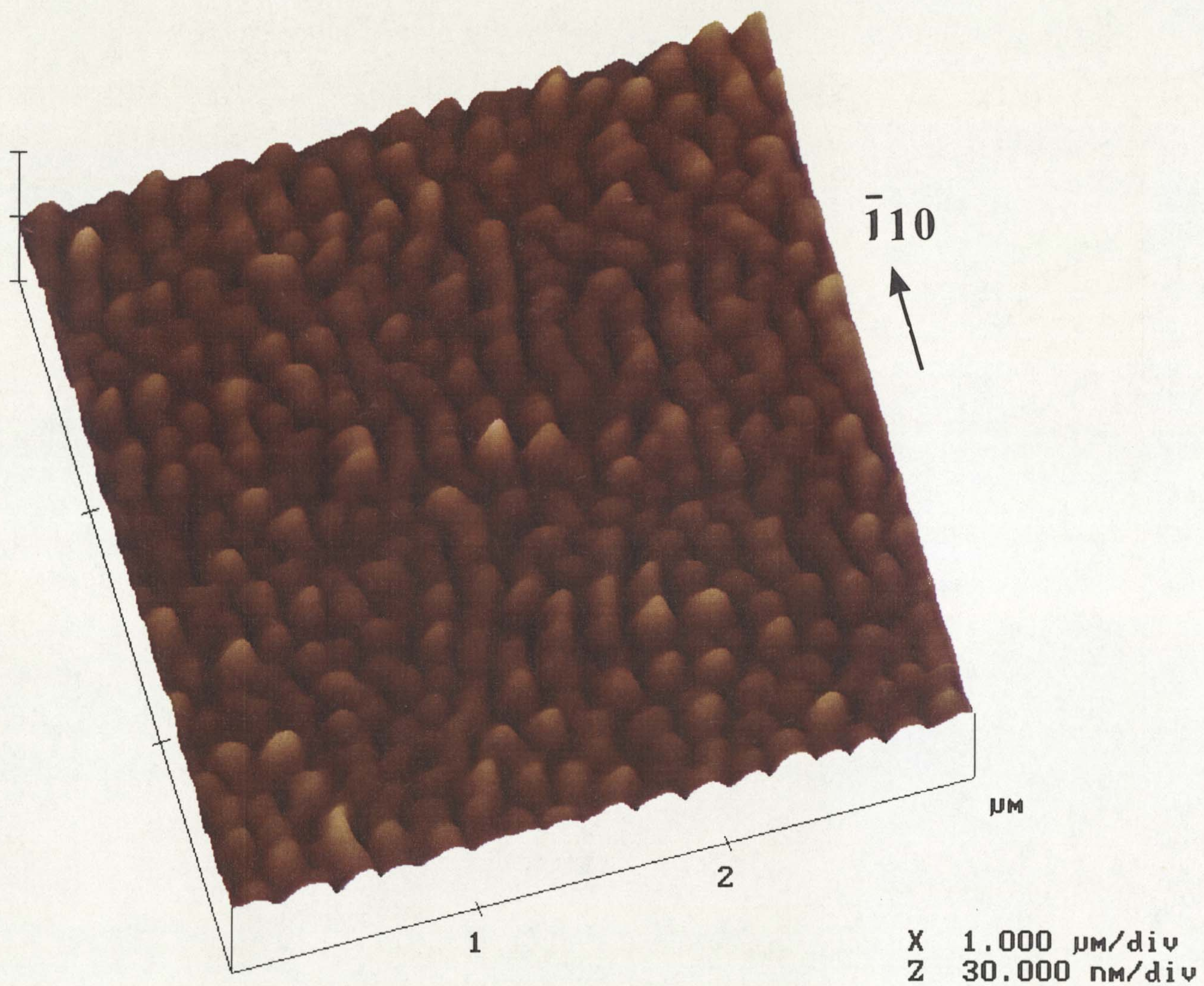

Figure 6.11: AFM micrograph of the surface ripple structure observed in laser assisted CBE at a substrate temperature of 357°C and a laser power of 2.5W.

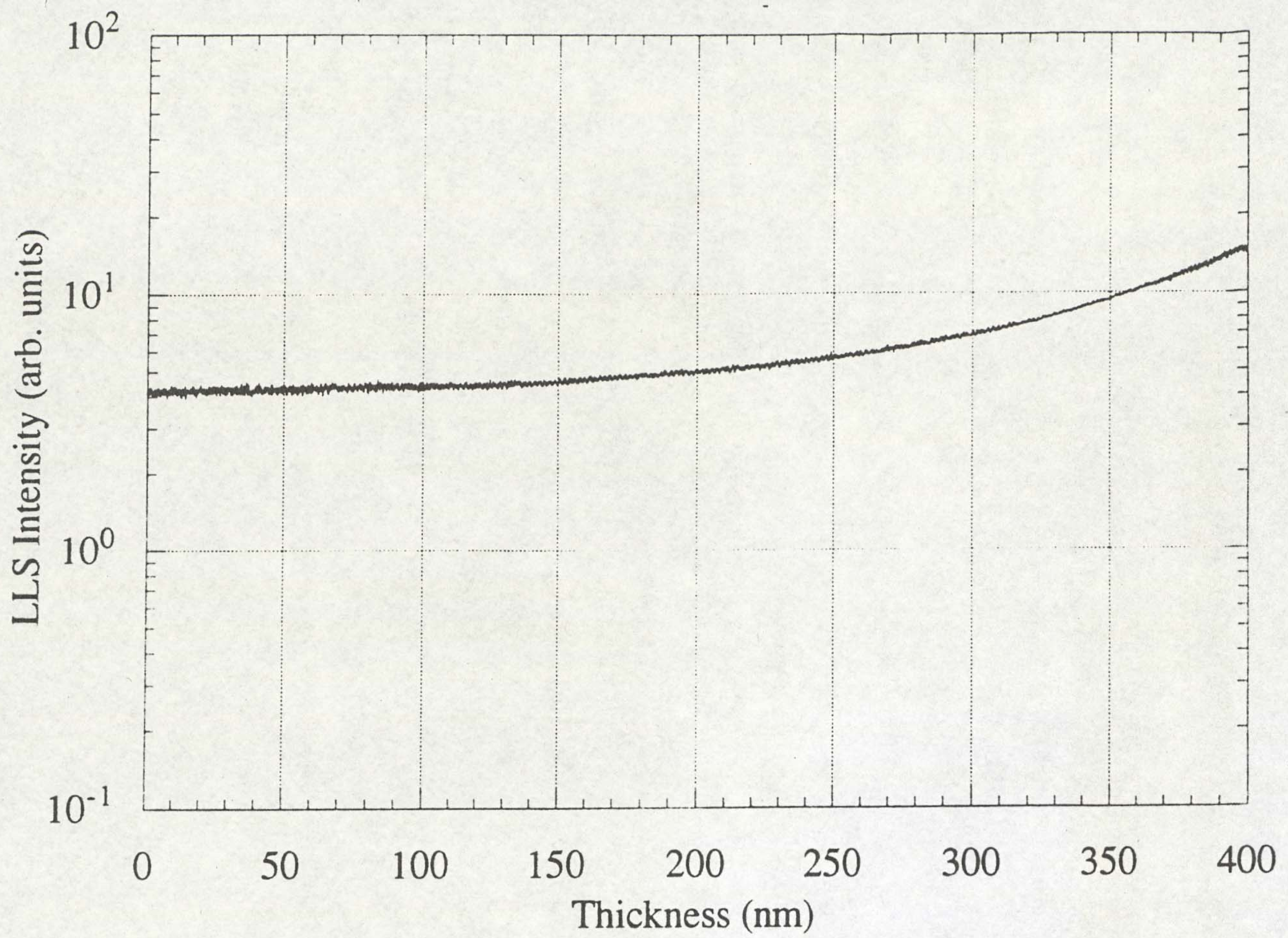

Figure 6.12: Laser light scattering trace of the development of the surface ripple pattern at a substrate temperature of 357°C and 2W laser power.

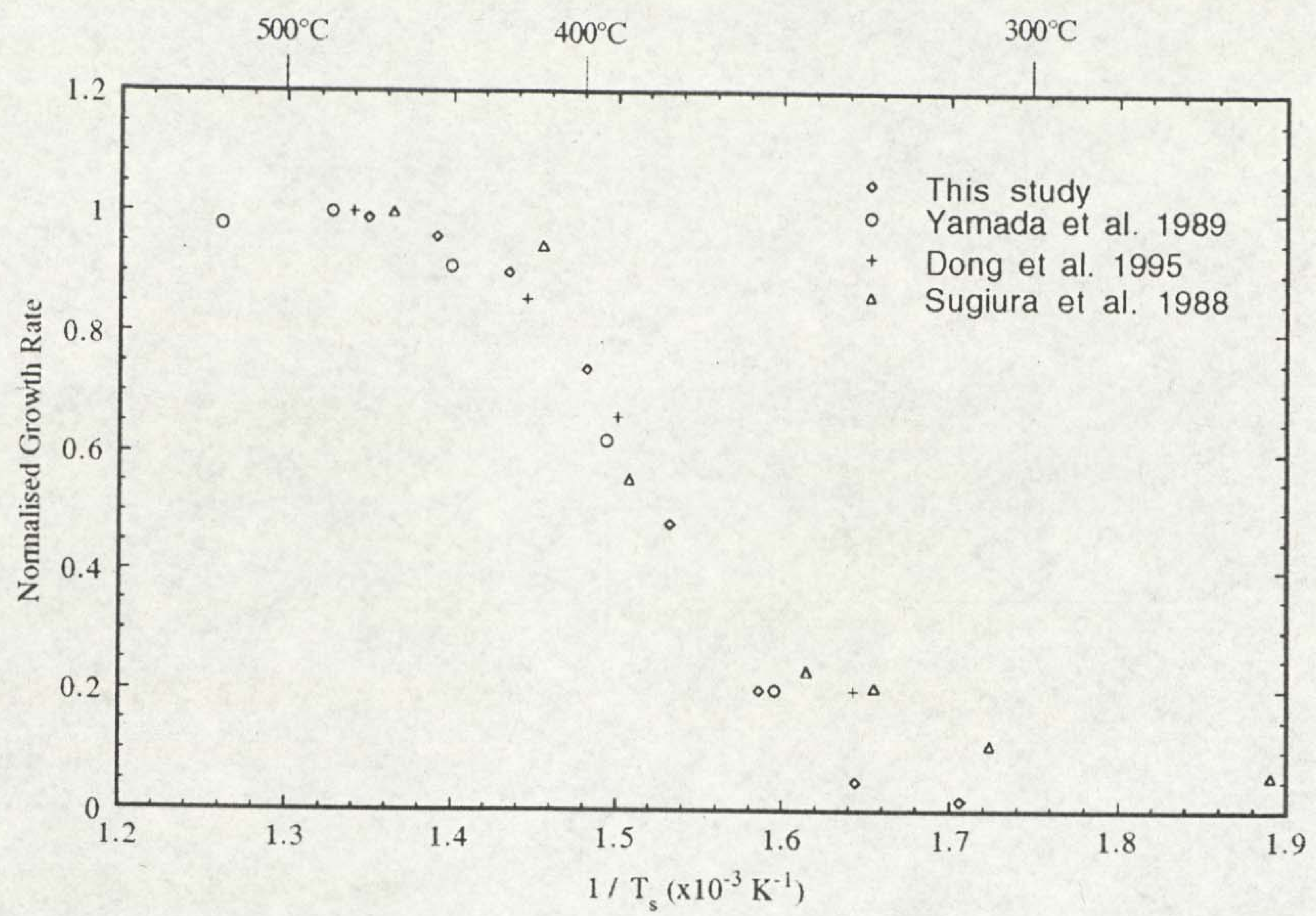

Figure 6.13: Temperature dependence of CBE growth of GaAs, as reported by a number of workers.

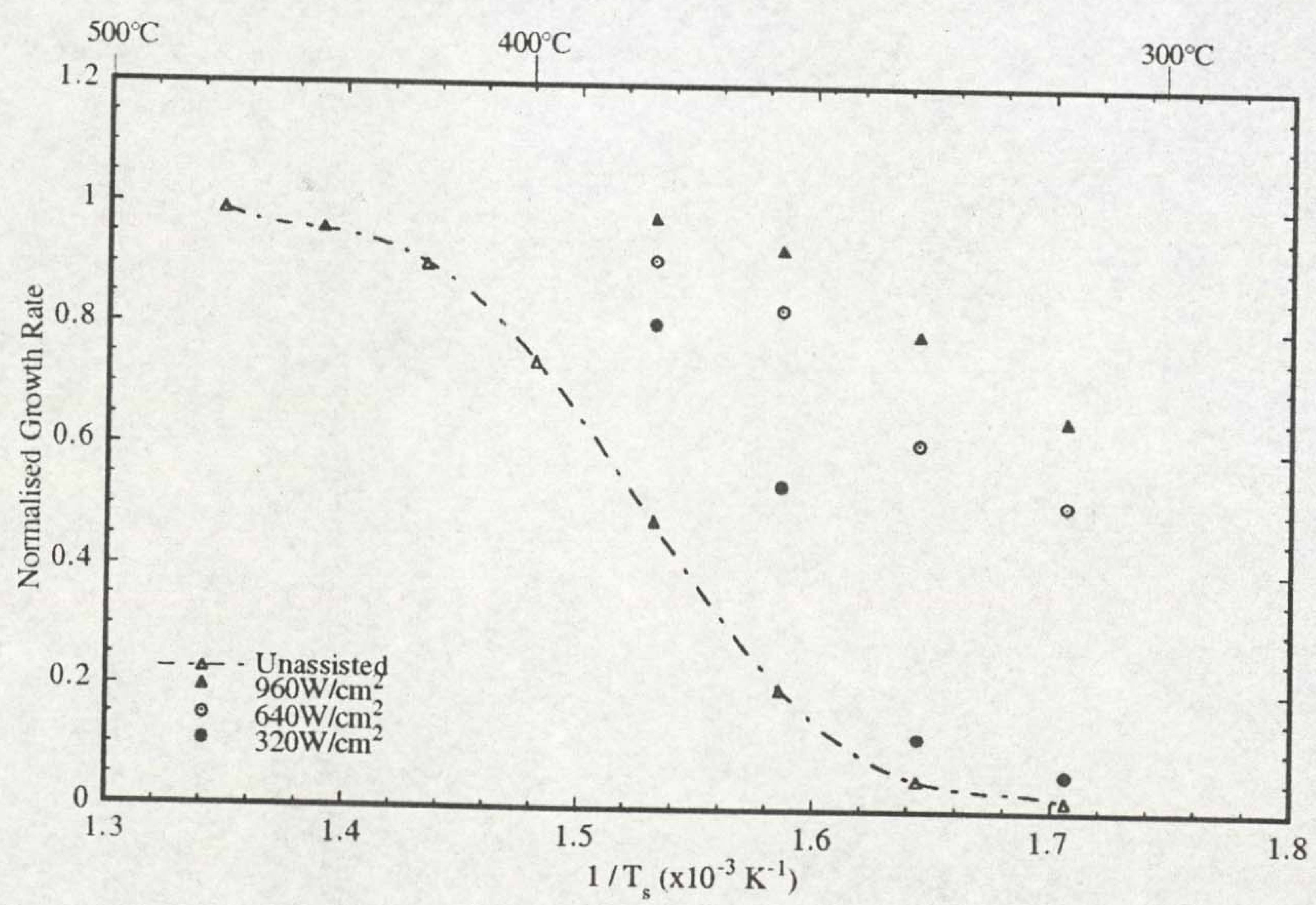

Figure 6.14: Temperature dependent growth rate of laser assisted CBE.

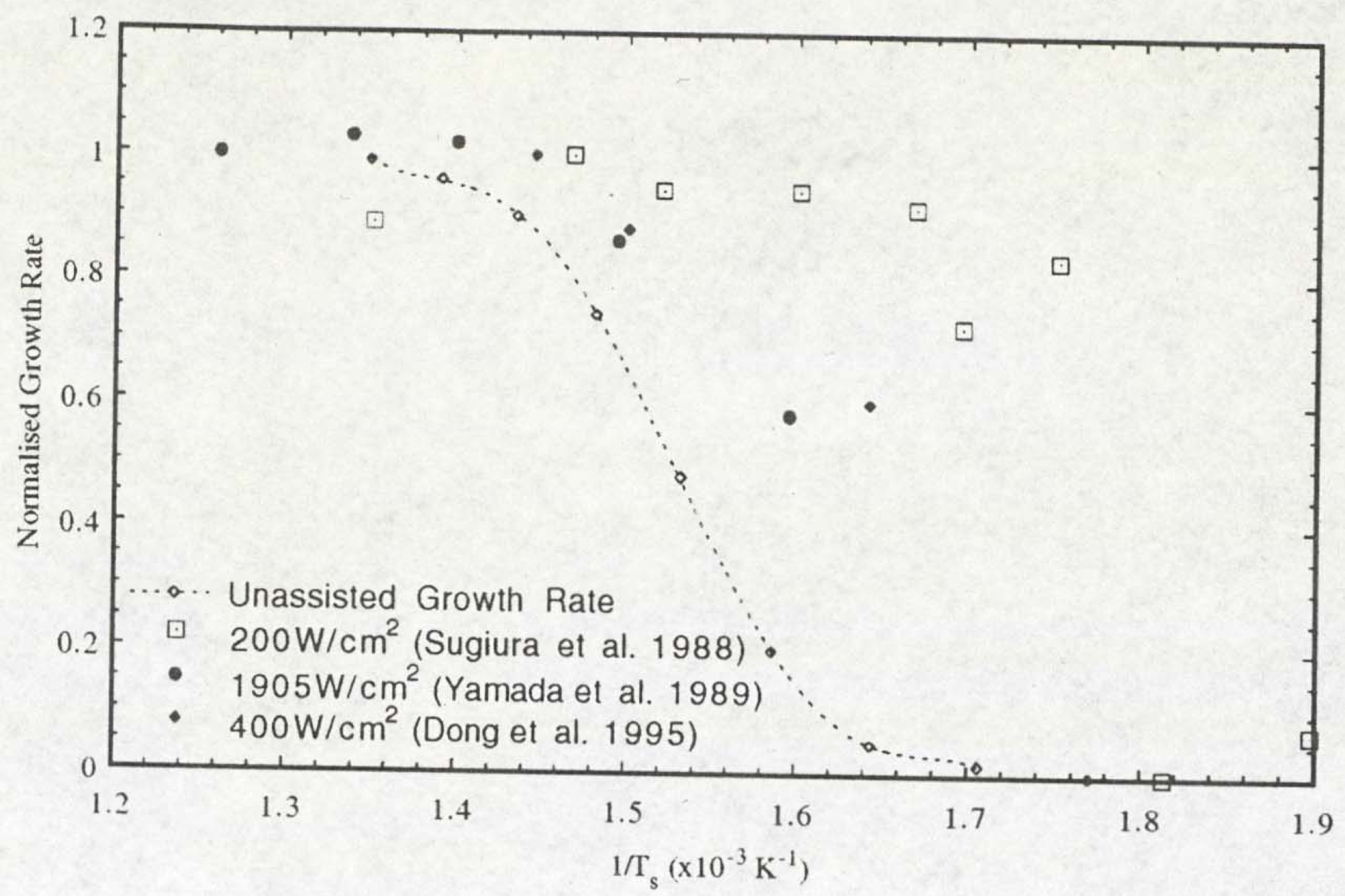

Figure 6.15: Temperature dependent growth rate of laser assisted GaAs as reported by other studies.

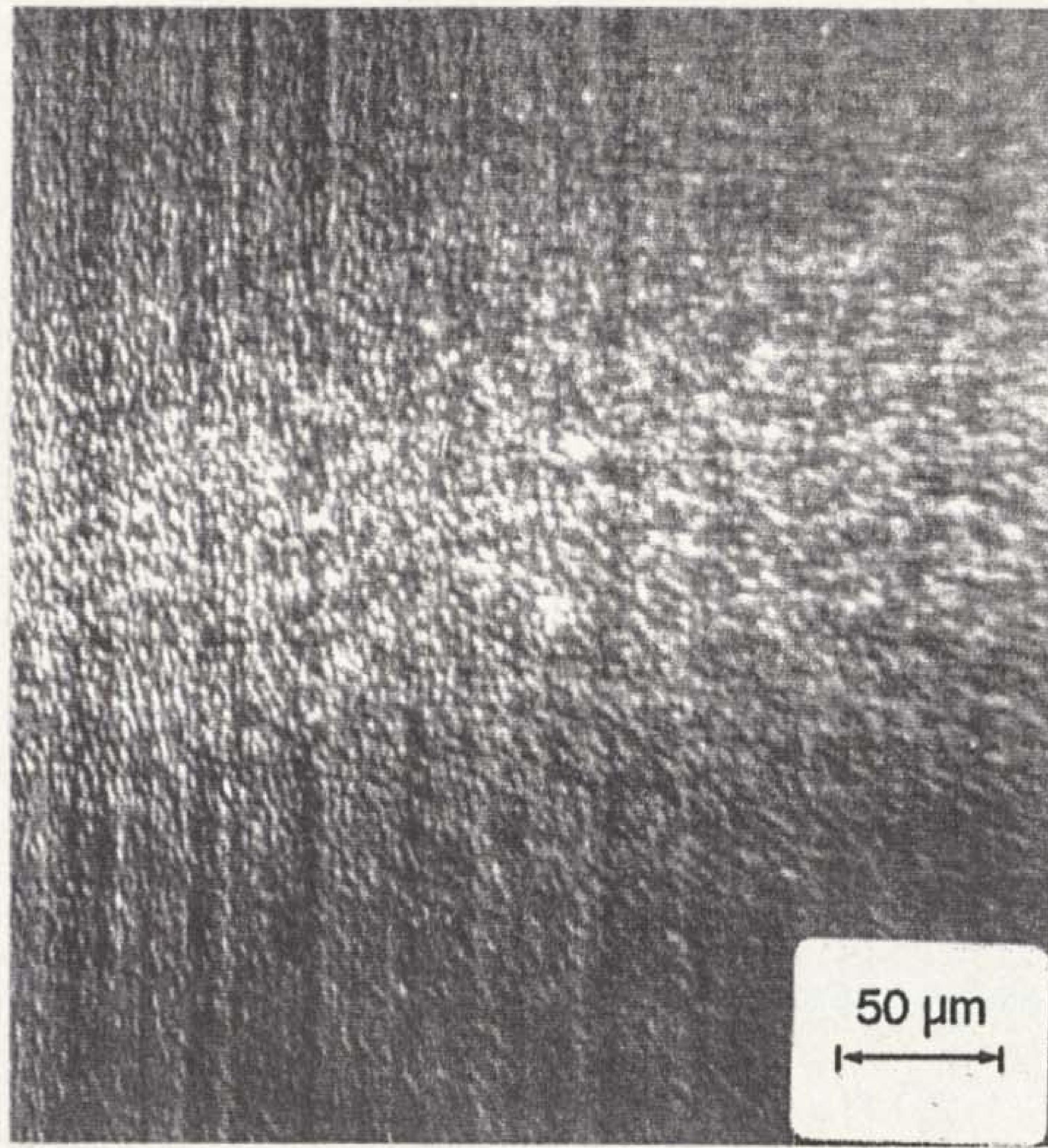

(a) Low magnification overview.

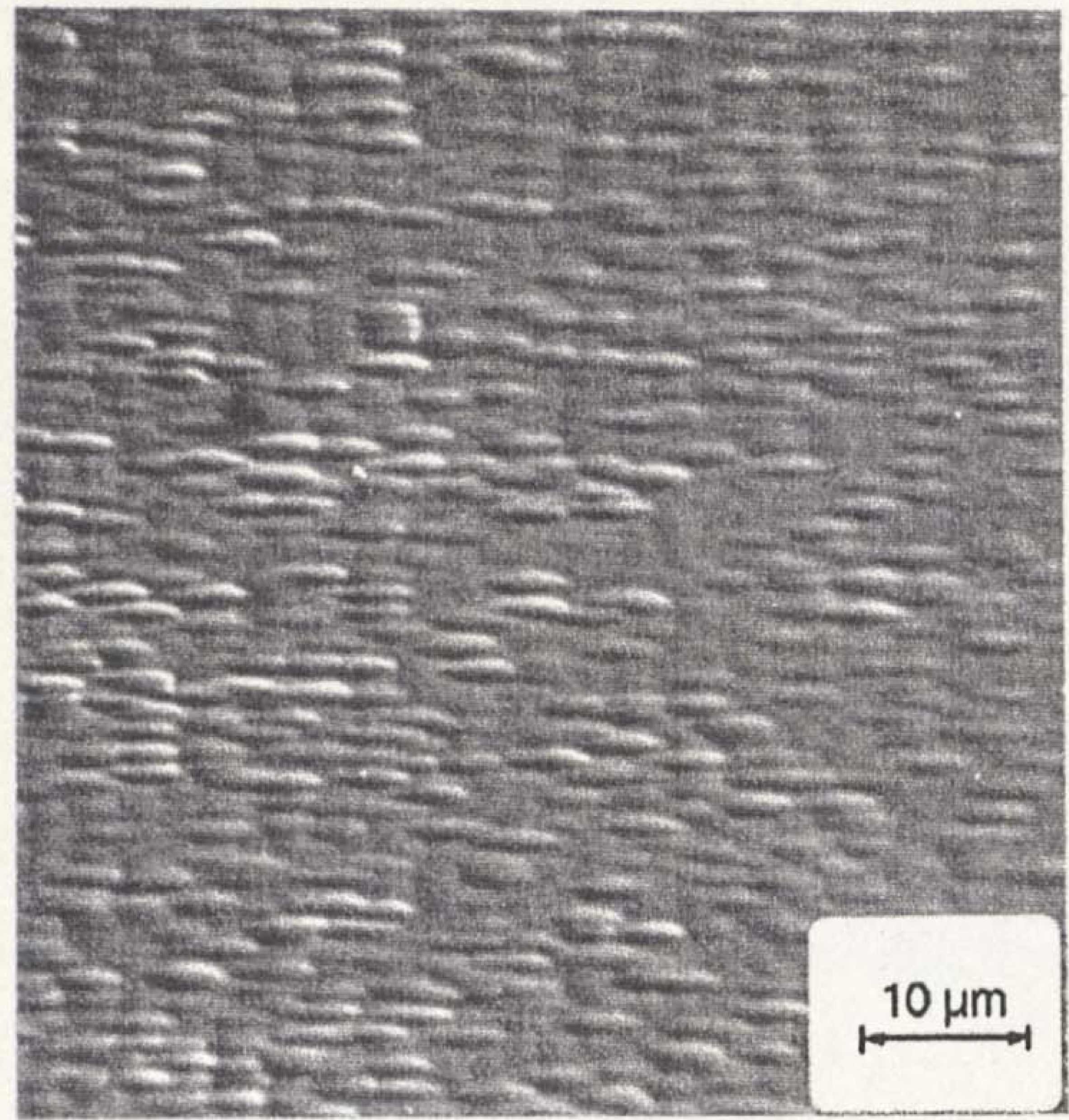

(b) At the centre of the laser area.

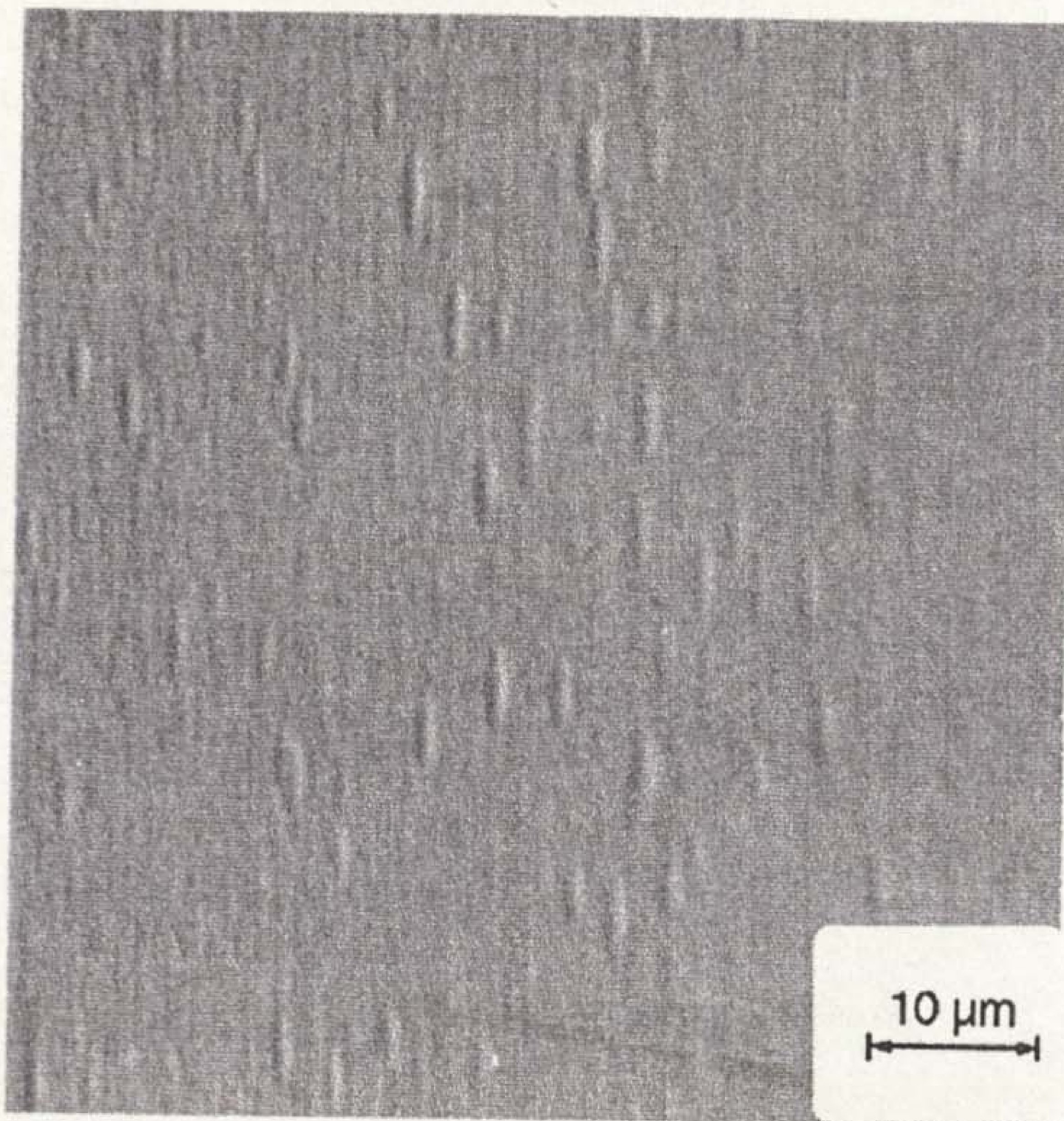

(c) A few mm from the laser area.

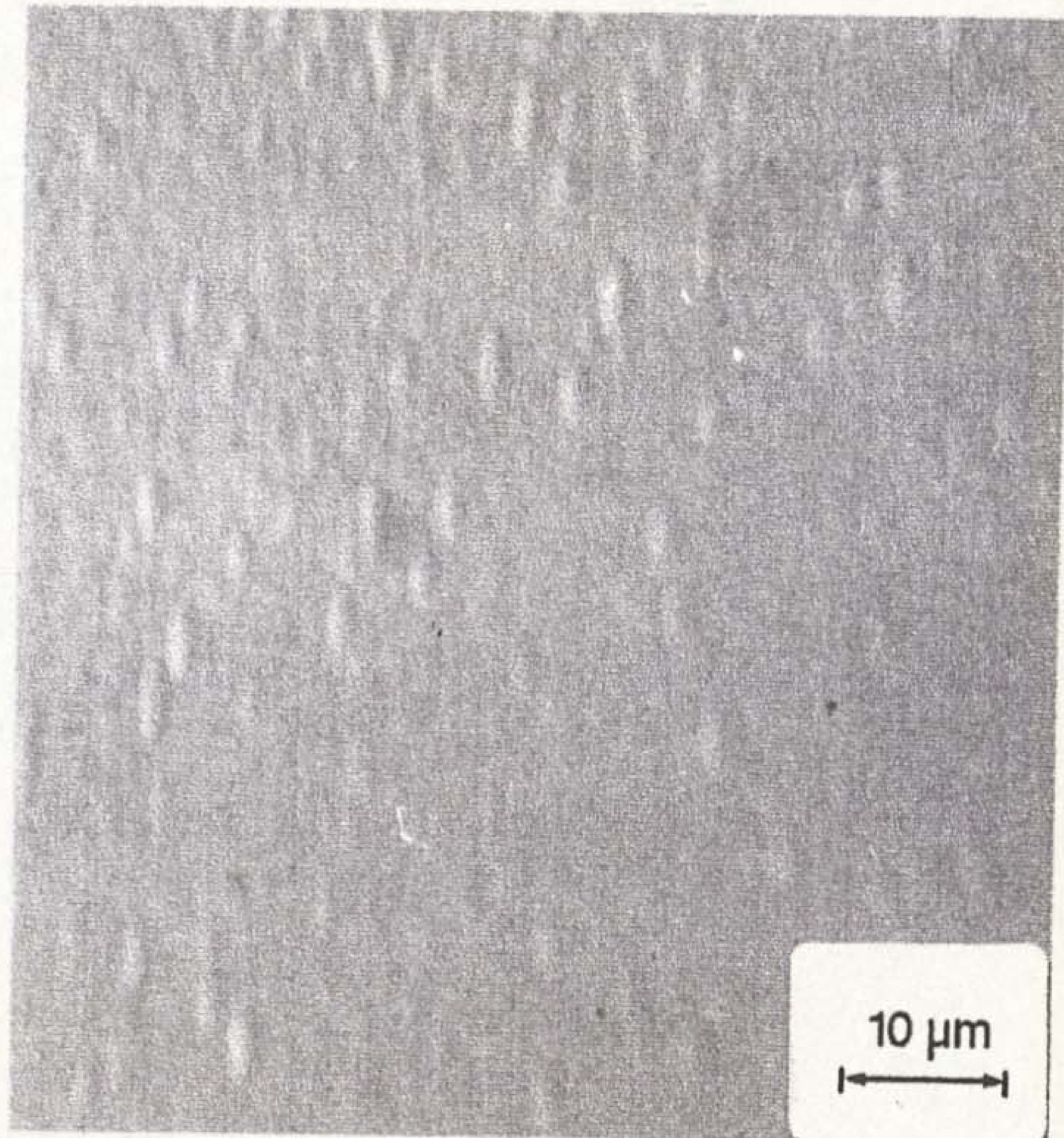

(d) A few cm away from the laser area.

Figure 6.16: Nomarski optical micrographs of the surface morphology in and adjascent to laser irradiated area of laser power 2.25W. The GaAs layer grown was at a substrate temperature of 600°C and the layer was 500nm thick away from the laser area.

CHAPTER SEVEN
CONCLUSIONS

7.1 Laser Modified CBE

7.2 Laser light scattering studies

7.3 Suggestions for further work

7.1 Laser Modified CBE

Focused continuous-wave (514.5nm) argon ion laser radiation increases the growth rate of GaAs grown by CBE using TEG and arsine thermally cracked to As_2 in an injector cell in substrate temperature range of 313-450°C. This enhancement is by a factor of up to 20 depending on laser power / radius, substrate temperature and group V : group III flux ratio.

By measuring the mean growth rate over the entire laser irradiated area by laser interferometry, during the early stages (around the first 150nm) of cw and chopped Ar+ laser assisted CBE of GaAs, it has been demonstrated that for substrate temperatures above 360°C there is a strong photothermal contribution to the enhancement. The cw growth rate with increasing laser power was consistent with increasing substrate temperature, and the growth rate of chopped beam assisted GaAs varied with chopping frequency at the frequency expected from local heating. The temperature rise required to account for all the cw enhancement is around 30% above that predicted from a heat conduction equation, assuming infinite dimensions. It is suggested that this difference is due to the finite substrate dimensions.

A surface ripple structure, partially aligned along the <110> directions, is observable in the laser affected area at high laser powers and substrate temperatures between 360-450°C. This is consistent with thermally induced elastic strain in the laser affected area resulting in variations in local growth rate. The development of the ripple structure is followed in real time using diffusely reflected light from the Ar+ laser and it is shown that the ripples start to appear after ~150nm of growth. Unintentional carbon incorporation is also reduced in the laser affected area, consistent with a local temperature rise.

Below a substrate temperature of 360°C a step change in the growth rate with laser power is observed. This step change indicates a deviation in the origin of the enhancement from purely photothermal. The position and sharpness of the step change in terms of laser power and the GaAs growth rate are dependant on the group V: group III flux ratio, indicating that the As_2 surface coverage has an important role in the growth kinetics of both unassisted and laser assisted CBE. A decrease in V:III ratio results in increased growth rates at lower laser powers and the step change moving to lower laser power and becoming broader. Laser assisted CBE at low substrate temperatures (~313°C), and high (>5:1) V:III flux ratios, where the step change is greatest result in the greatest growth rate selectivity with high laser power. These conditions also resulted in well defined laser assisted features.

Laser reflectometry, also known as dynamic optical reflectometry (DOR) and laser interferometry, is demonstrated suitable for monitoring the growth rate of laser assisted CBE of GaAs.

Laser modified CBE of GaAs at substrate temperatures above 490°C result in a growth rate inhibition. This is consistent with the photothermal effect observed below 490°C. However measurement was not obtained by laser interferometry due to the inhibition being small (<10%) and the temperature dependence of the refractive index. Above 490°C laser radiation, at laser powers required to produce an inhibition observable by Nomarski interference microscopy, also results in the development during growth of a surface 'cross-hatch' pattern of ridges aligned along the <110> directions, extending up to 6mm from the laser irradiated area. Such 'cross-hatch' patterns are believed to be associated with dislocations parallel to the surface, and indicate that thermally induced plastic deformation has occurred. An etch pit density study of one such sample revealed no net change in threading dislocation density in the region with respect to areas away from the laser area. However a number of those present were at the end of etched ridges,

associated with segments parallel to the surface. It is suggested that the plastic deformation has occurred by the movement of threading dislocations already present from the underlying substrate without the nucleation of additional dislocations. This is consistent with the calculated thermal strain and density of threading dislocations originating from the substrate. The plastic deformation is thus not a significant problem in Ar+ modified CBE, and under the correct condition may possibly reduce the local threading dislocation density.

7.2 Laser light scattering studies

LLS has been demonstrated to be a valuable in-situ monitoring technique since it is relatively simple to set up, and is compatible with most growth techniques. It gives valuable information on the surface topography at a scale which usually dominates growth, and which is related to surface processes. Orientation information is achieved by substrate rotation during normal data acquisition. Interference oscillations are also exhibited for epilayers of differing refractive index, as in specular laser interferometry (DOR), making LLS suitable for monitoring the growth of optically active structures.

It has been shown that pre-growth annealing epi-ready substrates can result in the development of an island morphology that is maintained during growth. The islands are around 1μm in lateral diameter and a few nm in height, and are associated with substrate-epilayer contamination due to desorption of previously deposited species from the cryopanel as a result of radiant heating from the substrate stage. By outgassing the substrate heater stage and the arsine cracker cell for a few hours before substrate loading the interface quality can be improved to that seen under clean MBE conditions. Surface pits are then observed as in MBE up to 6nm in depth but less than 100nm across. These pits fill during growth of GaAs to leave a surface dominated by islands a few monolayers in height and around 1μm across. Growth of GaAs leads to an initial reduction in

scattered light intensity due to smoothing but the islands remain and elongate, observable by LLS as a broadening of the trace due to a $\sin^2(\varphi)$ intensity relation with substrate orientation (of angle φ).

Growth of $In_xGa_{1-x}As$ ($x \leq 0.25$) epilayers on GaAs results in the development of a 'cross-hatch' pattern of ridges aligned along the <110> directions, at the onset of significant relaxation. The scattering is caused by the ridges, not the dislocations themselves, and they are identifiable by LLS as sharp spikes when, during rotation, the scattered light detector is aligned along each <110> direction. This demonstrates LLS as a suitable technique for detecting the presence of significant relaxation, although direct correlation to the level of relaxation was not produced. It is suggested that the directional ridges are due to the presence of a laterally varying strain field altering the local growth rate, primarily due to misfit dislocations lying above the GaAs - $In_xGa_{1-x}As$ epilayer interface.

Laser light scattering has been demonstrated to be sensitive to the pseudomorphic to island growth transition during high misfit (7.2%) InAs on GaAs heteroepitaxy. The transition results in an increase in scattered light intensity after ~1nm thickness of growth by a factor of around 5 over the subsequent 1.5nm thickness of growth. Coalescence of the islands is observed as a more gradual increase. LLS is thus suitable for monitoring the formation of self organised islands, also referred to as quantum dots or discs when buried in GaAs or AlGaAs.

7.3 Suggestions for further work

There are a number of areas of this work which merit further attention and expansion.

Ar+ laser inhibited CBE of GaAs is being extended to higher substrate temperatures (>625°C). Above 625°C the GaAs growth rate decreases by over an order of magnitude in 100°C. Local growth rate reduction due to laser radiation to around a third of the unirradiated growth rate has been measured with laser interferometry. However the morphology of the grown material has yet to be investigated.

The Ar+ modified CBE studies are being extended to AlGaAs and InGaAs, where changes in composition result from irradiation. It should be possible to measure these changes using laser interferometry. A PhD student is carrying out the work.

New precursors for both group III and V sources should be investigated for Ar+ modified CBE. Laser assisted CBE using tris-dimethylamino arsenide has been demonstrated to be feasible at substrate temperatures below that required with arsine cracked to As_2 in an injector cell, and a non thermal component indicated by Dong *et al.* 1994.

Study into laser modified CBE patterning, by the use of diffractive optics, holography, or beam scanning, to produce device structures must be undertaken if the field is to continue as an engineering field of study. The scale of the written features is severely limited by the system design. The distance between the optics and the substrate (over 0.3m) and system vibration limits the feature size presently to over 0.1mm. This should be addressed.

The work will be extended to UV lamp modified CBE. A PhD student is investigating assistance to GaAs growth rate and also changes in dopant incorporation using CBr_4 as a carbon dopant source. The use of a UV lamp as the light source has the possible advantage over an Ar+ laser in that the whole wafer may be irradiated at relative power

density, and the photon energy is closer to that required to photo-dissociate TEG in the gas phase.

The effect of Ar+ laser irradiation on the threading dislocation density merits further attention. This study suggests plastic deformation does occur at high substrate temperatures and the laser powers used, but only by the movement of threading dislocations originating from the substrate. It may be possible to locally reduce the threading dislocation density by causing those present to move across and away from the laser irradiated area. This may improve device performance of devices grown by laser modified CBE, and suggests a possible use of the laser to anneal device structures.

LLS would be suited to the monitoring of multilayer structures in much the same way as laser reflectometry (DOR).

LLS as a technique can be applied to many chemical and growth systems. It, along with other optical techniques, can be applied to non UHV environments. In CBE or MOVPE it could be used to evaluate growth using new precursors or used when problems arise associated with the growth system and surface morphology. LLS could be applied to the MBE growth of AlGaAs where poor surface topography is sometimes observed.

LLS may also be suitable for calibrating or monitoring the thickness of InAs grown in the formation of self organised quantum dots.

REFERENCES

Abrahams, M.S, C.J. Buiocchi, J. Appl. Phys. 36 (1965) 2855.

Adachi, S., J. Appl./ Phys. 58(3) (1985) R1.

Armstrong, J.V., T. Farrell, T.B. Joyce, P. Kightley, T.J. Bullough and P.J. Goodhew, J. Cryt. Growth 120 (1992) 84.

Arthur, J.R., J. Appl. Phys. 39 (1968) 4032.

Aspnes, D.E., S.M. Kelso, R.A. Logan and R. Bhat, J. Appl. Phys. 60(2) (1986) 754.

Aspnes, D.E., W.E. Quinn and S. Gregory, Appl. Phys. Letters 57 (1990) 2707.

Beanland, R., J. Appl. Phys. 72 (1992) 4031.

Beanland, R., C. Kiely and R.C. Pond in 'Handbook in semiconductors 3a' Ed S. Mahajan, , (1994).Elsevier.

Benninghoven, A., F.G. Rudenauer and H.W. Werner, 'Secondary Ion Mass Spectrometry' (1987) John Wiley.

Beuermann, Th. and M. Stoke, Chemtronics 4 (1989) 189.

Binning, G., C. Quate, C.H. Gerber, Phys. Rev. Letters 56 (1986) 930.

Blakemore, J.S., J. Appl. Phys. 53(10) (1982) R123

Bluhm, H., U.D. Schwartz, F. Hermann, P. Paufler, Appl. Phys. A 59 1994 23.

Brice J.C, EMIS datareview RN=2001 'Properties of gallium arsenide (1989) pp18

Brodsky, M.H. (ed) 'Properties of gallium arsenide' EMIS Data review series 2 (1990) INSPEC.

Brown, E.R., J.R. Soderstrom, C.D. Parker, L.J. Mahoney, K.M. Molvar and T.C. McGill, Appl. Phys. Letters 58 (1991) 2291.

Brueck, S.R.J. and D.J. Ehrlich, Phys. Rev. Letters 48 (1982) 1678.

Carslaw, H.S. and J.C. Jaeger, 'conduction of heat in solids' (1959) Oxford Uni. Press.

Celii, F.G., L.A. Files-Sesler, E.A. Beam and H.-Y. Lui, J. Vac. Sci. Technol. A 11 (1993) 1796.

Cho, A.Y., Appl. Phys. letters 19 (1971) 467.

Church, E.L., H.A. Jenkinson, and J.M. Zavada, Opt. Eng.16 (1977) 360.

Church, E.L., H.A. Jenkinson, and J.M. Zavada, Opt. Eng.18 (1979) 125.

Cullis, A.G., A.J. Pidduck and M.T. Emeny, J. Cryst Growth 158 (1996) 15.

Davies, G.J., P.J. Skevington, E.G. Scott, C.L. French and J.S. Foord, J. Cryst Growth 107 (1991) 999.

Dong, H.K., B.W. Liang, M.C. Ho, S. Hung and C.W. Tu, J. Cryst Growth 124 (1992) 181.

Dong, H.K., N.Y.Li, C.W. Tu, M. Geva and W.C. Mitchel, Mat. Res Symp. Proc. 340 (1994) 173

Drigo, A.V., A. Aydinli, A. Carnera, F. Genova, C. Rigo, C. Ferrari, P. Franziosi and G. Salviati, J. Appl. Phys. 66 (1989) 1975.

Dugdale 'private communication' (1996).

Dunstan, D.J., S.J. Young and R.H. Dixon, J. Appl. Phys. 70 (1991) 3038.

Dunstan, D.J., P. Kidd, P.F. Fewster, N.L. Andrew, R. Grey, J.P.R. David, L. Gonzalez, A. Sacedon and F. Gonzalez-Sanz, Appl. Phys. Letters 65 (1994) 839.

Effer, D., J. Electrochem. Soc. 112 (1963) 1020.

Egorov, A. U., A.E. Zhukov, P.S. Kop'ev, N.N. Ledenstov, M.V. Maximov and V.M. Ustinov, Workshop of the Eighth International MBE conference, Osaka, Japan, Aug.-Sep. (1994) 385 .

Farrell, T., J.V. Armstrong and P.Keightley, Appl. Phys. Letters 59 (1991) 1203.

Farrell, T., J.V. Armstrong, T.B. Joyce, T.J. Bullough, P. Kightley and P.J. Goodhew, J. Cryt. Growth 120 (1992) 395.

Farrell, T., 'private communication' (1995).

Fischer, M., R. Luckerath, P. Balk and W. Richer, Chemtronics 3 (1988) 156.

Foord, J., J. Appl. Phys. 68 (1990) 4053.

Foxon, C.T., Joyce, B.A., Current topics in mats. sci. vol. 7 (1981) N. Holland Pub. Co.

Fitzgerald, E.A., Mater Sci Rep. 7 (1991)87.

Gerard, J.M., J.B. Genin, J. Lefebre, J.M. Moison, N. Lebouche and F. Barthe, J. Crystal Growth 150 (1995) 351.

Grabmaier, J.B, C.B. Watson, Phys. Status Solidi 32 (1969) K13.

Huang, K.F., K.Tai, J.L. Jewell, R.J. Fischer, S.L. McCall and A.Y. Cho, Appl. Phys. Letters 54 (1989) 2192.

Heavens, O.S., 'Optical properties of thin films' (1995) London Butterworths Sci. Pub.

Hussien, S.A., A.A. Fahmy, N.A. El-Masry and S.M. Bedair, J. Appl. Phys. 67 (1990) 3853.

Heavens, O.S., Optical Prop. of Thin Sol. Films, Butterworths Pub. LTD (1955).

Iga, R., H. Sugiura and T. Yamada, Japan J. Appl. Phys. 61 (1992) 1423.

Iga, R., H. Sugiura and T. Yamada, Semicond. Sci. Technol. 8(1993) 1101.

Irvine, S.J.C., J. Bajaj and H.O. Sankur, J. Cryt. Growth 124 (1992) 654.

Isu, T., M. Hata, Y. Morishita, Y. Nomura, S. Goto and Y. Katayama, J. Cryst. Growth 120 (1992) 45.

Jeppesen, S., M. Miller, B. Junno, B. Kowalski, I. Maximov, D, Hessman, A. Petersson and L. Samuelson, proceedings of ICCBE 5. (to be published)

Joyce, B.A. and R.R. Bradley, Phil. Mag. 14 (1966) 289.

Joyce, T.B., T.J. Bullough, P. Kightley, C.J. Kiely, Y.R. Xing and P.J. Goodhew, J. Cryst. Growth 120 (1992) 206.

Joyce T.B PhD Thesis (1993).

Joyce, T.B., T.J. Bullough, and S. Westwater, J. Cryt. Growth 146 (1995) 394.

Kamiya, I., D.E. Aspnes, L.T. Florez and J.P. Harbison, Phys. Rev. B46 (1992) 1589.

Kitabayashi, H. and T. Waho, J. Crystal Growth 150 (1995) 152.

Laidler, K.L., J. Chem. Phys. 10 (1942) 43.

Lax, M., J. Appl. Phys. 48 (1977) 3939.

Le Corre, A., S. Durel, F. Clerot, B.Lambert, A. Poudoulec, S. Salaun and D. Lecrosnier, J. Cryst Growth 120 (1992) 353.

Martin, T. and C.R. Whitehouse, J. Cryst. Growth 105 (1990) 57.

Martin, T., C.R. Whitehouse and P.A. Lane, J. Cryst. Growth 107 (1991) 969.

Martin, T., C.R. Whitehouse and P.A. Lane, J. Cryst. Growth 120 (1992) 25.

Martin, Y., C.C. Williams, V. Wickramasinginge, J. Appl. Phys. 61 1989 4723.

Mathis, B.S and A.M Bonnot, Diamond and Rel. Mats. 'to be published'(1996).

Mifsud, V.J., P.W. Sullivan and D. Williams, J. Cryst Growth 105 (1990) 289.

Miller and Rozgonyi Defect characterization, Electrochem Soc. (1978) pp229.

Nabetani, Y., N. Yamamoto, T. Tokuda and Sasaki, J. Crystal Growth 146 (1995) 363.

Neave, J.H., B.A. Joyce and P.J. Dobson, Appl. Phys. A 34 (1984) 179.

Nelson, H., RCA Review 24 (1963) 603.

Olsen, G.H., J. Cryst. Growth 31 (1975) 223.

Orme, C., M.D. Johnson, J.L. Sudijono, K.T. Leung and D.G. Orr, Appl. Phys. Letters 59 (1994) 860.

Oron, M. and G. Sorenson, Appl. Phys. Letters 35 (1979) 782.

Panish, M.B., J. Electrochem. Soc. 127 (1980) 2729.

Parker, E.H.C. (ed) 'The technol. and Physics of MBE' (1985) Plenum, New YorkPub.Co.

Pickering, C., Thin Solid Films 206 (1991) 275.

Rytz-Froidevaux, Y., R.P. Salathe and H.H. Gilgen, Appl. Phys. A 37 (1985) 121.

Schooley, A.H., Proc. IRE 50 (1962) 426.

Shitara, T., J. Zhang, J.H. Neave and B.A. Joyce, J. Appl. Phys. 71 (1992) 4299.

Smith, G.W., A.J. Pidduck, C.R. Whitehouse, J.L. Glasper and J.Spowart, J. Crystal Growth 127 (1993) 966.

Stringfellow, G.B., R. Stall, W. Koschel, Appl. Phys. Letters 38 (1991) 156.

Tsang, W.T., Appl. Phys. Letters 45 (1984) 1234.

Tsang, W.T., J. Cryst. Growth 105 (1990) 1.

Tu, C.W., H.K. Dong, and N.Y. Li, Mats. Chem. and Phys. 40 (1995) 260.

Van Buuren, T., M.K. Weimeier, I. Athwail, K.M. Colbow,J.A. Mackenzie, T, Tiedje, P.C. Wong and K.A.R. Mitchell, Appl. Phys. Letters 59 (1991) 464

van de Ven, J, J.L. Weyher, J.E.A.M. van den Meerakker, J.J. Kelly, J. Electrochem. Soc.: Solid State Sci. 134 (1987) 989.

LIVERPOOL
UNIVERSITY
LIBRARY

Vasquez, R.P., B.F. Lewis and F.J. Grunthaner, J. Vacuum Sci. Technol. B1 (1983) 791.

Veuhoff, E., W. Pletschen, P. Balk and H. Luth, J. Cryst. Growth 55 (1981) 30.

Xie, Q., P.Chen and A. Madhakur, Appl. Phys. Letters 65 (1994b) 2051.

Xie, Q., P.Chen, A.Kalburge, T.R. Ramachandran, A. Nayfonov, A. Konkar and A. Madhakur, J. Crystal Growth 150 (1995) 357.

Yang, K., E. Mirabelli, Z.-C. Wu and L.J.Schowalter, J. Vac. Sci. Technol. B11 (1993) 1011.

Zipperian, T.E., L.R. Dawson, T.J. Drummond, J.E. Schirber and I.J. Fritz, Appl. Phys. Letters 53 (1988) 975.